September 30, 2015

Mechanical and Thermal Analysis of the LCLS-II Cryogenic Distribution System (I_p = 1.5)

Bob Wands
Ingrid Fang

Table of Contents

Introduction and Summary

The cryogenic distribution system (CDS) for LCLS-II was analyzed for all relevant loadings using the criteria of ASME B31.3, "Process Piping," augmented by B31E-2010 "Standard for the Seismic Design and retrofit of Above-Ground Piping Systems."

The specific components analyzed were:

1. Straight horizontal section
2. Anchor modules
3. Vertical expansion Joint
4. Transfer line supports
5. Cryomodule feedcap
6. Cryomodule feedcap support

Thermal results (temperatures and heat leaks) are reported for each analysis. Worst-case combinations of gravity, pressure, cool down, vacuum, and seismic loading are applied, and the resulting stresses in all components are shown to be below the material allowable stress.

Description of Loadings

The CDS is subjected to both thermal and mechanical loadings.

For the thermal analysis, specified cryogenic fluid temperatures are applied directly on the inner surfaces of the pipes, and heat fluxes from radiation are applied on the outer surfaces of the pipes. The radiation heat fluxes applied are 1.5 W/m^2 for the 55 K shield, and 0.15 W/m^2 for the 2K and 5 K lines.

For the stress analysis, the following mechanical loadings are applied:

1. Thermal contraction (cool down) – this loading is the result of thermal contractions due to cooling down the system to its operating temperature. It may cause stress issues where materials of different thermal contractions are joined.

2. Internal Pressure – this is a maximum allowable working pressure as defined in UG-98 of the ASME BPVC Section VIII, Div. 1.

3. Dead Weight – this is the loading due to gravity acting on the mass of the components

4. Seismic – this loading is the result of base acceleration during a seismic (earthquake) event. ASCE-7 was used to calculate this load. (see Appendix A)

5. External pressure – this loading is used in this analysis in two ways. First, as insulating vacuum, it is used to provide the large axial force to be resisted by the feedcap support structure, and second, it is used to simulate the leak checking operations, which involve the evacuation of individual pipes, and which, in the region of flex hoses, may impose loads on internal piping components.

6. Pressure imbalance at the vacuum breaks – this loading accounts for the possibility of differential pressure across the vacuum breaks. This differential pressure is a maximum when one side of the vacuum break is evacuated, and the other side is pressurized by a fault event. This loading occurs only in the central anchor module and the bottom elbow of the vertical transfer line.

Analysis Approach

The analysis approach to the CDS is detailed in Appendix A. To summarize: ASME B31.3-2014, "Process Piping" is the standard to which the LCLS-II transfer line will be designed and built. B31Ea-2010, "Standard for the Seismic Design and Retrofit of Above-Ground Piping Systems" specifies the design requirements for seismic loadings. ASCE 7-10, "Minimum Design Loads for Buildings and Other Structures" is used to determine the peak spectral accelerations, and the load combinations for an allowable stress design.

The basic load combinations are[6]

1. $D + F_{ip} + F_{ep} + T$
5. $D + F_{ip} + F_{ep} + 0.7E + T$
8. $0.6D + 0.7E + 0.6F_{ip} + 0.6F_{ep}$

where D = dead weight
F_{ip} = internal pressure on pipes
F_{ep} = external pressure on vacuum shell
T = thermal contraction (self-straining) effects
E = seismic effects (per ASCE 7-10)

In this analysis, the factor of 0.7 is applied only to the horizontal seismic acceleration, resulting in an applied acceleration of 0.89 g. The vertical seismic acceleration is taken at its full value.

For evaluating stresses it does not specifically address, B31.3 permits the methods of ASME Section VIII, Div. 1 and 2 to be used. Particularly useful in this analysis are the stress linearization (stress classification line) procedures of Div. 2, Part 5, "Design by Analysis."

Material Properties

Four materials are used in the LCLS-II CDS: 304 stainless steel, 6061-T6 aluminum, OFHC copper, and G-10 fiberglass epoxy. Currently, the temper of the OFHC copper is not specified. It is assumed for the purposes of this analysis that the copper is ASTM B601 temper H01.

Table I summarizes the material properties for the metallic components of the CDS. Values listed are those for room temperature. For 6061-T6, both welded and unwelded allowable stresses are given.

Table II summarizes the material properties and allowable stresses for G-10. The in-plane properties in the fill direction are used, as they are substantially lower than those in the warp and normal directions. The allowable stress is taken as 0.5 times the value of the lowest strength for each ultimate stress, resulting in an allowable stress of 18.5 ksi in tension and -20.5 ksi in compression.

Table I. Mechanical properties of metallic components and allowable stress

Material	Young's Modulus - psi	Poisson's Ratio	Ultimate Tensile Strength - ksi	Yield Strength - ksi	Allowable Stress – ksi	
304	28.3e6	0.3	75	30	20[1]	
6061-T6	10e6	0.3	42	35	14[1](unwelded)	8[5](welded)
OFHC Cu	17e6	0.3	30	10	6.7[5]	

Table II. Mechanical properties of G-10 and allowable stress[7]

Ultimate Tensile Strength - ksi		Ultimate Compressive Strength – ksi		Young's Modulus - psi		Poisson's ratio	Allowable Tensile Stress - ksi	Allowable Compressive Stress - ksi
Warp	Fill	Warp	Fill	In-plane	Normal			
60	37	-54	-41	2.7e6	1.1e6	0.15	18.5	-20.5

The feedcap employs several bolted connections. The bolts are specified as BS EN ISO 3506, Grade 2, Property Class 70. This is a 304 stainless steel with 700 MPa (100 ksi) tensile strength, and a 0.2% proof strength of 450 MPa (65.3 ksi). The allowable stress for this bolt is taken as 2/3 of the 0.2% proof strength, or 43.5 ksi.

The attachment of lines A, B, C, and D to the shield plate of the feedcap involves the epoxy bonding of G-10 to SS304. The strength of this bond is not specified. The approach taken here is to assess the bond stresses, and suggest a minimum bond strength based on that assessment.

Apart from the strength-related mechanical properties, the temperature-dependent physical properties (thermal conductivity and thermal contraction) were also required for all materials in the analysis. These are given in Tables III through VI.

Table III. Physical properties of SS304

Temp - K	k – W/m-k	ΔL/L from 300 K
4	0.272	2.97E-03
8	0.677	2.98E-03
10	0.904	2.99E-03
20	2.169	3.00E-03
40	4.67	2.98E-03
60	6.647	2.90E-03
80	8.114	2.78E-03
100	9.224	2.61E-03
120	10.101	2.41E-03
140	10.834	2.19E-03
160	11.479	1.94E-03
180	12.071	1.67E-03
200	12.633	1.39E-03
220	13.178	1.10E-03
240	13.714	8.05E-04
260	14.247	5.04E-04
280	14.779	1.99E-04
300	15.309	0

Table IV. Physical properties of G-10 (in-plane)

Temp - K	k – W/m-k	ΔL/L from 300 K
4	0.073	2.46E-03
6	0.097	2.46E-03
8	0.118	2.45E-03
10	0.136	2.45E-03
15	0.172	2.43E-03
20	0.198	2.42E-03
25	0.220	2.40E-03
30	0.239	2.38E-03
40	0.274	2.34E-03
50	0.306	2.29E-03
70	0.366	2.19E-03
100	0.448	1.99E-03
120	0.498	1.83E-03
150	0.568	1.58E-03
200	0.674	1.09E-03
250	0.772	5.37E-04
300	0.864	0

Table V. Physical properties of 6061-T6

Temp - K	k – W/m-k	ΔL/L from 300 K
4	3.29	4.14E-03
8	6.68	4.15E-03
10	8.42	4.15E-03
20	17.2	4.16E-03
40	32.8	4.12E-03
60	45.8	4.02E-03
80	56.8	3.86E-03
100	66.2	3.65E-03
120	74.5	3.40E-03
140	81.7	3.11E-03
160	88.2	2.78E-03
180	94.0	2.42E-03
200	99.2	2.03E-03
220	103.	1.61E-03
240	108.	1.19E-03
260	112.	7.44E-04
280	115.	2.94E-04
300	119.	0

Table VI. Physical properties of OFHC Copper

Temp - K	k – W/m-k	ΔL/L from 300 K
4	320	3.37E-03
8	622	3.31E-03
10	778	3.28E-03
20	1367	3.12E-03
40	1163	2.81E-03
60	670	2.51E-03
80	500	2.20E-03
100	443	1.88E-03
120	421	1.57E-03
140	411	1.27E-03
160	406	9.82E-04
180	402	7.06E-04
200	400	4.71E-04
220	398	2.85E-04
240	396	1.29E-04
260	395	5.10E-05
280	393	1.30E-05
300	392	0.00E+00

B31.3 Requirements for Wall Thickness of Pipe under Internal Pressure

Paragraph 304.1.2 of B31.3 states that, "for t < D/6, the internal pressure design thickness for straight pipe shall be not less than that calculated in accordance with either eq. (3a) or eq. (3b)."

$$t = \frac{PD}{2(SEW + PY)} \quad (3a)$$

$$t = \frac{P(d + 2c)}{2[SEW - P(1 - Y)]} \quad (3b)$$

where t = pressure design wall thickness
P = internal design gage pressure
D = outside diameter of pipe
d = inside diameter of pipe
S = stress value for material from Table A-1
E = quality factor from Table A-1A or A-1B
W = weld joint strength reduction factor in accordance with para. 302.3.5(e)
Y = coefficient from table 304.1.1, valid for t <D/6 and materials shown
c = sum of mechanical allowances (thread or groove depth) plus corrosion and erosion allowances.

Parameters for LCLS-II Piping

The cross section of the LCLS-II in the straight section is shown in Fig. 1. The line designations A-F will be used throughout this report. Parameters for eqns. 3a and 3b are given in Table VII. Resulting wall thicknesses are given in Table VIII. The operating temperatures of each line are summarized in Table IX.

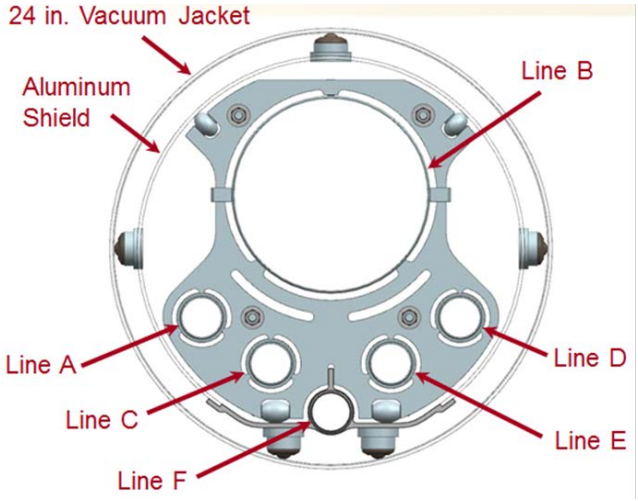

Figure 1. Cross-section of transfer line straight section

S = 25 ksi for 304

Table VII. Parameters for Calculating Minimum Wall Thickness of Transfer Line

Line	Material	OD - in	P (psi)	S (psi)	E*	W	Y	c
A	SS304L	2.375	300	20000	0.8	1	0.4	0
B	SS304L	10.75	60	20000	0.8	1	0.4	0
C	SS304L	2.375	300	20000	0.8	1	0.4	0
D	SS304L	2.375	300	20000	0.8	1	0.4	0
E	SS304L	2.375	300	20000	0.8	1	0.4	0
F	6061-T6 Al	2.45	300	8000**	1**	1	0.4	0

* Stainless steel pipe is assumed to be electric-fusion welded, single butt joint, no radiography.
** Aluminum pipe is seamless, but lengths are joined by welding, so welding allowable stress is used

Is it just a conservative approach to consider to get welded pipe without x-ray or do we really accept this type of supply ?

Table VIII. Calculated Minimum Wall Thickness and Actual Wall Thickness of Transfer Line piping

Line	t – eqn 3a (in)	t – eqn 3b (in)	t – actual (in)
A	0.022	0.020	0.109
B	0.020	0.020	0.134
C	0.022	0.020	0.109
D	0.022	0.020	0.109
E	0.022	0.020	0.109
F	0.045	0.040	0.191

Table IX. Operating temperatures of lines

Line	Temperature - K
A	2.5
B	2
C	4.5
D	5.5
E	35
F	55

A is 4.5
B is 2
C is 5
D is 7

Sizing of Transfer Line Vacuum Jacket

External Pressure

The vacuum jacket for the transfer line is sized using the procedures of the ASME Code, Section VIII, Div. 1, UG-28, in accordance with the requirements of para. 304.1.3 of B31.3.

The parameters for the cylindrical vacuum jacket are:

D_o = outside diameter of shell = 24 in
L = length of shell = 1400 inches (approximate length between anchors in straight section)
t = 0.25 in
$D_o/t = 96$
$L/D_o = 58.3$

Given $D_o/t > 10$, the procedures of UG-28(c)(1) can be used.

Entering Fig. G of Div. 2, Part D, with the value of $D_o/t = 96$, and L/D = 58.3, the Factor A is found to be 0.00012.

The vacuum shell material is 304 stainless steel. Entering Fig. HA-4, applicable to this material, with the value of A = 0.00012 shows that this factor falls to the left of the curves given. Therefore, by UG-28(c)(1) Step 7, the allowable pressure can be calculated from

$$P_a = 2AE/3(D_o/t)$$

Where E = Young's modulus of shell material = 28.3e6 psi

Substituting gives

$$P_a = 2(0.00012)(28.3e6)/(3(96)) = 23.6 \text{ psi}$$

This is well above the operating pressure differential of 15 psi under vacuum.

Internal Pressure

For internal pressure, the vacuum jacket may see a maximum of 7 psi differential. For P = 7 psi, S = 20 ksi, D = 24 in, d = 23.5 in, and E, W, Y and c as for the internal piping as listed above, the required wall thickness is governed by equation 3a and is 0.005 in. This is well below the available wall thickness of 0.25 inches.

FE Model Verification

Linear static finite element simulations were used to generate the results that follow. Verification consisted of reaction force checks against the input, as well as common sense evaluation of deformations to determine that they conform to the expected directions and approximate magnitudes. Mesh density was varied where necessary to verify stress convergence through the thickness of pipes and plates. Contact behavior between parts was limited to the linear characterizations of either full bonding, or, for a few interfaces, sliding without separation.

Stress Evaluation

The finite element method is well known for producing high stresses at structural discontinuities (stress concentrations). These concentrations occur in nature, but are exacerbated by the analysis since in most practical FE models, the discontinuities are defined by corners that are mathematically sharp, i.e., have an infinitely small radius. Calculated local stresses at such discontinuities can greatly exceed the yield stress. However, it is well known that for ductile, statically loaded structures, stress concentrations can be safely ignored. This is because the ductility ensures that a small amount of yielding can occur without fracture, allowing the internal forces to redistribute to the large volumes of less stressed material nearby, while the static loading ensures that fatigue will not be a consideration. The main issue in dismissing high FE stresses as concentrations is the subjectivity of deciding if they are in fact concentrations.

In this report, two methods are used to evaluate the stresses in regions where the calculated FEA value is greater than the membrane stress allowable. The first is the stress linearization approach using stress classification lines. This is from the ASME Code, Section VIII, Div. 2. This approach decomposes the stresses along a stress classification line (SCL) passed through the part into a constant (membrane) stress, and a linearly varying bending stress, which are statically equivalent to the calculated stress state. This process mitigates the effect of a concentration, since the concentration is typically a very small region at one end along the line, and does not have a large effect on the forces and moments. It is applicable to shells and heads associated with pressure parts.

The second method is more subjective. It involves looking closely at a stress plot of a region of high stress, and attempting to illustrate that it is surrounded by material at a much lower stress, and that the stress attenuates rapidly as the distance from the concentration increases.

Transfer Line Straight Section

The FE model of the transfer line straight section is shown in Fig. 2. This model is periodically symmetric. Two symmetry planes are exploited – the one between the individual spiders in a pair, and the one at the halfway point between two adjacent spider pairs. For reference, spider pairs are spaced 120 inches apart. The model is half this length, or 60 inches.

All thermal heat loads are expressed as two times the values produced by the model, so that they actually represent a 120 length of transfer line, with a single spider pair in the middle.

How many layers ?. 1.5 W/m2 seems ok for TS. 0.15 W/m2 seems high (3 times)

To simulate radiative loading, a heat flux of 1.5 W/m^2 was applied to the 50 K shield surface. heat flux of 0.15 W/m^2 was applied to the 5 K surfaces.

The symmetric thermal boundary conditions prohibit any flow of heat across the symmetry planes..

The symmetric structural boundary conditions prohibit any rotation of the end surfaces of the pipes at the symmetry cuts about the X or Y axis. This is done at the spider end by fixing the axial (Z) displacement of all surfaces. At the midplane cut, allowances must be made for thermal contraction, so a remote point is used for each line A-F that allows it to contract toward the spider, but does not allow rotation. The vacuum shell does not contract and can be given a Z constraint at both ends. The shield, which is cut in Z periodically by design, can be allowed to contract without rotation restrictions.

The vertical “fin” on line F loosely engages the slot in the spider to resist the lateral motions of the X-direction seismic accelerations. One side of this fin was attached to the spider in a way that allowed sliding (for thermal contraction) but no separation.

The following loads were considered in the combinations given on Page 5:

1. Cool down
2. All pipes pressurized to their MAWP
3. 0.89 g acceleration in X (seismic)
4. 1.4 g acceleration in Y (deadweight + seismic)
5. 0.2 g acceleration in Y (deadweight – seismic)

The critical load combination corresponds to Combination 5, and consists of cool down plus MAWP plus X-acceleration plus 1.4 g Y-acceleration. (There is external pressure only on the vacuum shell, which has been independently sized for this load, and which does not impose this load on any other component in this analysis.)

This model was not subjected to axial (Z-direction) seismic loading, as there is no provision for reacting axial forces except at the central anchor module, which is considered in a separate analysis.

The total weight of the model is 550 lbs. This translates to a total weight of 1100 lbs for each 120 inch long section of transfer line, or 110 lbs/ft

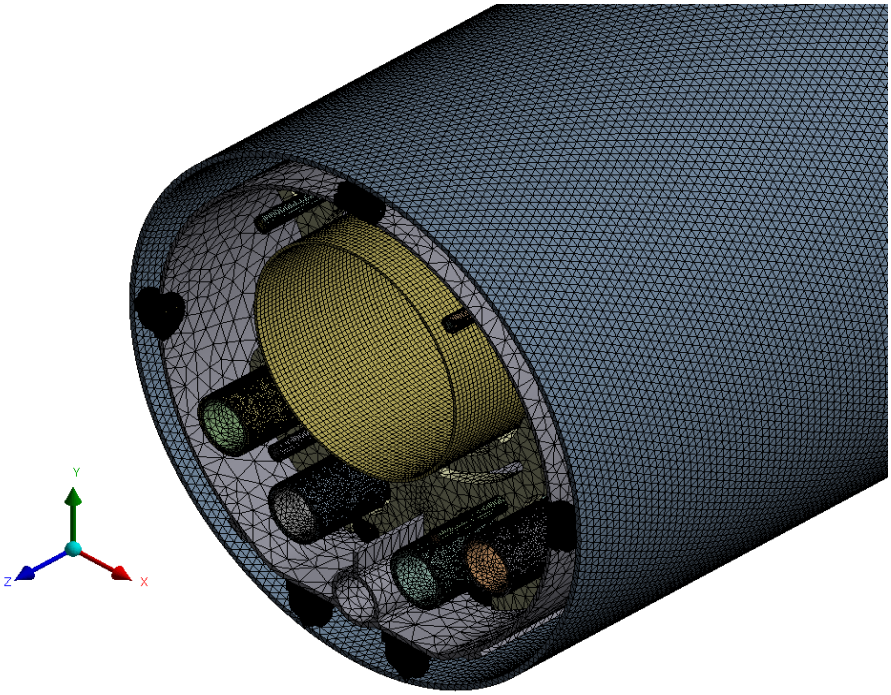

Figure 2. FE model of TL straight section

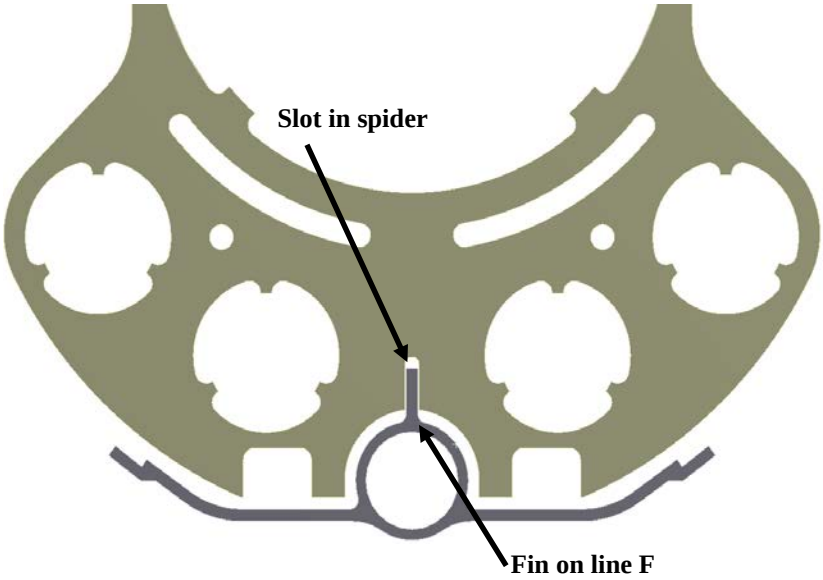

Figure 3. Fin/slot geometry for reacting lateral (X-dir) seismic loads

Thermal Results

The heat leak to the internal lines is given in Table X. The total heat leak to 300 K is 15 W. This includes the radiative heat load between 300 K and 50 K of 7.8 W, and the radiative heat load between 50 K and 5 K of 0.78 W. This heat leak should be interpreted as that for each 120 inch length of transfer line supported by a spider pair.

The temperature profile in the spider is shown in Fig. 4.

Table X. Heat leaks for straight section lines

Line	Radiation – W	Conduction – W	Total – W
A	**-0.04**	**-0.03**	**-0.07**
B	**-0.21**	**-0.10**	**-0.31**
C	**-0.04**	**-0.05**	**-0.09**
D	**-0.04**	**-0.03**	**-0.07**
E	**-0.04**	**-0.02**	**-0.06**
F	**-3.92**	**-3.01**	**-6.93**
Note: Negative sign indicates heat flow into line			

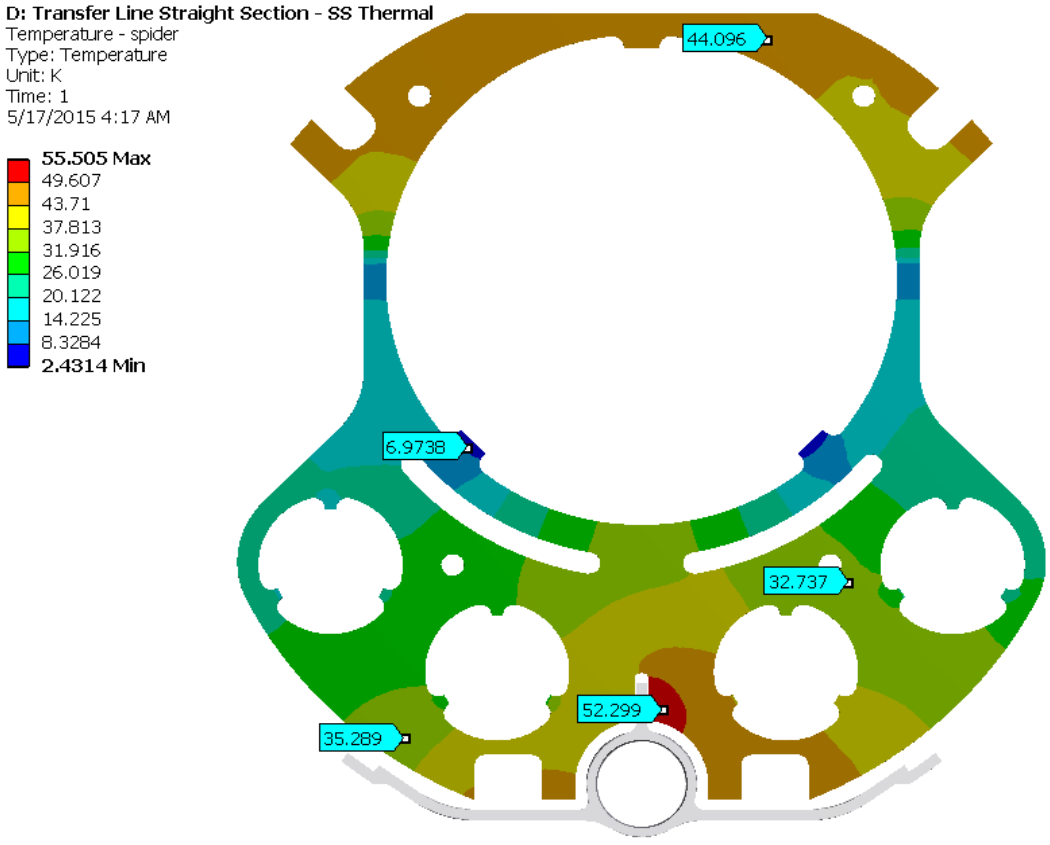

Figure 4. Temperature profile in spider

Stress Results

As state previously, the critical load combination corresponds to Combination 5, and consists of cool down plus MAWP plus Y-acceleration plus X-acceleration

The maximum and minimum principal stresses in the spider of the straight section were examined, and it was found that the compressive stress limit is most closely approached. (Note: the von Mises criterion – equivalent stress – is not applied to the G-10, as it is not an isotropic ductile material.) The minimum principal stress, shown in Fig. 5, occurs at one of the protrusions that support the fiberglass pipe sleeves, and is -16.1 ksi. This is below the G-10 compressive allowable stress of -20.5 ksi.

Figure doesn't seem to be in accordance with the max load mentionned

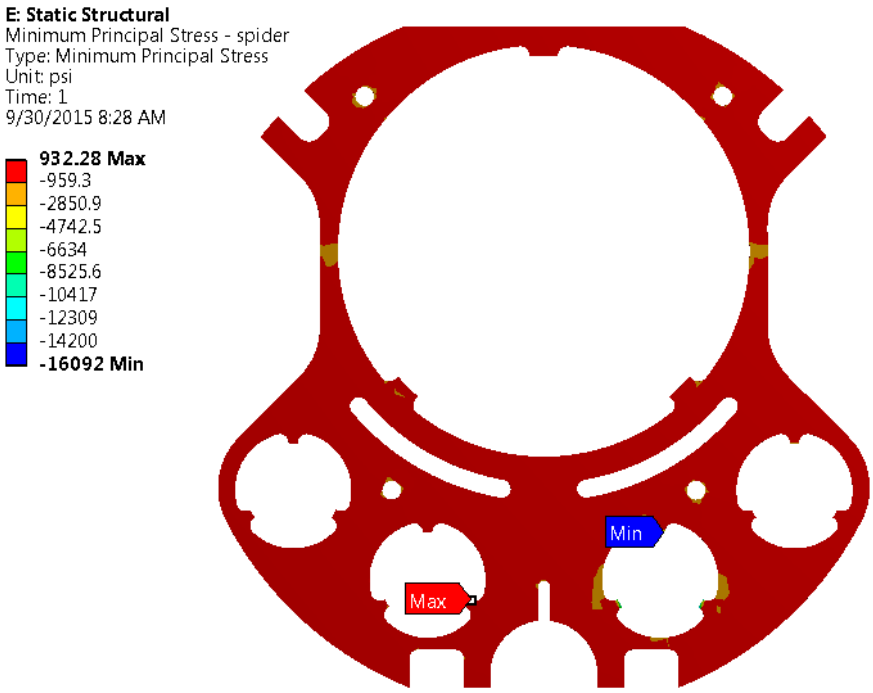

Figure 5. Minimum principal stress in spider in straight section

The stresses in the SS304 piping are shown in Fig. 6. The maximum of 13.6 ksi is less than the membrane allowable stress of 20 ksi.

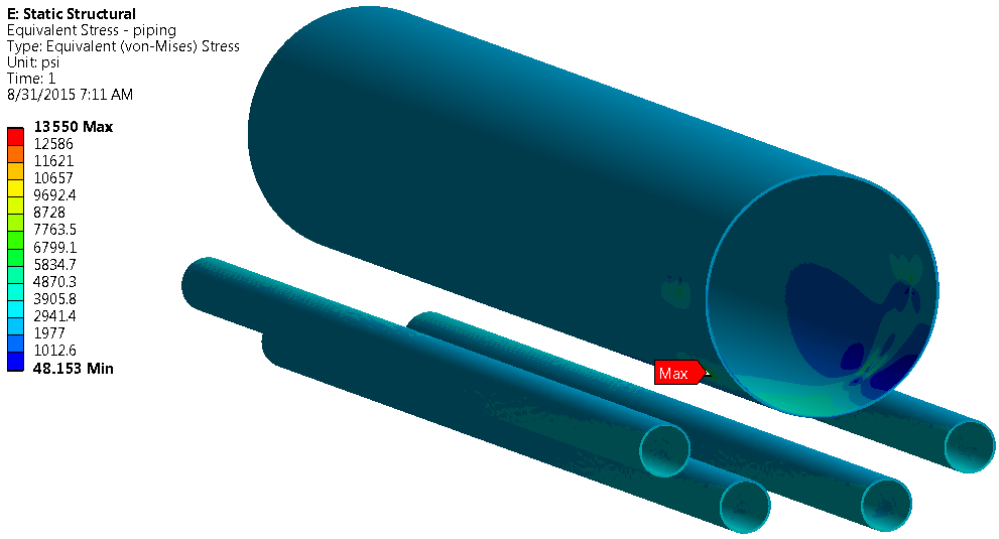

Figure 6. Stresses in straight section piping

The stresses in the 6061-T6 extrusion of line F are shown in Fig. 7. The maximum of 15.9 ksi is greater than the membrane stress allowable of 12 ksi for the material. To assess the stress more critically, a stress classification line was passed through the high stress region (Fig. 8). The resulting primary membrane stress, Pm, of 2.3 ksi, and the primary membrane plus bending, Pm+Pb, of 15.9 ksi, are both below the allowables of 12 ksi and 18 ksi, respectively.

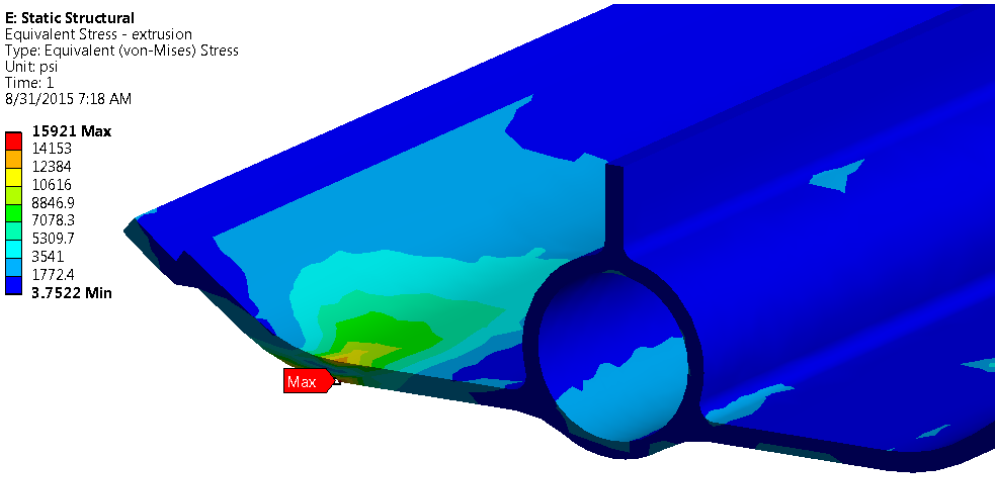

Figure 7. Stresses in line F aluminum extrusion

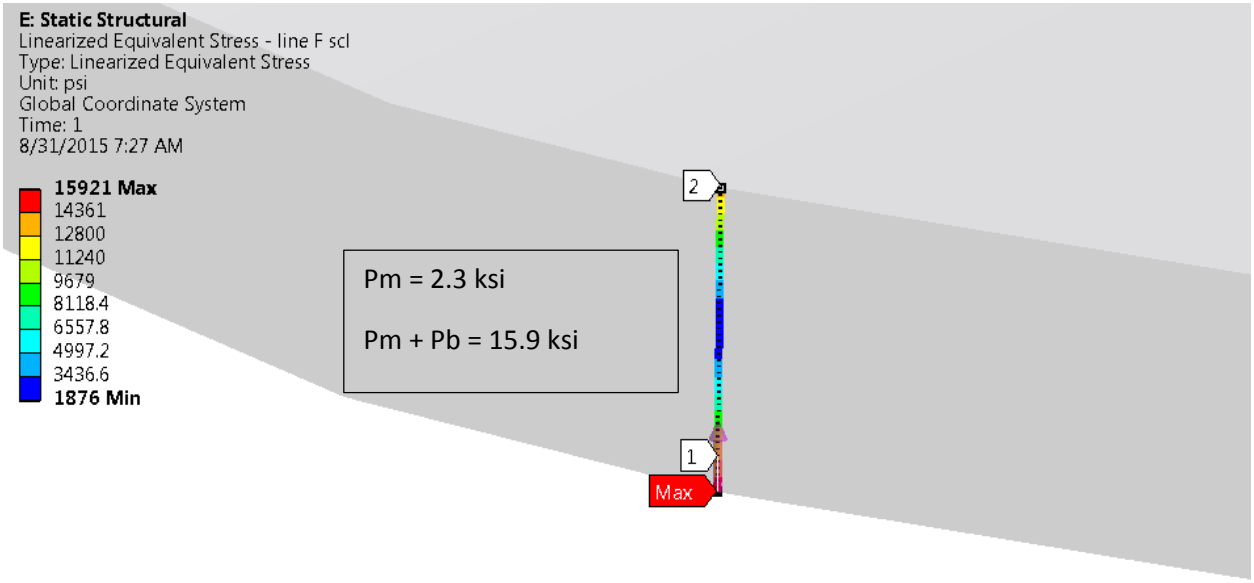

Figure 8. Stress classification line through extrusion

The piping loads are transmitted to the vacuum shell through the interaction of the aluminum shield with ball transfers that roll against the vacuum shell. These are specified as Ball Transfer Systems, LLC, 25 MPS stainless steel, capacity 550 lbs. A 120 inch length of internal piping weighs approximately 635 lbs, and is supported under normal conditions by two ball transfers. This results in a load of about 317 lbs on each ball transfer. With a total Y-direction dead-weight plus seismic acceleration of 1.4 g, each ball transfer will see a total load of about 445 lbs. This is still under the rated capacity.

Transfer Line Horizontal Anchor Module

The horizontal anchor module provides axial (Z-direction) horizontal anchoring for 70 m of pipe. All thermal contractions take place relative to the anchor module. It provides the reaction for all axial accelerations, and delivers these forces to the walls of the enclosure through a truss structure. (The analysis of this structure is presented later in this report.)

The following loads were considered in the combinations given on Page 5:

1. Cool down
2. All pipes pressurized to their MAWP
3. 0.89 g acceleration in X (seismic)
4. 1.4 g acceleration in Y (deadweight + seismic)
5. 0.2 g acceleration in Y (deadweight – seismic)
6. 0.89 g acceleration in Z (seismic)
7. 22 psia overpressure of the vacuum space on the left hand side of the vacuum break
8. 22 psia overpressure of the vacuum space on the right hand side of the vacuum break

The critical load combination correspond to Combination 5, and consists of cool down plus MAWP plus 1.4 g Y-acceleration plus Z-acceleration plus differential pressurization of 22 psi across the vacuum break, additive to the axial (Z) acceleration effects.

The finite element model of the anchor module is shown in Fig. 9. This module sits in the middle of a 70 m long straight section of transfer line. It provides the only support against axial (Z-direction) loadings.

To correctly represent the internal piping loads, as well as the proper constraints offered by the spider pairs to lateral loading, the model was extended axially in both directions to the midpoint between the anchor and the adjacent spider pair. At these ends each pipe was permitted to move axially without resistance, but was constrained against lateral motion and bending rotation.

The mass of the 35 m of pipe on each side was simulated with point mass elements associated with the ends of the internal piping as well as the vacuum jacket. These elements react with the gravitational and seismic accelerations to provide the correct loads to the anchor module.

Constraint was applied on a circumferential surface on the anchor module, with the intent to simulate the actual constraint applied by the anchor module support.

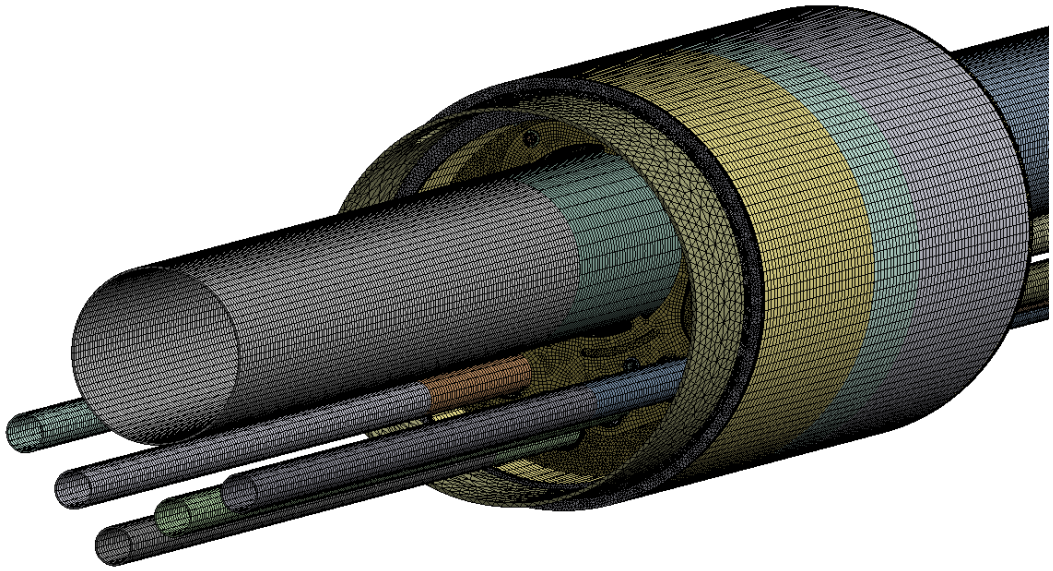

Figure 9. Finite element model of transfer line anchor module

Thermal Results

The total heat load from 300 K is approximately 20 W. This includes approximately 1.5 W of radiation to the 2 K surfaces, and 2.5 W of radiation to the 50 K surfaces.

The heat leak to the various lines is summarized in Table XI.

The temperature profile in the pantleg that runs from the adapter plate to the room temperature vacuum shell is shown in Fig. 10. This is the main conductive path out of the cold region, and the temperature difference between the two ends is 240 K.

Table XI. Calculated heat loads on pipes in anchor module

Line	Radiation - W	Conduction - W	Total - W
A	**-0.19**	**-0.61**	**-0.80**
B	**-0.80**	**-1.89**	**-2.69**
C	**-0.18**	**-0.52**	**-0.70**
D	**-0.19**	**-0.63**	**-0.82**
E	**-0.18**	**-0.41**	**-0.60**
F	**-0.92**	**-13.53**	**-14.45**
Note: Negative sign indicates heat flow into line			

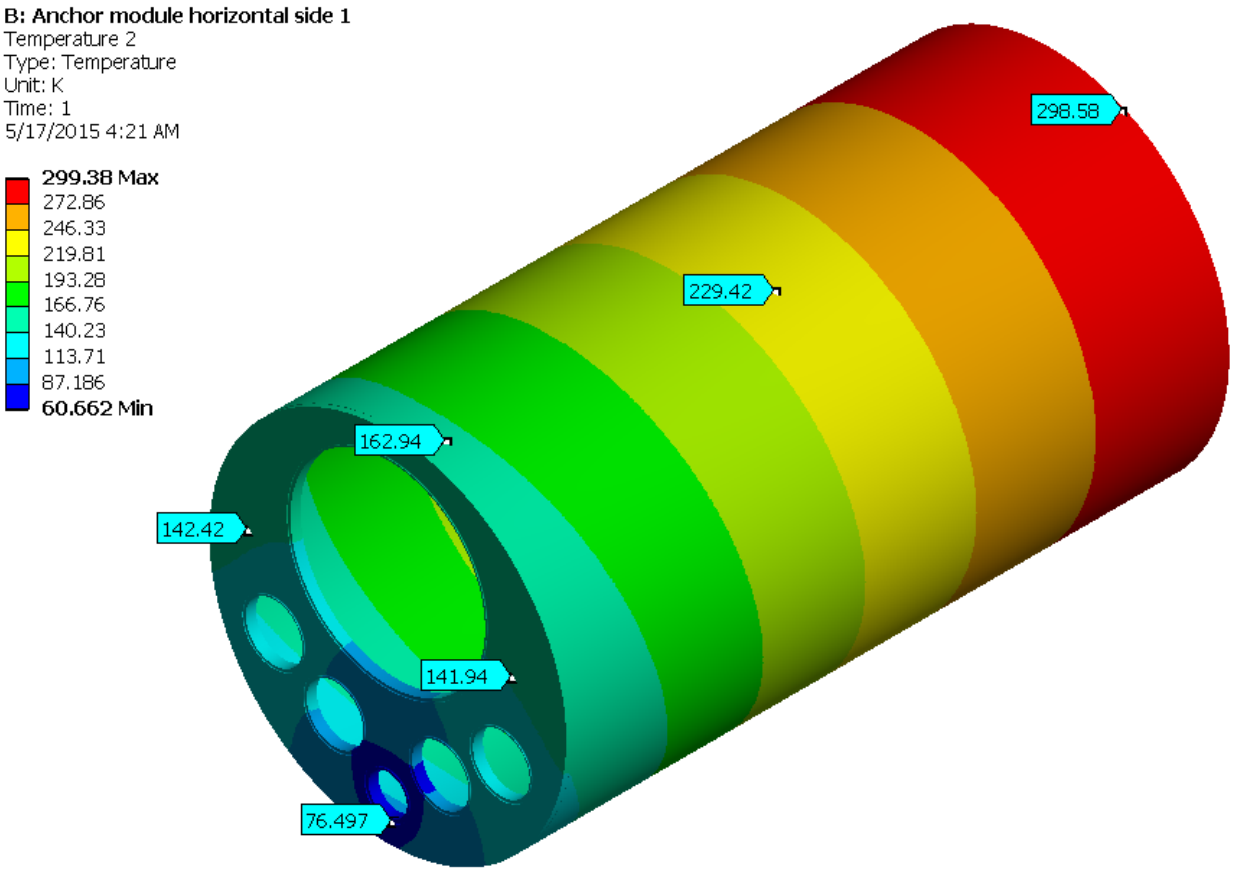

Figure 10. Temperature profile in adapter plate and pantleg of anchor module

Stress Results

As previously stated, the critical load combination corresponds to Combination 5, and consists of cool down plus MAWP plus 1.4 g Y-acceleration plus Z-acceleration plus differential pressurization of 22 psi across the vacuum break, additive to the axial acceleration effects. All following discussion is in the context of this load combination.

Fig. 11 shows the resulting stress in the adapter plate. The maximum stress of 19 ksi is below the allowable for primary membrane of 20 ksi.

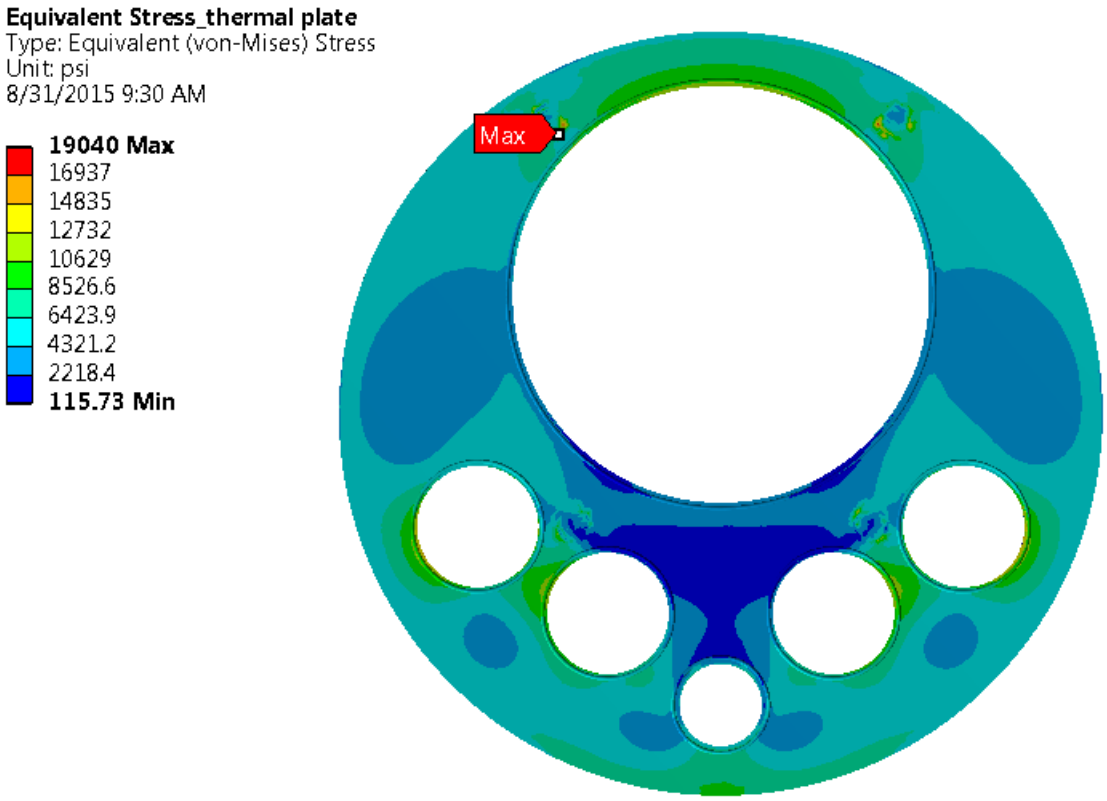

Figure 11. Stresses in adapter plate

The stresses in the piping are shown in Fig. 12. The maximum stress is 10.9 ksi, and occurs where line C contacts the G-10 spider. This is well below the membrane stress allowable of 20 ksi.

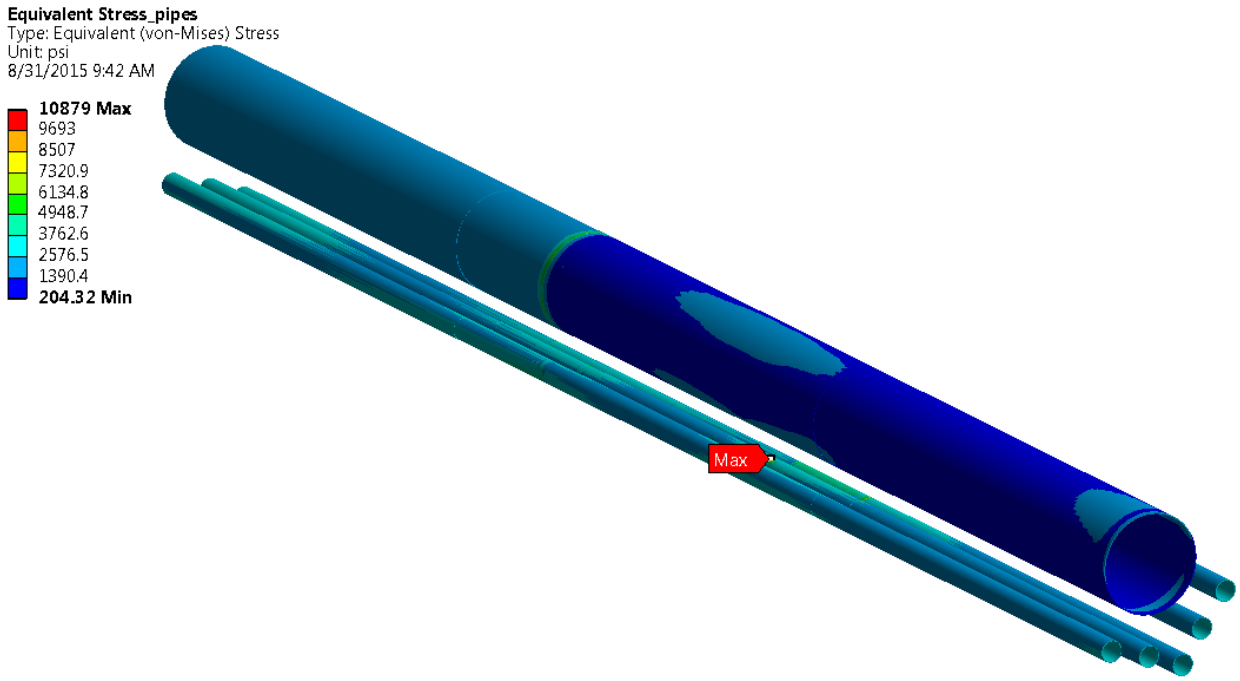

Figure 12. Stresses in piping

The maximum and minimum principal stresses in the spider were examined. The minimum principal stress was closest to its limit. This stress, shown in Fig. 13, is a minimum of -15.4 ksi, and occurs at the location of a sleeve which is part of the attachment of the spider to the large adapter plate. This stress is below the allowable compressive stress for G-10 of -20.5 ksi.

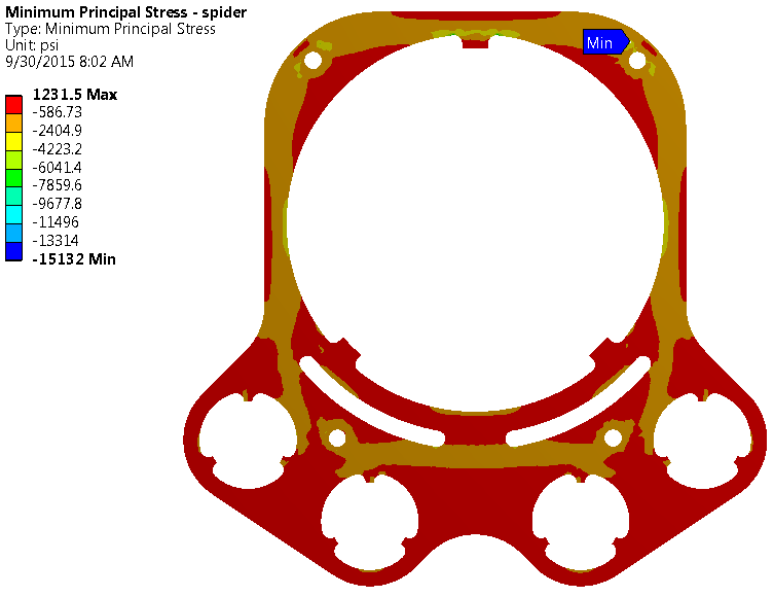

Figure 13. Minimum principal stress in G-10 spider of anchor module

The stresses in the vacuum jacket are shown in Fig. 14. The maximum is 13.1 ksi, occurring at the ends. Though the model terminates as shown, the simulation actually includes the effect of 35 m of vacuum jacket on either side of the model through the use of point mass elements, as explained previously. The stresses shown are due to the interaction of these mass elements with the faces used to define them. The maximum stress of 10.5 ksi is well below the maximum allowable stress of 20 ksi for primary membrane stress.

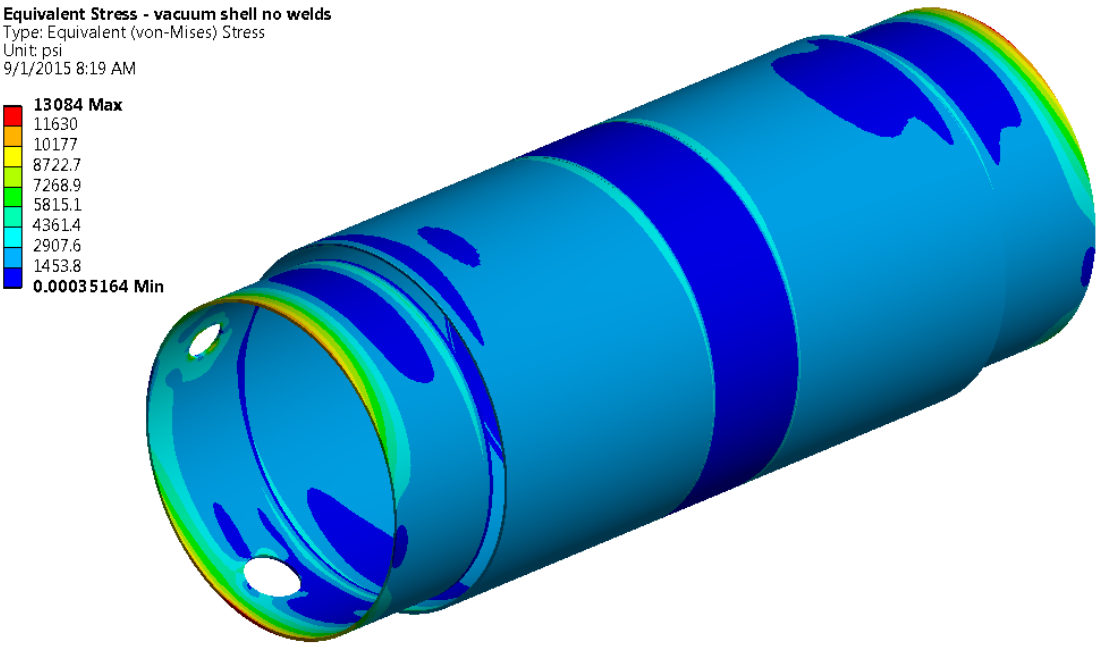

Figure 14. Stresses in vacuum jacket

The stresses in the pantleg that runs from the OD of the adapter plate to the vacuum shell are shown in Fig. 15. The maximum stress is 23.6 ksi. To determine that the stresses through this region are within the stress limits, a stress classification line was passed through the part (Fig. 16). This indicates that the primary membrane stress, Pm, is 4.0 ksi, and primary membrane plus bending stress, Pm + Pb, is 23.5 ksi. These stress are below the limits of 20 ksi, and 30 ksi, respectively.

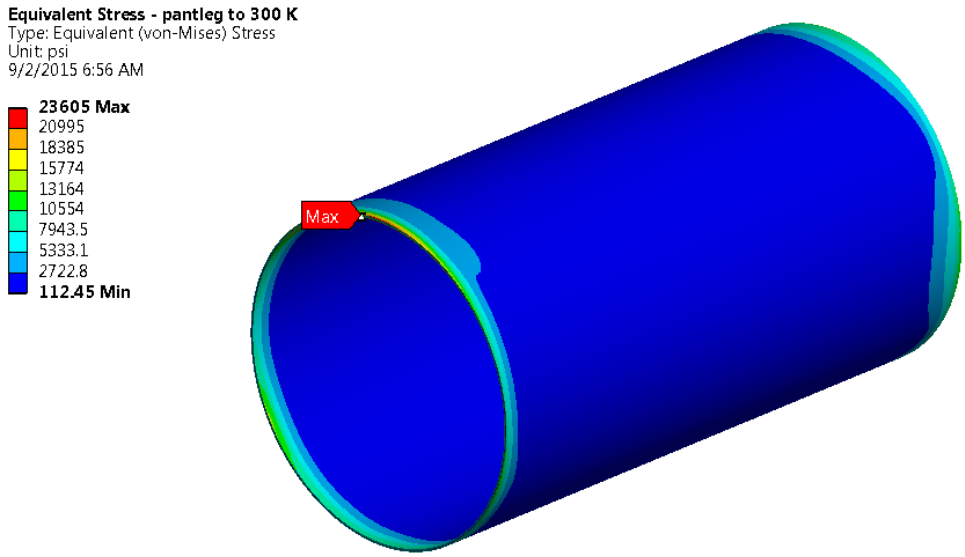

Figure 15. Stresses in adapter plate pantleg

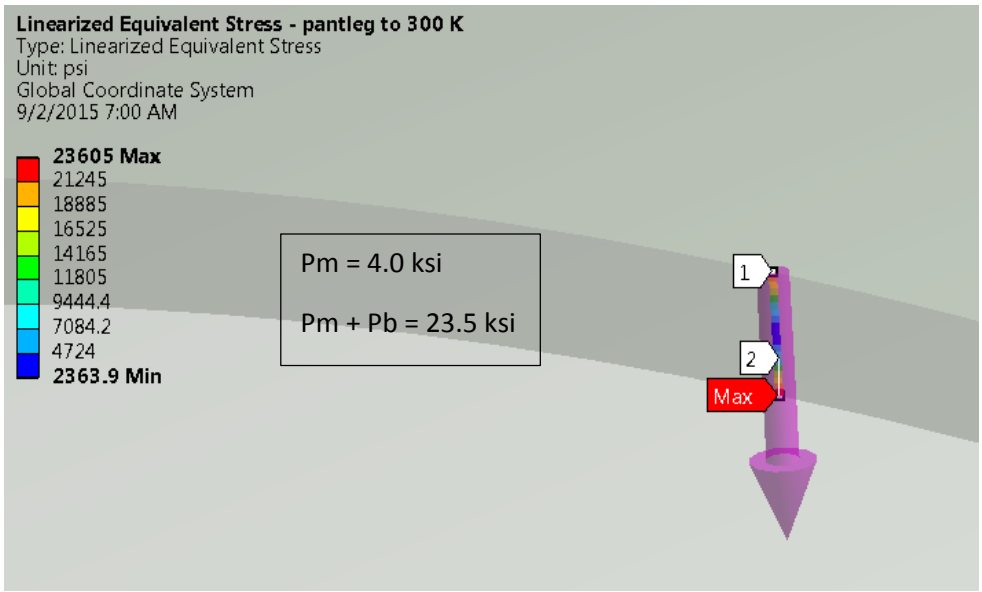

Figure 16. Stress classification line through adapter plate pantleg

The most highly stressed weld is the weld attaching the adapter plate pantleg to the 300 K adapter plate. The stress in this weld is 29.3 ksi, as shown in Fig. 17. To determine that the stresses through this region are within the stress limits, a stress classification line was passed through the part (Fig. 18). This indicates that the primary membrane, Pm, is 20 ksi, and primary membrane plus bending stress, Pm + Pb, is 29 ksi. These stress are below the limits of 20 ksi, and 30 ksi, respectively.

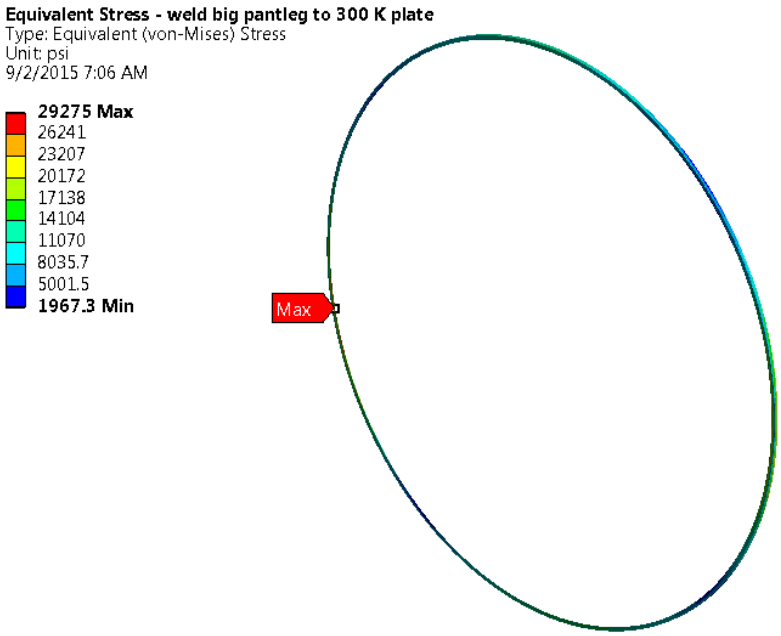

Figure 17. Stresses in weld between adapter plate pantleg and 300 K plate

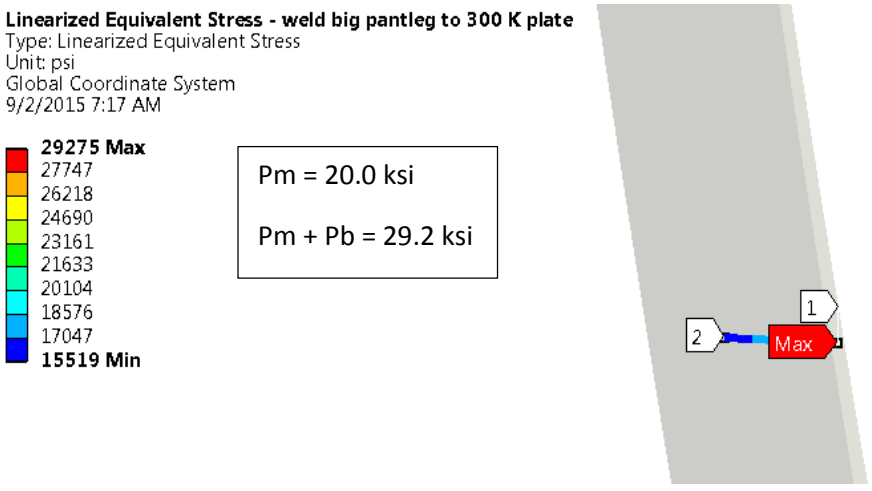

Figure 18. Stress classification line passed through weld between adapter plate pantleg and 300 K plate

The stresses in the pantleg of line B are shown in Fig. 19. The maximum stress is 22.4 ksi. To determine that the stresses through this region are within the stress limits, a stress classification line was passed through the part (Fig. 20). This indicates that the primary membrane, Pm, is 7.6 ksi, and primary membrane plus bending stress, Pm + Pb, is 20.5 ksi. These stress are below the limits of 20 ksi, and 30 ksi, respectively.

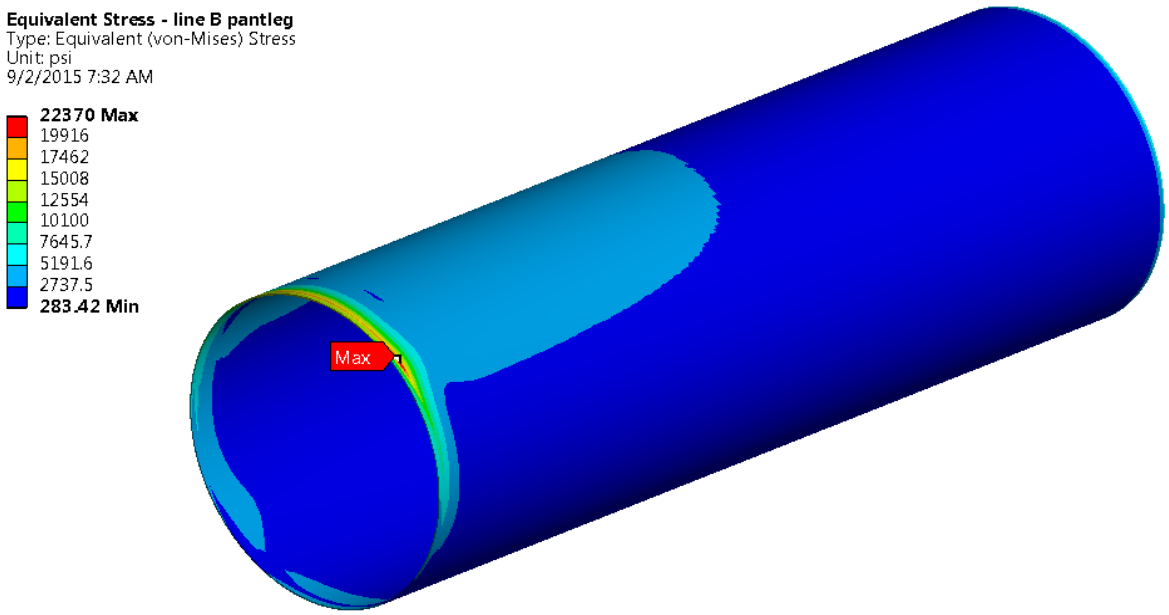

Figure 19. Stresses in line B pantleg

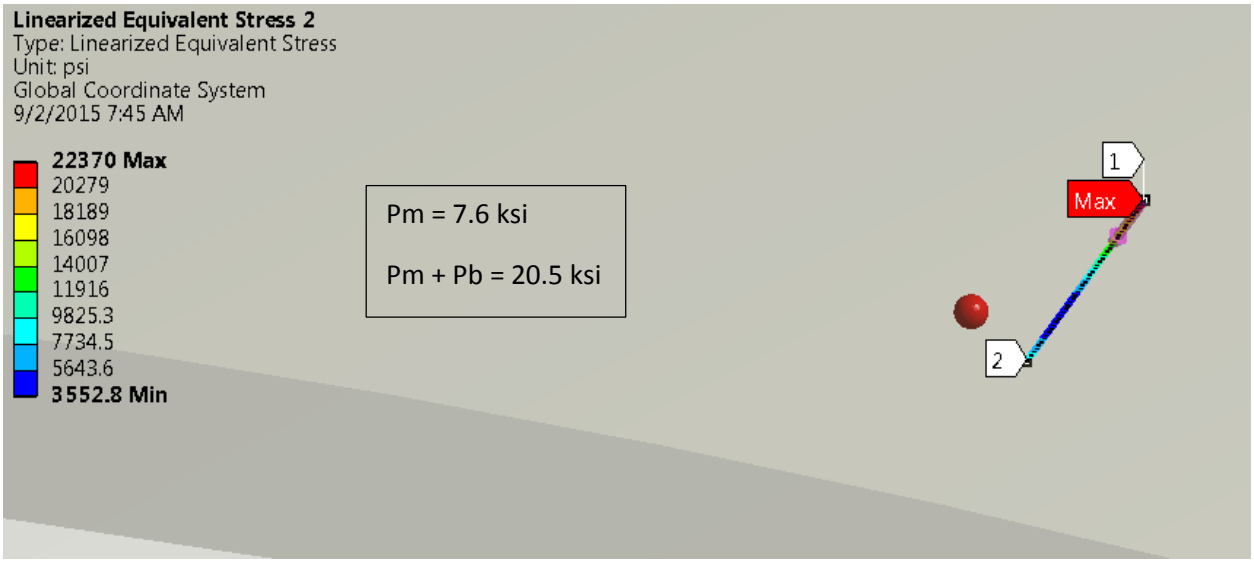

Figure 20. Stress classification line passed through line B pantleg

The stresses in the weld between the line B pantleg and the adapter plate are shown in Fig. 21. To determine that the stresses through this region are within the stress limits, a stress classification line was passed through the part (Fig. 22). This indicates that the primary membrane, Pm, is 12.2 ksi, and primary membrane plus bending stress, Pm + Pb, is 21.6 ksi. These stress are below the limits of 20 ksi, and 30 ksi, respectively.

All other welds in the anchor module show calculated stresses substantially below the allowable membrane stress of 20 ksi.

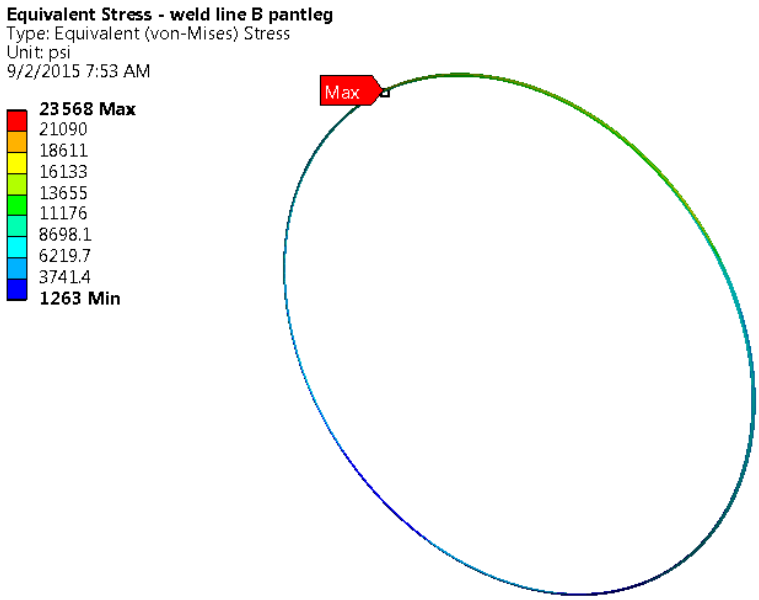

Figure 21. Stress in weld between line B pantleg and adapter plate

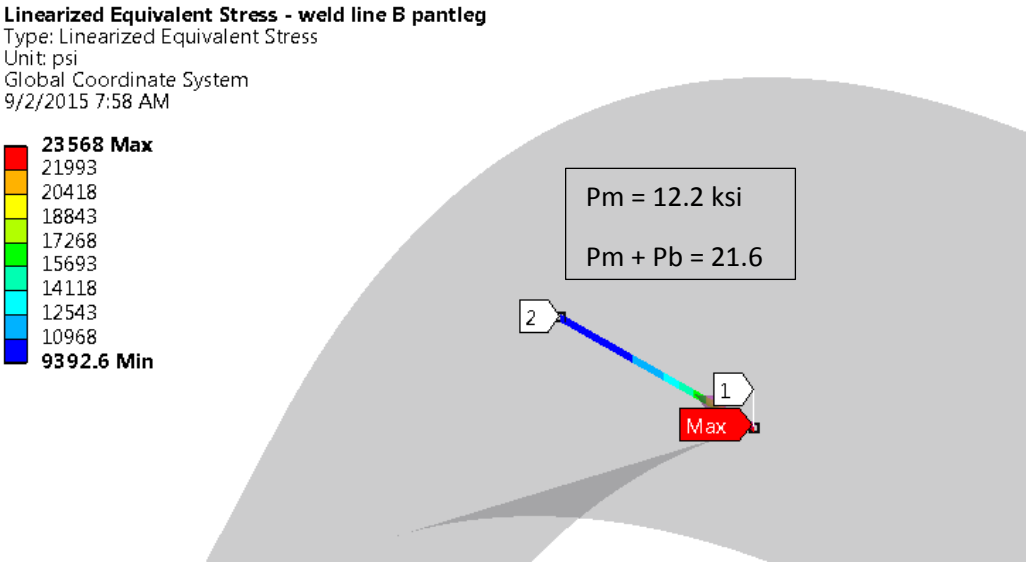

Figure 22. Stress classification line passed through weld between line B pantleg and adapter plate

The stresses in the small pantlegs are shown in Fig. 23.The maximum is 24.4 ksi. To determine that the stresses in this region are within the stress limits, a stress classification line was passed through the part. The results are shown in Fig. 24. The primary membrane stress, Pm, is 17.7 ksi. The primary membrane plus bending stress, Pm+Pb, is 22.7 ksi. Both stresses are less than the allowables of 20 ksi and 30 ksi, respectively.

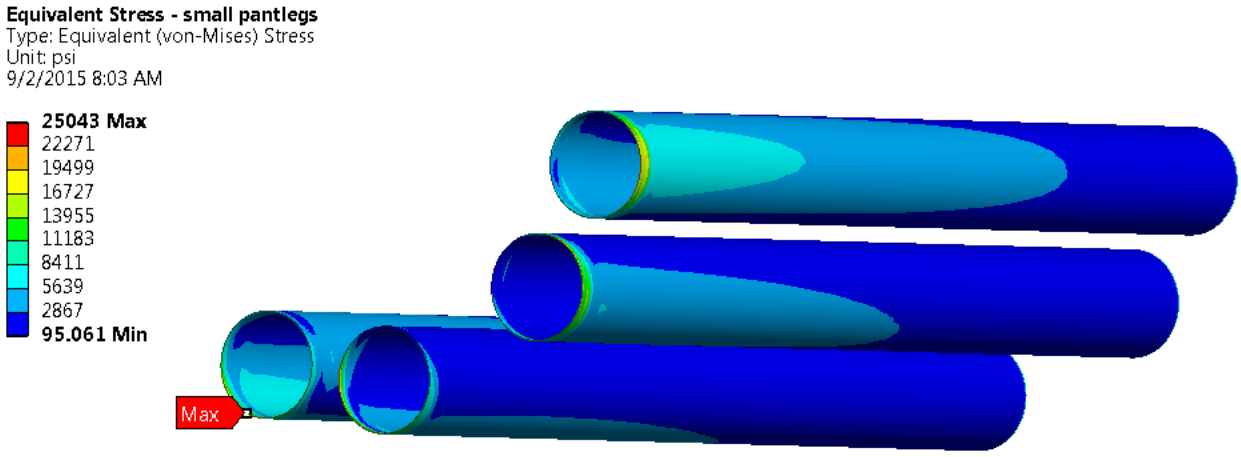

Figure 23. Stresses in pantlegs – maximum is in pantleg for line A

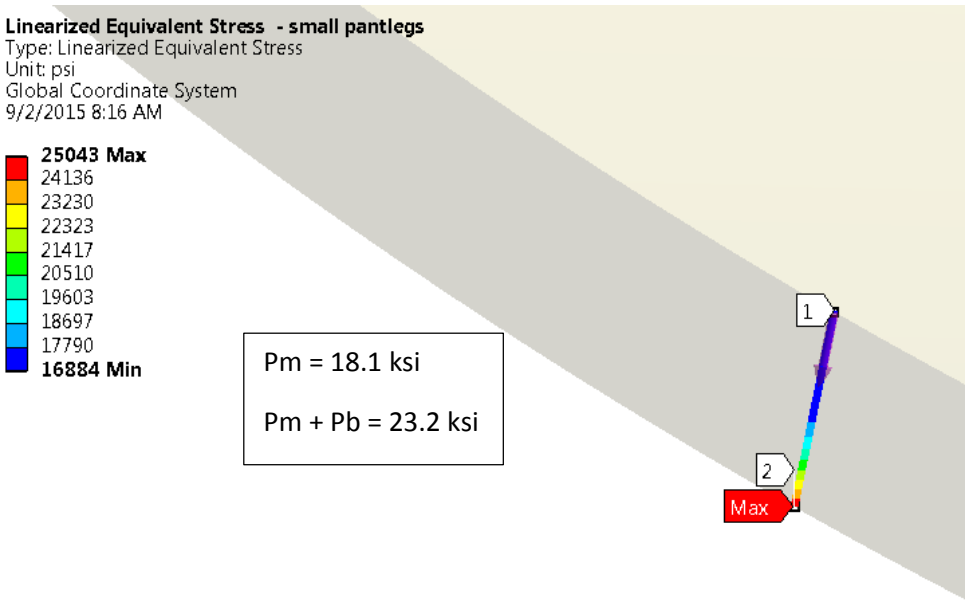

Figure 24. Stress classification line passed through line D small pantleg

Vertical Anchor Module

The vertical anchor module provides vertical anchoring for the relatively short vertical run of the transfer line, in a manner analogous to that of the horizontal anchor. The design of the vertical module is identical in all respects – only the details of the supported piping different.

The following loads were considered in the combinations given on Page 5:

1. Cool down
2. All pipes pressurized to their MAWP
3. 0.89 g acceleration in X (seismic)
4. 1.4 g acceleration in Y (deadweight + seismic)
5. 0.2 g acceleration in Y (deadweight – seismic)
6. 0.89 g acceleration in Z (seismic)
7. 22 psia overpressure of the vacuum space on the top side of the vacuum break
8. 22 psia overpressure of the vacuum space on the bottom side of the vacuum break

The critical load combination correspond to Combination 5, and consists of cool down plus MAWP plus 1.4 g Y-acceleration plus Z-acceleration plus differential pressurization of 22 psi across the vacuum break, additive to the Y-acceleration effects.

The solid model of the vertical anchor module is shown in Fig. 25(a). The finite element model of the anchor module is shown in Fig. 25(b). The finite element model does not include the horizontal portion of the anchor module assembly. The masses of the horizontal components are included in the finite element model through the use of lumped mass elements. This results in the anchor module having to react the entire mass of the horizontal section, although that section itself will have some resistance to motion coming from its interconnect to other structure.

The dead weight of the anchor is reacted by the lower support. The upper support is designed to provide lateral constraint, but does not share the vertical load. For this analysis, the upper support was reduced to its fundamental parts, which were then appropriately constrained.

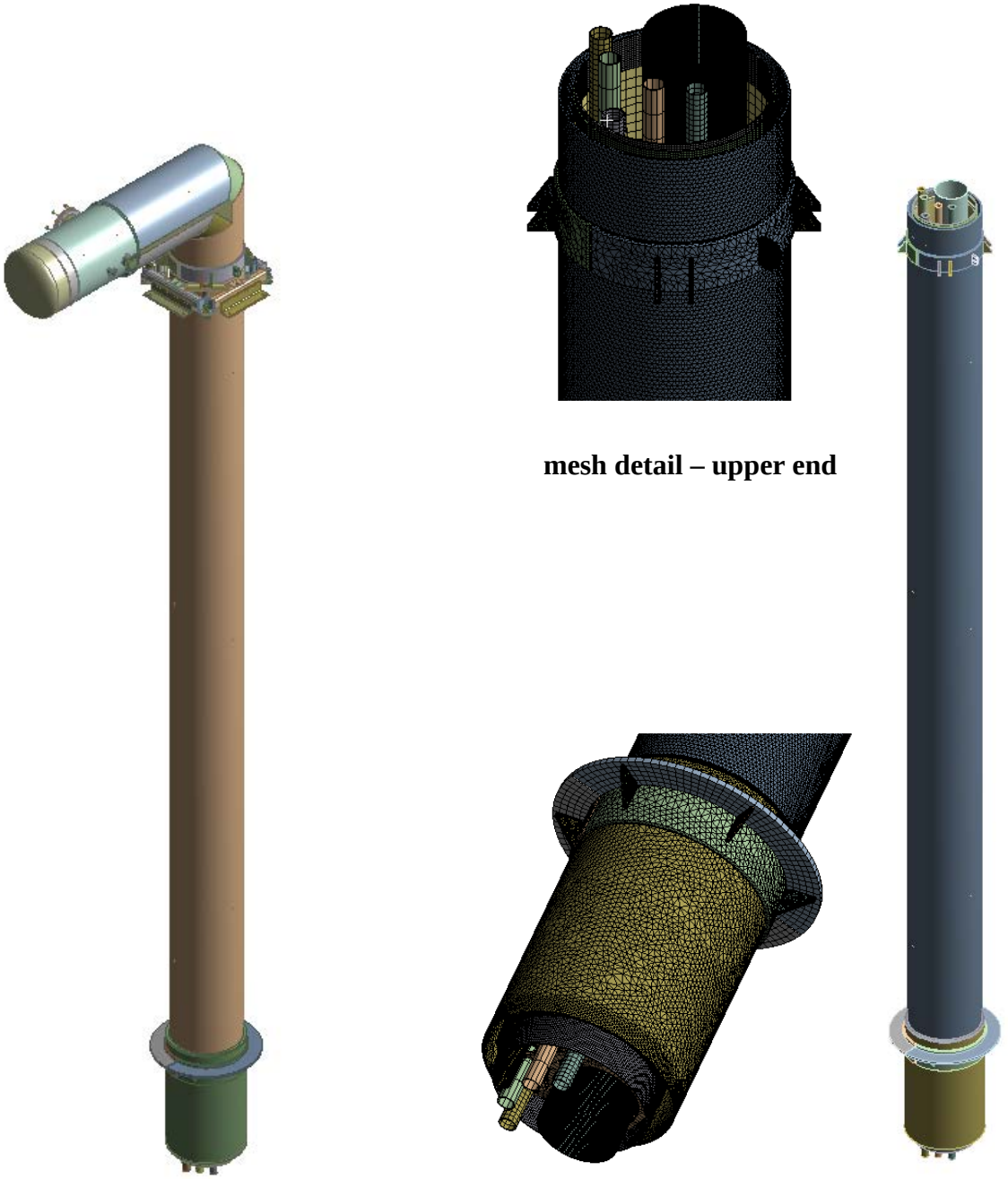

Figure 25. Finite element model of vertical anchor module

Thermal Results

The vertical anchor module is identical to the horizontal anchor module in the vacuum break region. All heat leaks and temperature profiles are therefore the same as those presented for the horizontal orientation. This simulation also includes spiders in the vertical section, and the heat leak and temperature profiles for these and related components are covered in the section of this report dealing with the horizontal straight section.

Stress Results

The critical load combination corresponds to a variation of Combination 5, and consists of cool down plus MAWP plus 1.4 g Y-acceleration plus Z-acceleration plus differential pressurization of 22 psi across the vacuum break, additive to the Y- acceleration effects. All following discussion is in the context of this load combination.

The stresses in the adapter plate are shown in Fig. 26. The maximum stress is 15.6 ksi, which is less than the membrane stress allowable of 20 ksi.

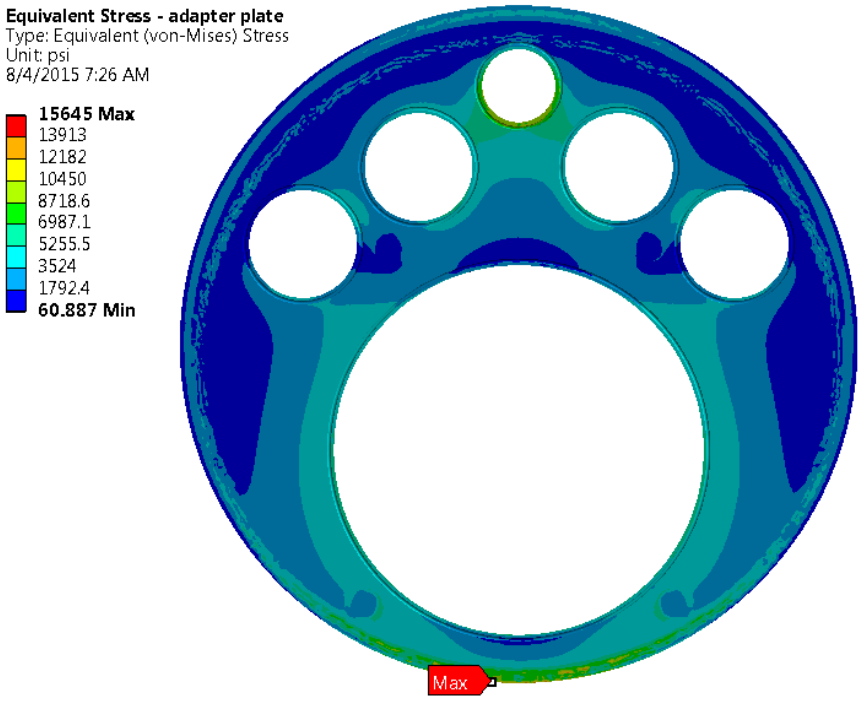

Figure 26. Stresses in adapter plate

The stresses in the piping are shown in Fig. 27. The maximum stresses occur in the upper portion of the model where line B contacts the fiberglass spiders, and are likely due primarily to the lateral accelerations, and the conservative assumption that the mass of the upper horizontal section (not explicitly included in the model) will be reacted by the spiders. This stress, 20.5 ksi, is slightly above the membrane stress allowable. However, as shown by the inset, this stress has the characteristics of a stress concentration (as opposed to a primary stress), attenuating rapidly as distance from the maximum stress increases. Therefore, the piping stresses are within the allowable stress limits.

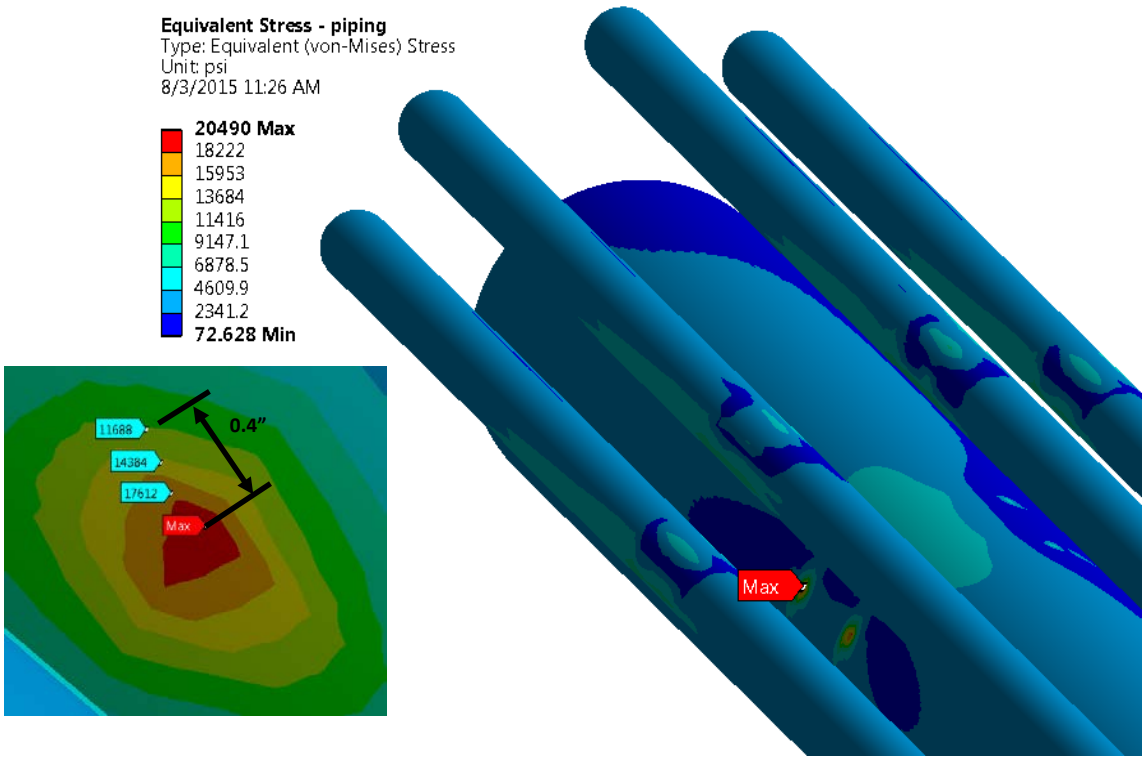

Figure 27. Stresses in piping

The maximum and minimum principal stresses in the spiders were examined. The maximum principal stress was closest to its limit. This stress, shown in Fig. 28, is a maximum of 12.1 ksi, and occurs at the location the pin connecting one of the small rollers to the spider. This stress is below the allowable tensile stress for G-10 of 18.5 ksi.

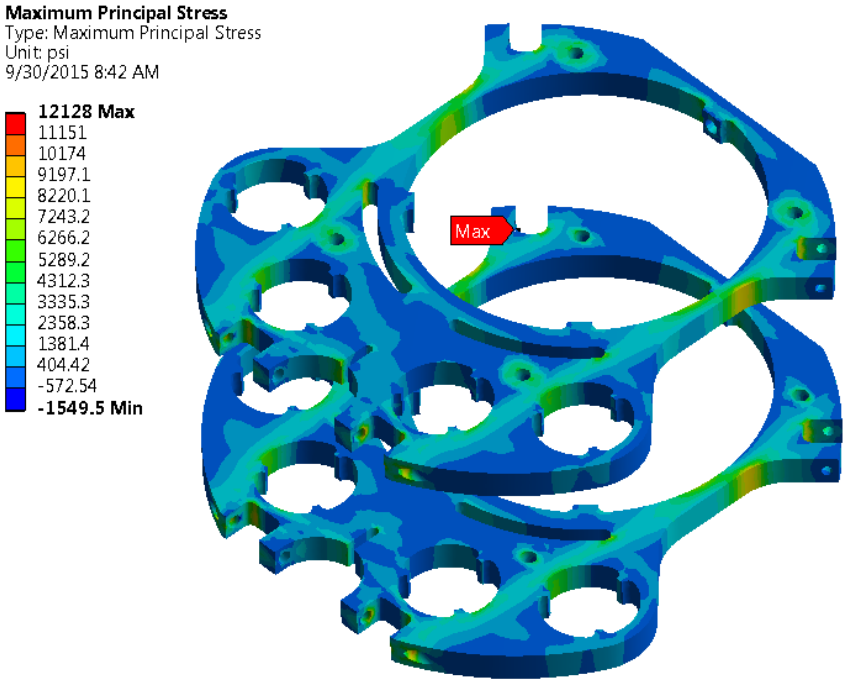

Figure 28. Stresses in G-10 spider of vertical anchor module

The most highly stressed region of the vacuum shell is the thin adapter plate that accommodates the change in vacuum shell diameter at the anchor. The stresses in this plate are shown in Fig. 29. The maximum stress is 20.2 ksi. To determine that the stresses through this region are within the stress limits, a stress classification line was passed through the part (Fig. 28). This indicates that the primary membrane, Pm, is 9.2 ksi, and primary membrane plus bending stress, Pm + Pb, is 18.2 ksi. These stress are below the limits of 20 ksi, and 30 ksi, respectively.

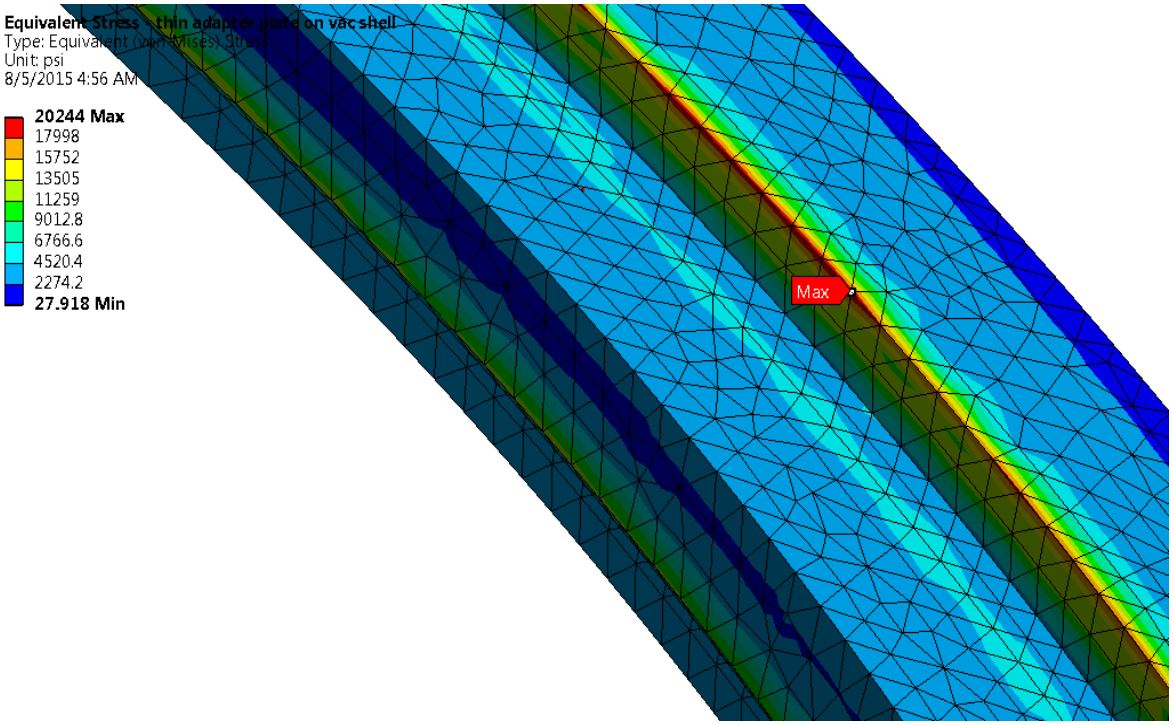

Figure 29. Stresses in thin adapter plate of vacuum shell

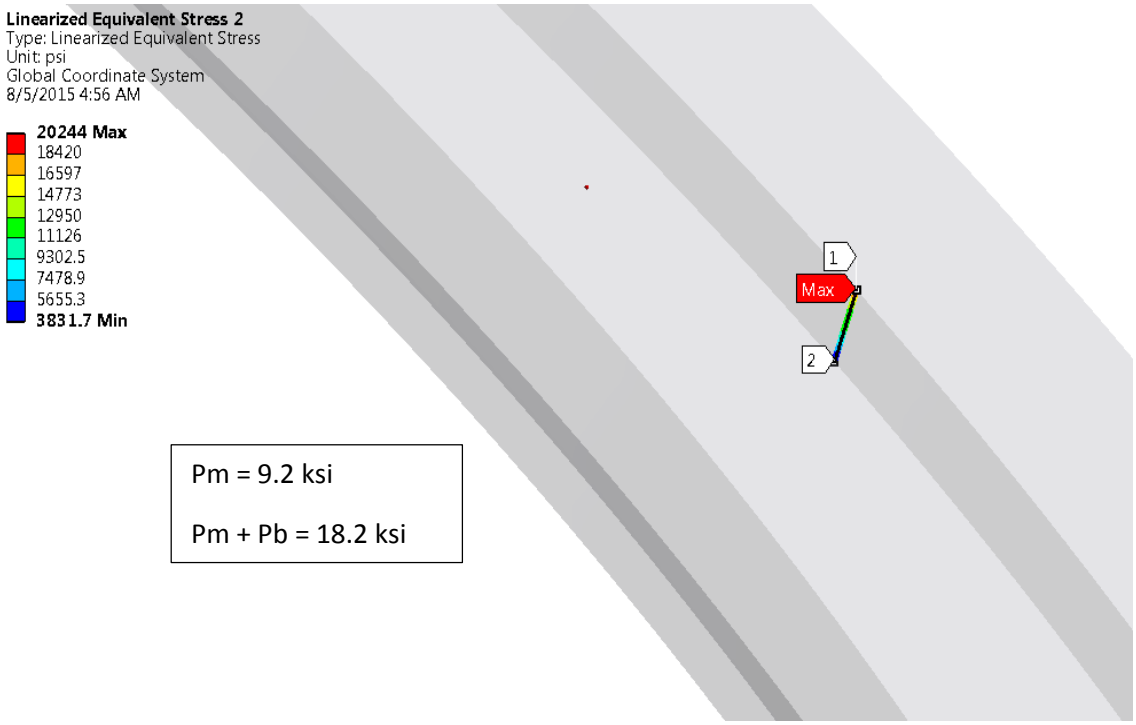

Figure 30. Stress classification line through thin adapter plate of vacuum shell

The stresses in the large pantleg that runs from the adapter plate to the 300 K plate are shown in Fig. 31. Stresses are a maximum 18 ksi at the weld at the adapter plate. This is below membrane stress allowable of 20 ksi.

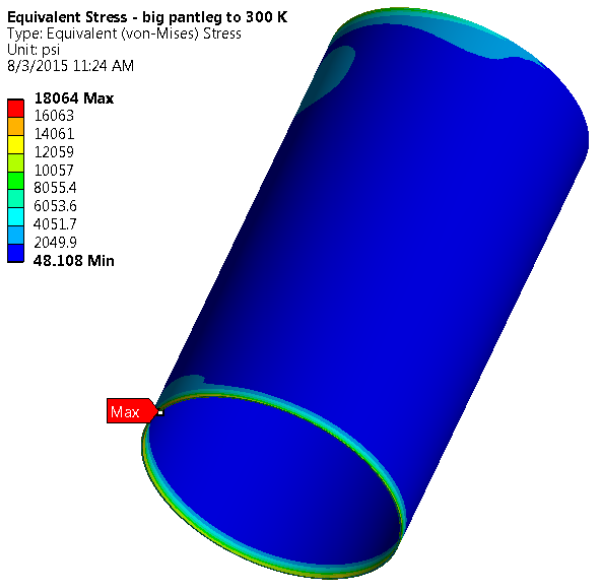

Figure 31. Stresses in large pantleg

Fig. 32 shows the stresses in the small pantlegs. The highest stress, in the pantleg for line E, is 9.5 ksi, which is well below the membrane stress allowable of 20 ksi.

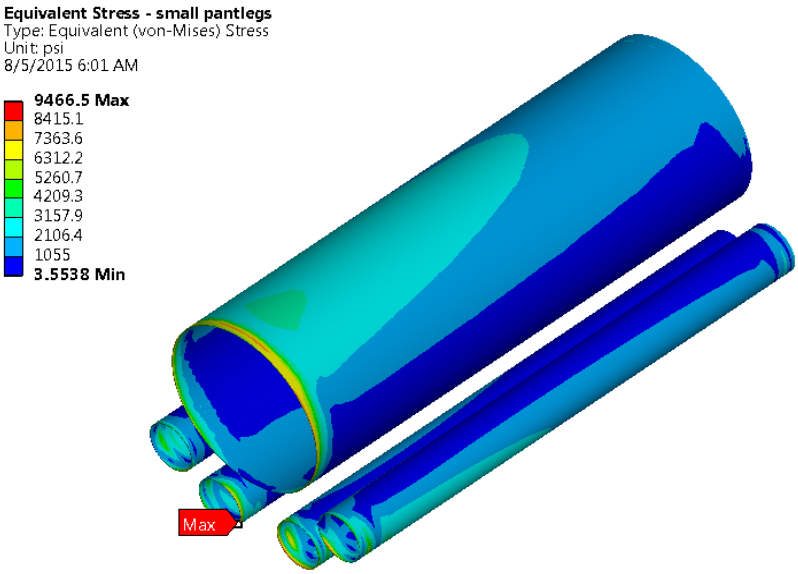

Figure 32. Stresses in small pantlegs

The stresses in all welds are shown in Fig. 33. For all but one weld, the stresses are less than the membrane stress allowable of 20 ksi. For the weld between the big pantleg and the 300 K plate, the maximum stress is 33.6 ksi. To determine that the stresses through this region are within the stress limits, a stress classification line was passed through the part (Fig. 34). This indicates that the primary membrane, Pm, is 7.4 ksi, and primary membrane plus bending stress, Pm + Pb, is 28 ksi. These stress are below the limits of 20 ksi, and 30 ksi, respectively.

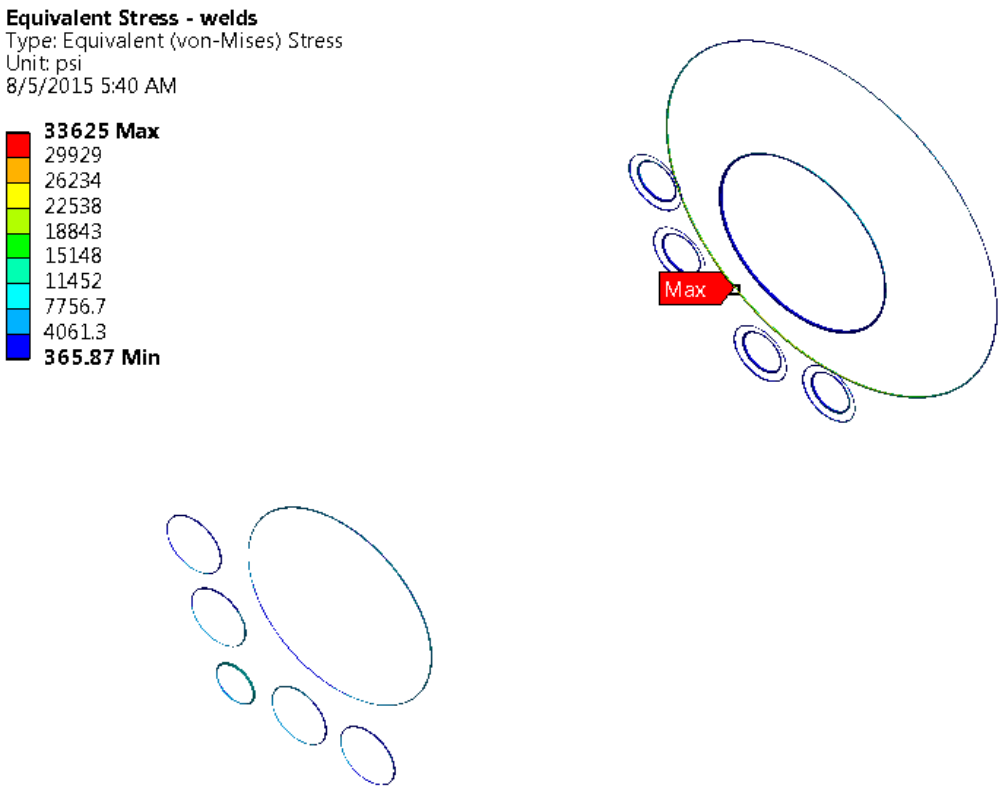

Figure 33. Weld stresses

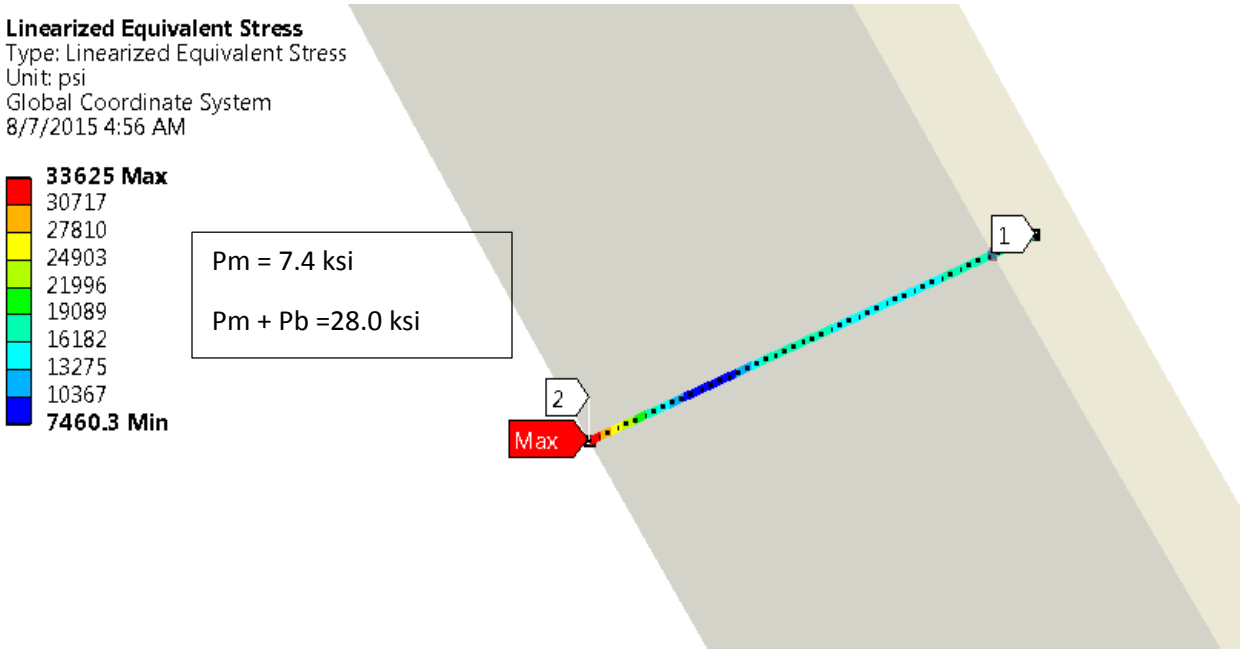

Figure 34. Stress classification line passed through weld between large pantleg and 300 K plate

Fig. 35 shows the stresses in the most highly-stressed region of the aluminum extrusion. The maximum stress, 4.4 ksi, occurs at the location of roller contact on the uppermost spider. This stress is well below the membrane stress allowable of 14 ksi for unwelded 6061-T6 aluminum.

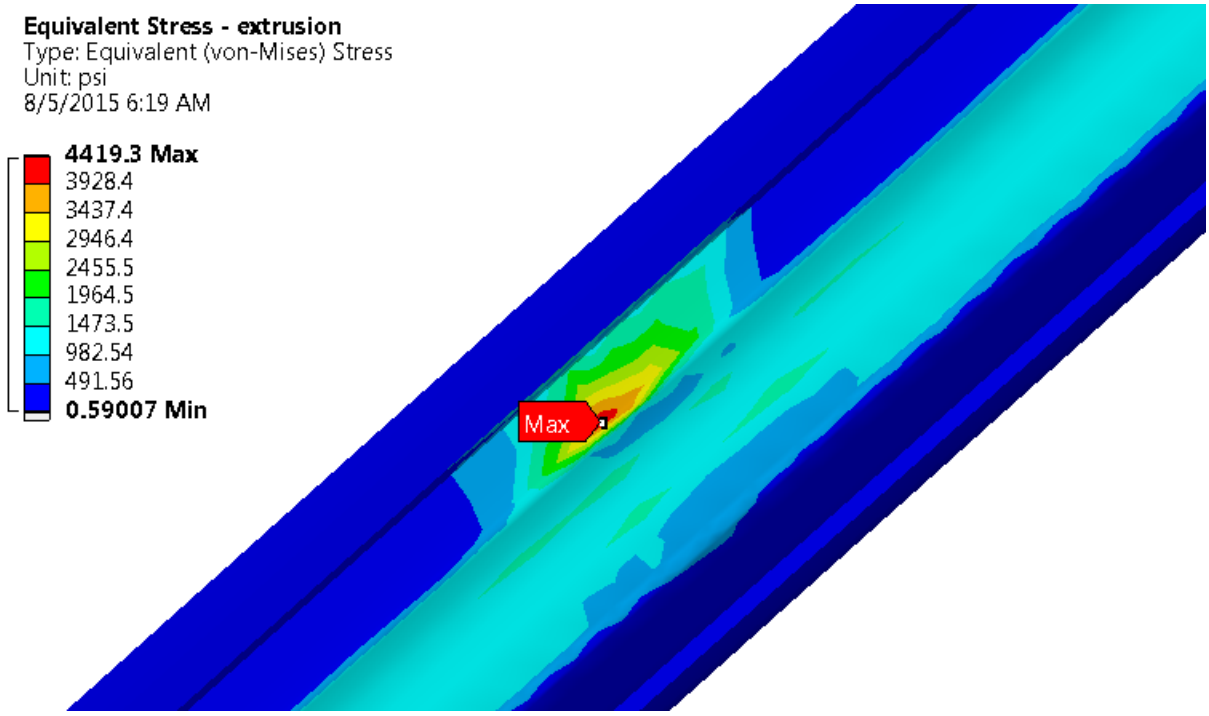

Figure 35. Stresses in aluminum extrusion

Vertical Expansion Joint - overview

The vertical expansion joint (Fig. 36) is designed to allow horizontal motion of the horizontal run of the transfer line during cool down. It consists of an elbow at the top, a vertical length containing flex hoses on each line, and an elbow at the bottom, which also contains the vacuum break between the transfer line and the cryomodule.

This line was analyzed with two separate models. One was of the top elbow, the other was of the bottom elbow. The vertical length was split between the two elbows. This is the same as assuming that any loads developed by the vertical length are shared equally between the top and bottom elbows. No significant lateral restraint is available in the vertical portion itself (i.e., the flex hoses are unconstrained between their ends) so all of the loads on each line will be delivered to the constraints available in the elbows.

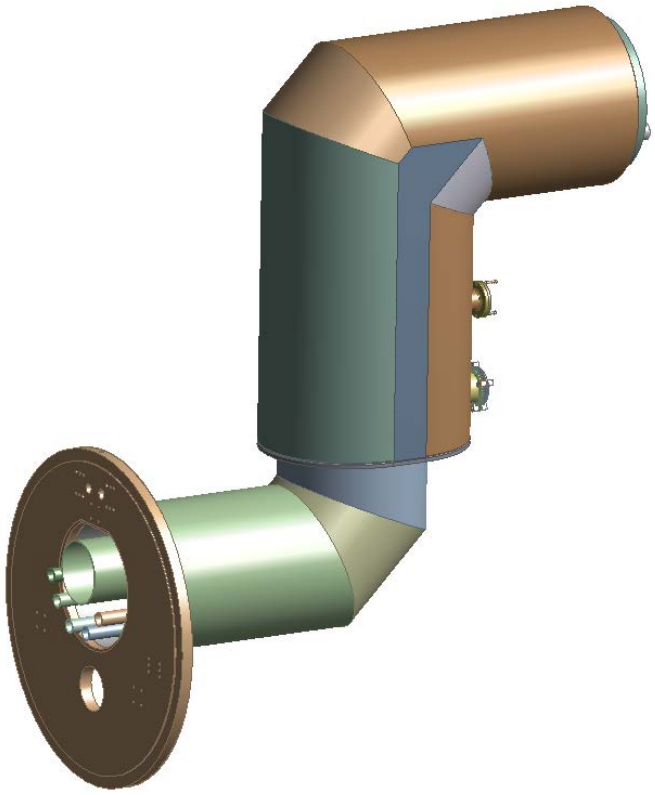

Figure 36. Solid model of vertical expansion joint

Top Elbow of the Vertical Expansion Joint

The following loads were considered in the combinations given on Page 5:

1. Cool down
2. All pipes pressurized to their MAWP
3. 0.89 g acceleration in X (seismic)
4. 1.4 g acceleration in Y (deadweight + seismic)
5. 0.2 g acceleration in Y (deadweight – seismic)
6. 0.89 g acceleration in Z (seismic)
7. 15 psi external pressure on all lines (leak-checking scenario)

The critical load combination corresponds to Combination 5, and consists of cool down plus MAWP plus X-acceleration plus 1.4 g Y-acceleration.

The top elbow FE model is shown in Fig. 37.

For the purposes of the stress analysis, the shield design is assumed to have the clearances and other provisions necessary to cool down stress-free. Therefore, the shield stresses are assessed for only the mechanical loads.

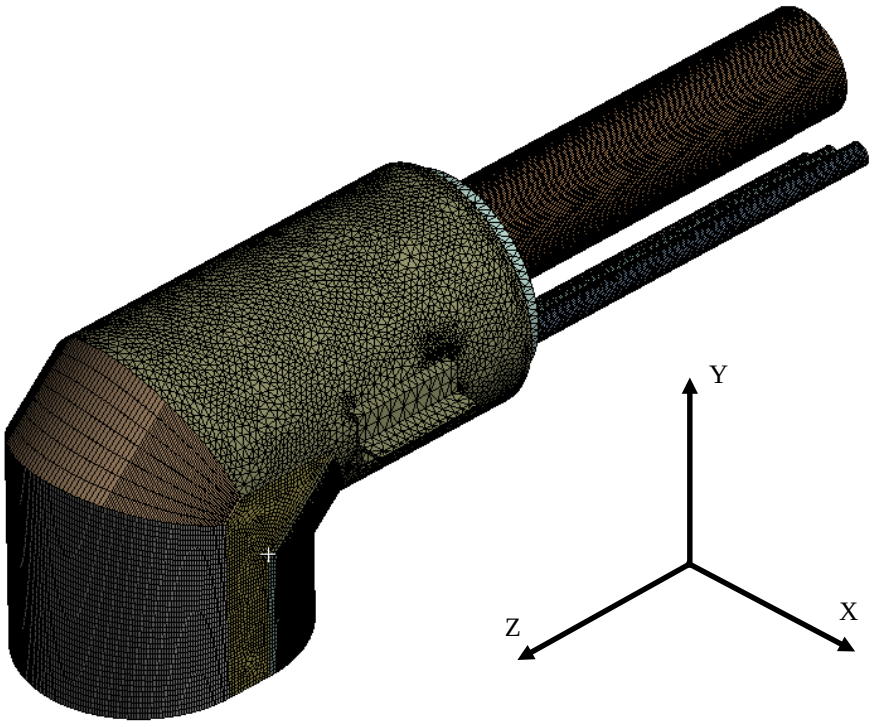

Figure 37. FE model of top elbow of vertical expansion joint

Thermal Results

The heat leaks calculated for each pipe are summarized in Table XII. The total heat leak to 300 K is 9 W. This includes approximately 0.6 W in radiation to the 2 K surfaces, and 3.8 W in radiation to the 50 K surfaces. Note: For this thermal simulation, it was assumed that the top two rollers on the spider do not make contact with the shield.

The temperature profile of a spider is shown in Fig. 38. Temperatures range from 2.5 K to 70 K.

Table XII. Heat load on pipes in top elbow of vertical expansion joint

Line	Radiation - W	Conduction - W	Total - W
A	**-0.20**	**-0.30**	**-0.49**
B	**-0.36**	**-0.10**	**-0.46**
C	**-0.23**	**-0.39**	**-0.62**
D	**-0.20**	**-0.36**	**-0.56**
E	**-0.23**	**-0.12**	**-0.35**
F	**-2.85**	**-3.19**	**-6.04**
Note: Negative sign indicates heat flow into line			

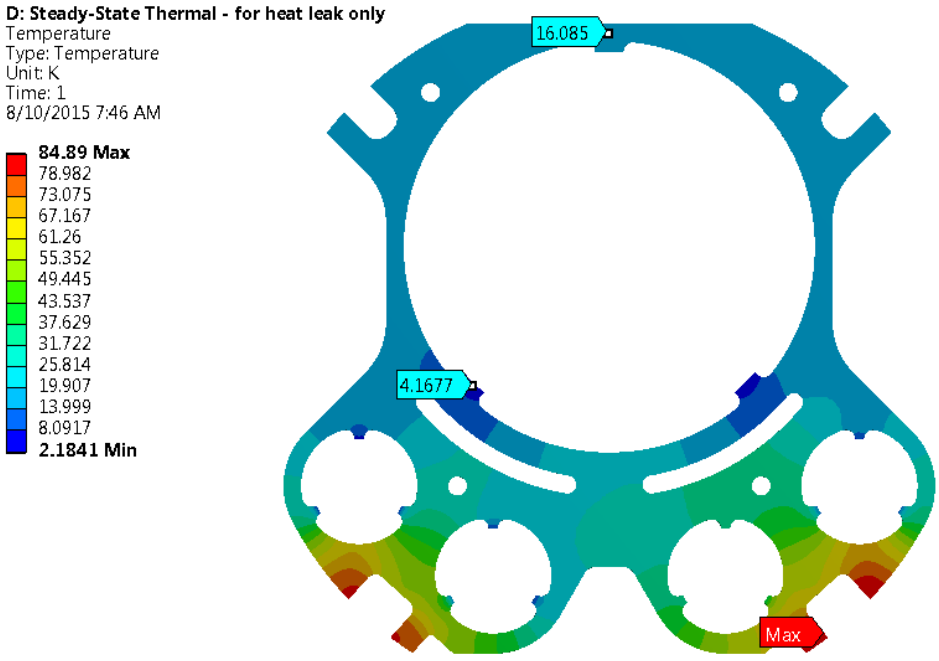

Figure 38. Temperature profile in spider in top elbow of vertical expansion joint

Stress Results

As previously stated, the critical load combination corresponds to Combination 5, and consists of cool down plus MAWP plus X-acceleration plus Y-acceleration. All further discussion is in regard to this loading condition.

The maximum and minimum principal stresses in the spiders were examined. The maximum principal stress was closest to its limit. This stress, shown in Fig. 39, occurs at one of the protrusions that support line B, and is a maximum of 14.9 ksi. This stress is highly concentrated, but still below the allowable tensile stress for G-10 of 18.5 ksi.

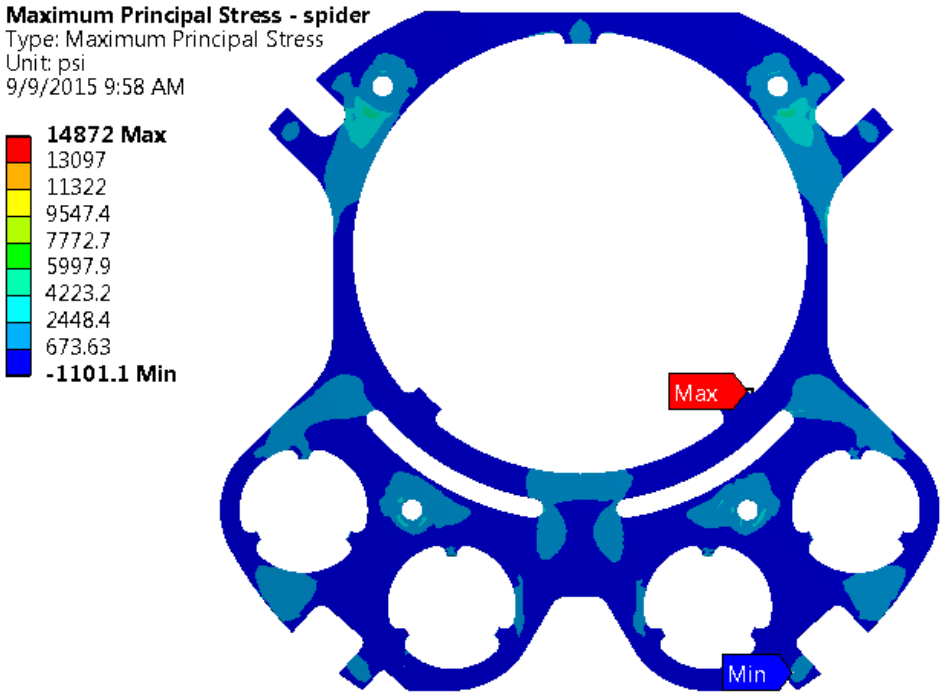

Figure 39. Maximum principal stresses in spider for top elbow of vertical expansion

The stresses in the piping are shown in Fig. 40. The maximum stress is at the contact region between line B and the G-10 spider. Fig. 41 shows a close-up, and illustrates the rapid attenuation of the stress as the distance from the maximum increases. The bulk of the stresses in all piping are well below the allowable membrane stress of 20 ksi.

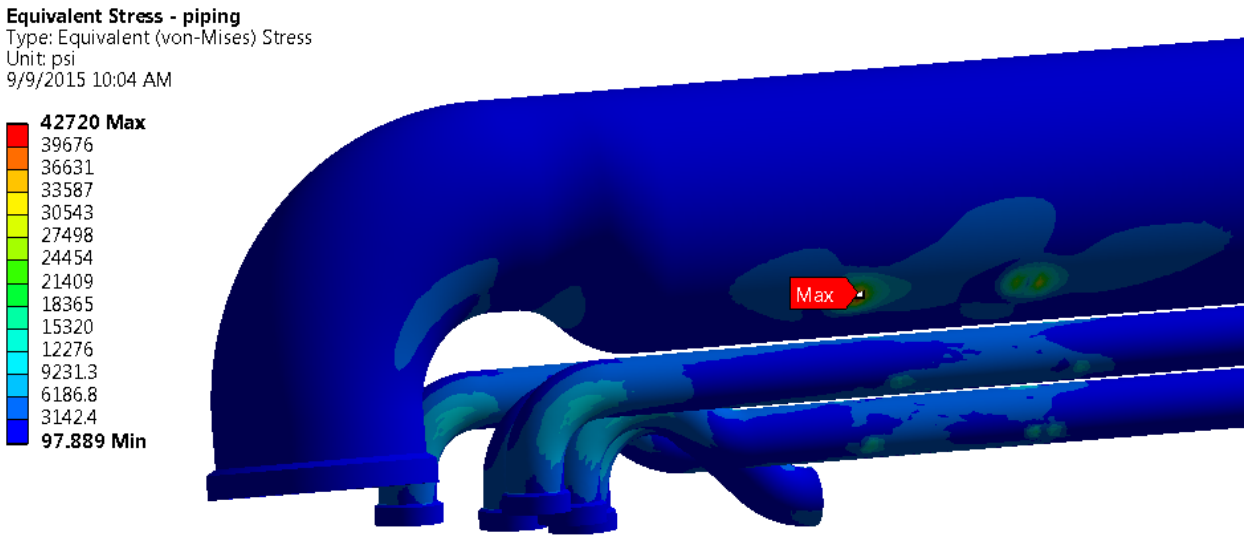

Figure 40. Stress in piping for top elbow of vertical expansion joint

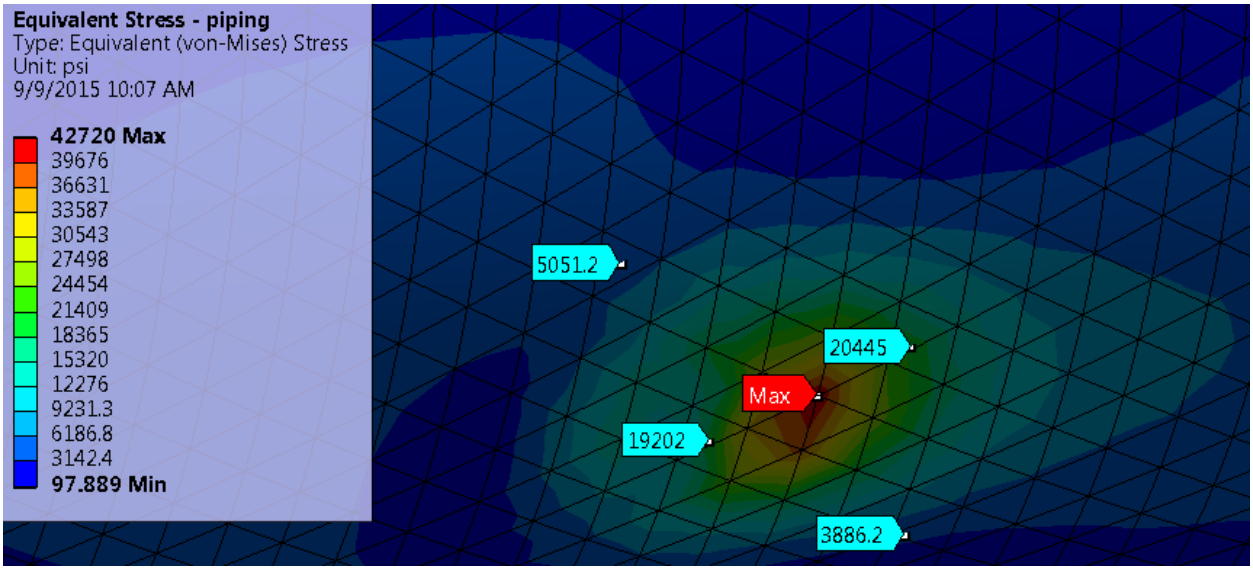

Figure 41. Close-up of stress concentration at contact of line B with G-10 spider

Two G-10 arcs provide the load path from the shield to the vacuum vessel. The maximum and minimum principal stresses in the spiders were examined. The maximum principal stress was closest to its limit. This stress, shown in Fig. 42, is a maximum of 2.4 ksi, well below the maximum allowable tensile stress of 18.5 ksi.

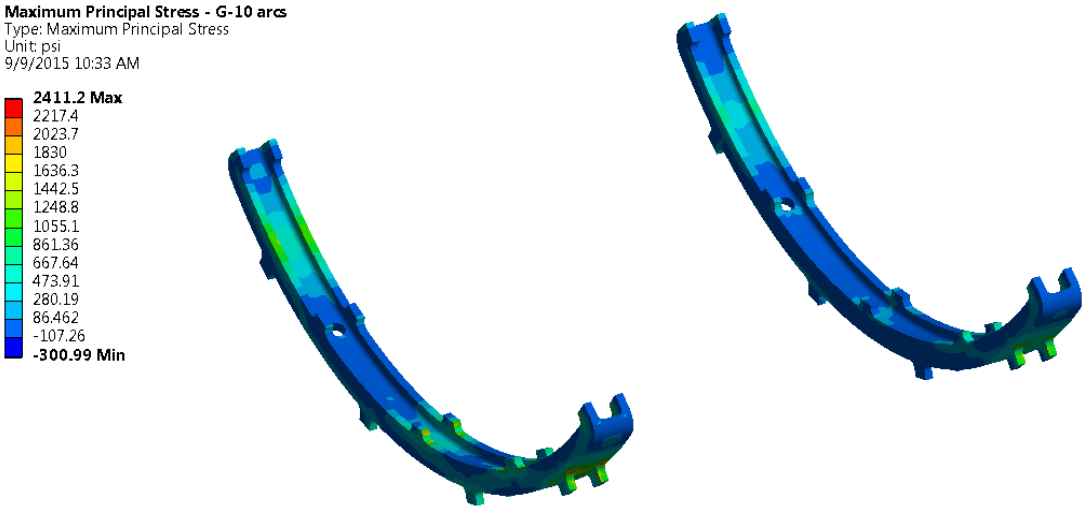

Figure 42. Maximum principal stress in G-10 arcs under

Fig. 43 shows the stresses in the shield. The stresses are well below the allowable membrane stress of 8 ksi for welded 6061-T6.

The bottom wheels of the spider are not considered in this analysis, but will be addressed in the next model.

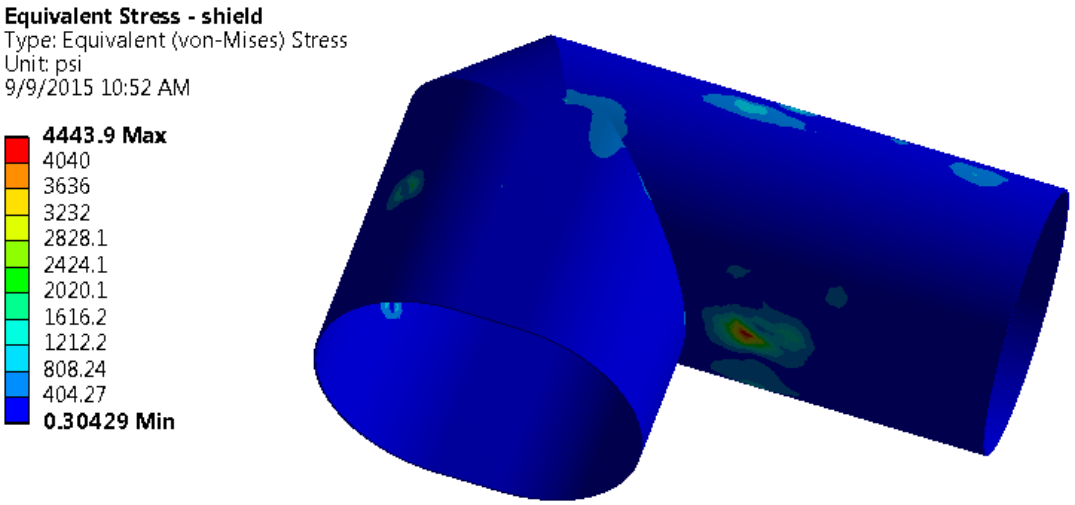

Figure 43. Stresses in shield under mechanical loads

Model of Vertical Expansion Joint Top Elbow for Roller Loads

The four G-10 rollers on the two spiders in the upper elbow of the vertical expansion joint must take the reaction produced by the lines A through E when they are pumped down for leak checking. This is because the flex hoses in the vertical run do not allow the development of the compressive stresses necessary for equilibrium without external support. (Note: Line F is not supported by the spider pair, and therefore does not contribute to the roller loads).

To estimate the roller loads, a half-model was created of only the spiders, lines A through C (lines A and C are identical to lines D and E in size), the shield, and the two fiberglass semi-circular pieces that support the shield on the vacuum vessel. This model is shown in Fig. 44. A vertically downward force of 832 lbs was applied to line B. A vertically downward force of 55 lbs was applied to each of lines A and C.

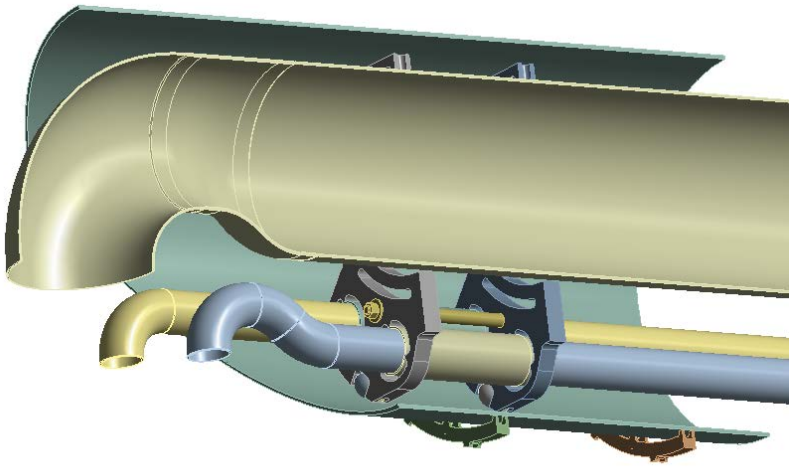

Figure 44. FE model for determination of roller loads during vacuum leak check

The results show that the maximum load occurs on the roller furthest away from the elbows, and is 500 lbs.

This roller is supported on a ½ in diameter stainless steel pin 2.9 inches long. The length of the roller is 1.5 inches. The length of bearing contact of the pin with the hole in the spider is 1.4 inches. The total projected bearing area with the spider is 1.4(0.5) = 0.7 inches, for a resulting bearing stress of 500/0.6 = 833 psi. The bearing stress of the pin in the roller hole is slightly less given its slightly greater length of engagement. These stresses present no issues for either the G-10 or stainless material.

Contact stresses between the curved roller surface and the shield surface are difficult to assess analytically in the context of a composite material, so an accurate mockup of the geometry was built, and subjected to a load of 1500 lbs. When the load was removed, no flat spot was noted on the roller, and there was no degradation of rolling ability.

Bottom Elbow of Vertical Expansion Joint

The following loads were considered:

1. Cool down
2. All pipes pressurized to their MAWP
3. 0.89 g acceleration in X (seismic)
4. 1.4 g acceleration in Y (deadweight + seismic)
5. 0.85 g acceleration in Z (seismic)
6. Pumpdown of lines for leak checking
7. 22 psia overpressure of the vacuum space on the cryomodule side of the vacuum break
8. 22 psia overpressure of the vacuum space on the expansion joint side of the vacuum break

The critical load combination corresponds to Combination 5, and consists of cool down plus MAWP plus 0.89 g acceleration in X plus 1.4 g acceleration in Y plus vacuum plus 22 psia overpressure on the cryomodule side of the vacuum break.

Note that, unlike the top elbow, the bottom elbow incorporates a vacuum break, and can therefore provide constraint against the Z-direction seismic loads.

The FE model of the bottom elbow is shown in Fig. 45.

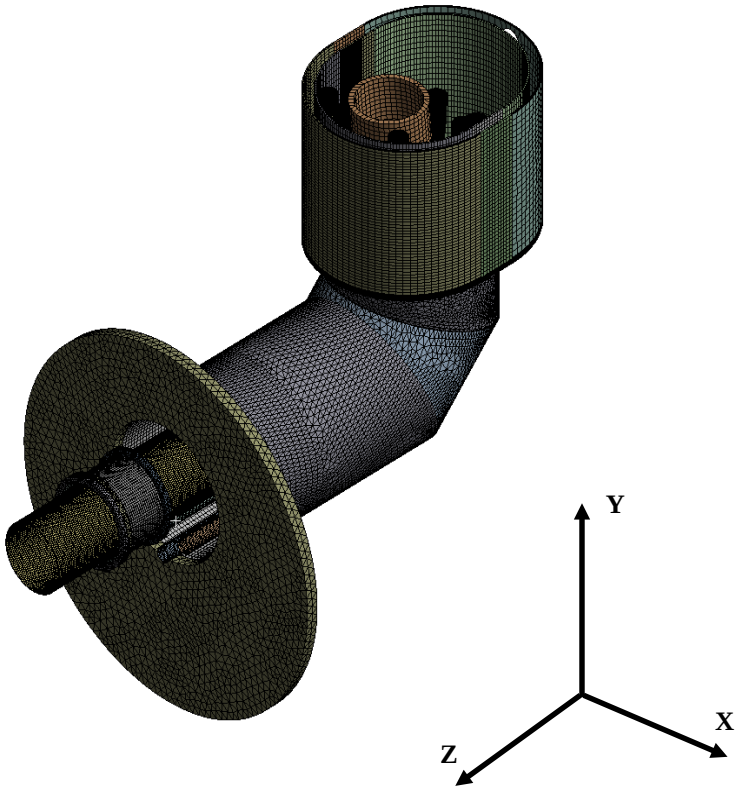

Figure 45. FE model of bottom elbow of vertical expansion joint

Thermal Results

The total heat load to 300 K is approximately 25 W. This includes approximately 0.6 W of radiation to the 2 K surfaces, and 3.8 W of radiation to the 50 K surfaces. Heat loads to pipes are summarized in Table XIII.

Temperature in the adapter plate and the pantleg connecting it to the 300 K vacuum vessel is shown in Fig. 46. The temperature profile is very similar to that of the anchor module, as should be expected.

Table XIII. Heat load on pipes in bottom elbow of vertical expansion joint

Line	Radiation - W	Conduction - W	Total - W
A	**-0.09**	**-0.51**	**-0.60**
B	**-0.33**	**-1.15**	**-1.48**
C	**-0.10**	**-0.71**	**-0.82**
D	**-0.10**	**-0.74**	**-0.85**
E	**-0.11**	**-0.21**	**-0.31**
F	**-2.75**	**-17.09**	**-19.84**
Note: Negative sign indicates heat flow into line			

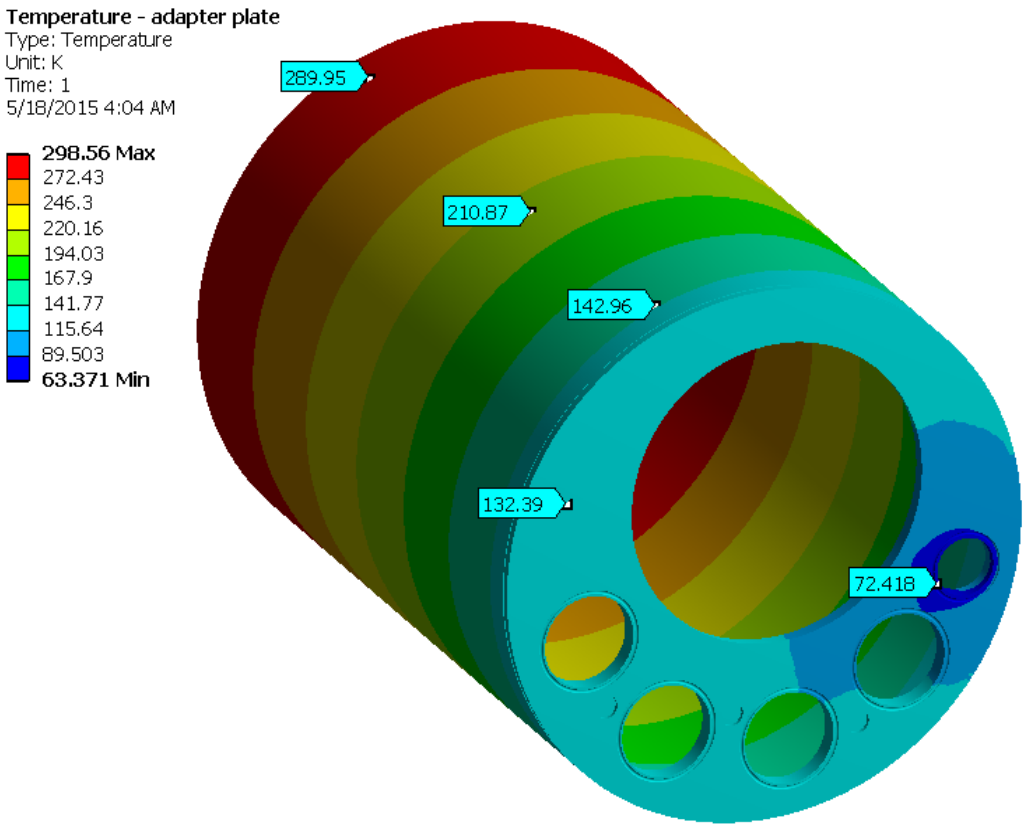

Figure 46. Temperature profile in adapter plate and pantleg of bottom elbow of vertical expansion joint

Stress Results

The analysis of the bottom elbow examined a unique loading which was not assumed to combine with any other loading. This was the simulation of the leak checking operation on the lines. Each line was assumed to be evacuated, and to have no support available against the tendency to expand in the vertical direction, due to the flex hoses in the assembly. This loading is not critical for the small diameter lines A, C, D, E, and F, but for line B it requires that a special truss structure be attached to the adapter plate, and extend to the centerline of the line B elbow, thus supporting it against vertical motion.

The resulting stresses for this load case are shown in Fig. 47. Apart from highly localized concentrations where the bracket attaches to the adapter plate, the stresses are all well below the allowable of 20 ksi.

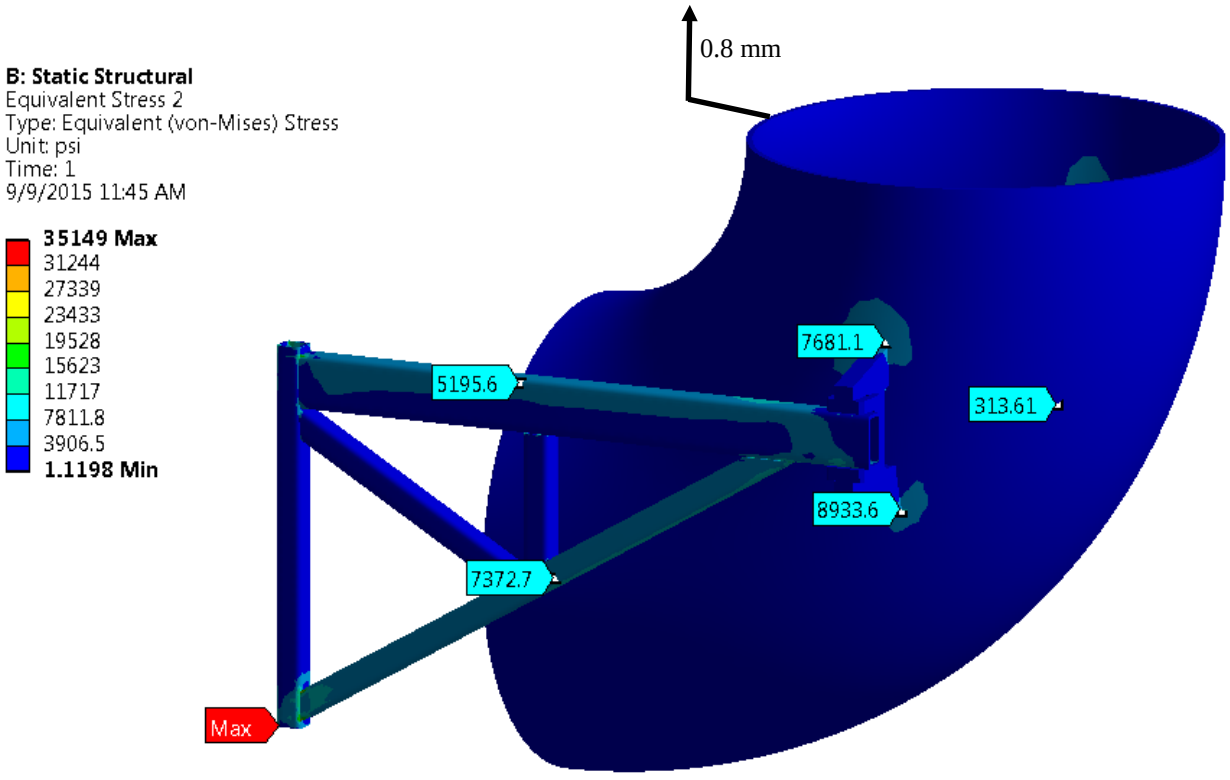

Figure 47. Stresses in support truss on line B during leak testing

Apart from the just-described unique leak-checking load case, the critical load combination corresponds to Combination 5, and consists of cool down plus MAWP plus 1.4 g acceleration in Y plus 0.89 g acceleration in Z plus vacuum plus 22 psia overpressure on the cryomodule side of the vacuum break.

All further discussion is with regard to this loading only.

The stresses in the adapter plate are shown in Fig. 48. They are a maximum of 13.4 ksi at a concentration on the outer radius at the weld line, but still lie below the allowable stress of 20 ksi.

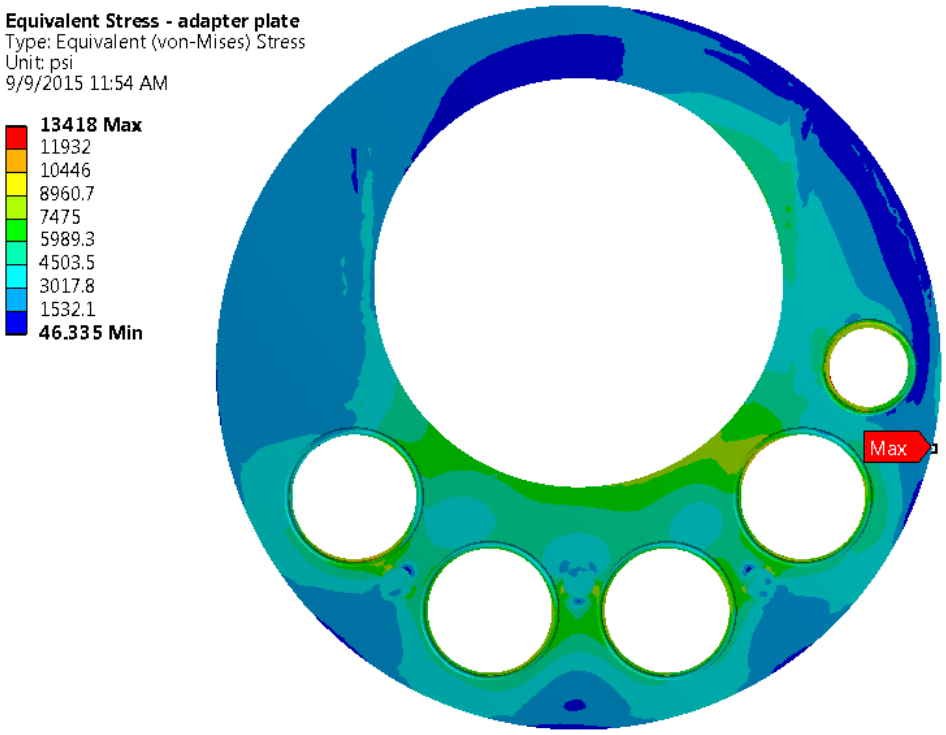

Figure 48. Stresses in adapter plate for bottom elbow of vertical expansion joint

The deformation of the line B bellows is shown is shown in Fig. 49. The resulting stresses in the pantleg and line B bellows are shown in Fig. 50, and all lie below the allowable of 20 ksi.

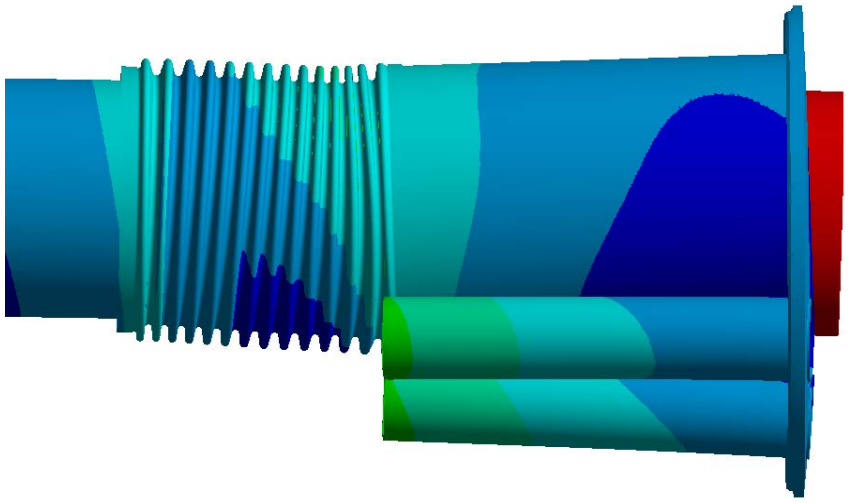

Figure 49. Deformation under load (scaled for clarity)

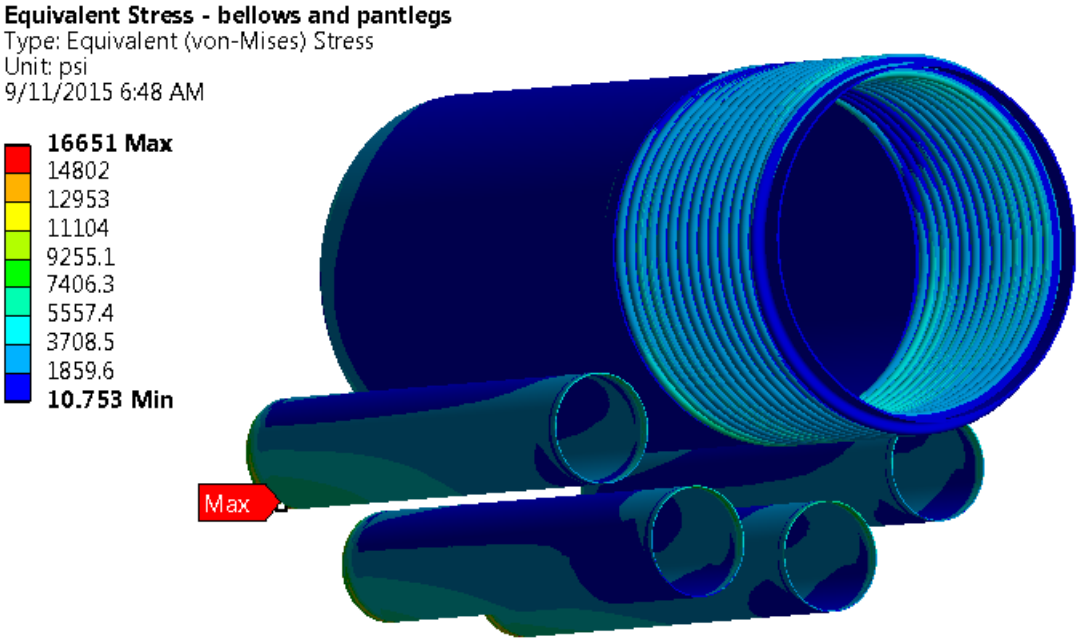

Figure 50. Stresses in pantlegs and bellows

The stresses in the welds on the pantlegs and adapter plates are shown in Fig. 51. The weld on line F to the adapter plate is the most highly stressed, with a maximum stress of 17.4 ksi. This is well below the maximum allowable primary membrane stress of 20 ksi.

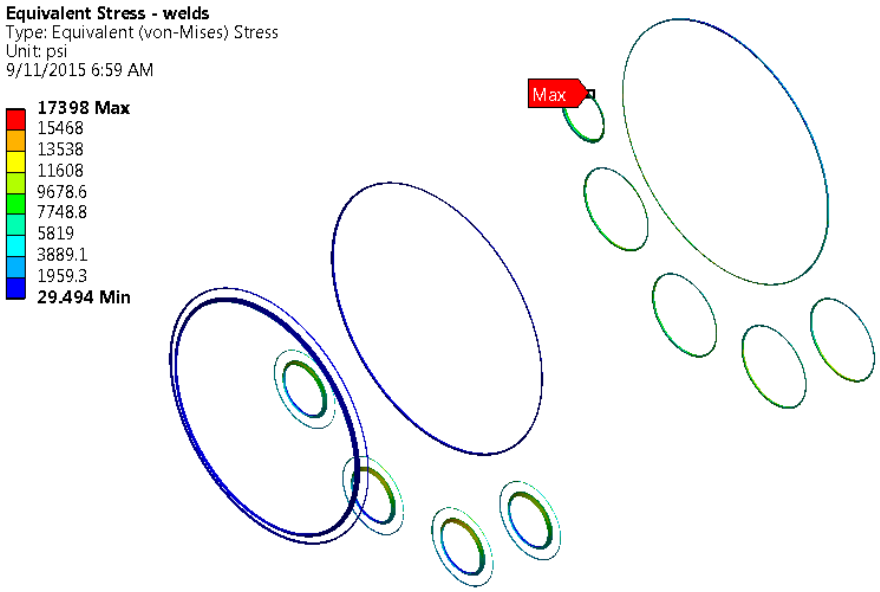

Figure 51. Stresses in welds on bottom elbow of vertical expansion joint

The stresses in the piping are shown in Fig. 52. The maximum stresses occur in the first 45 degree elbow of the lines, but do not exceed the primary membrane stress allowable of 20 ksi.

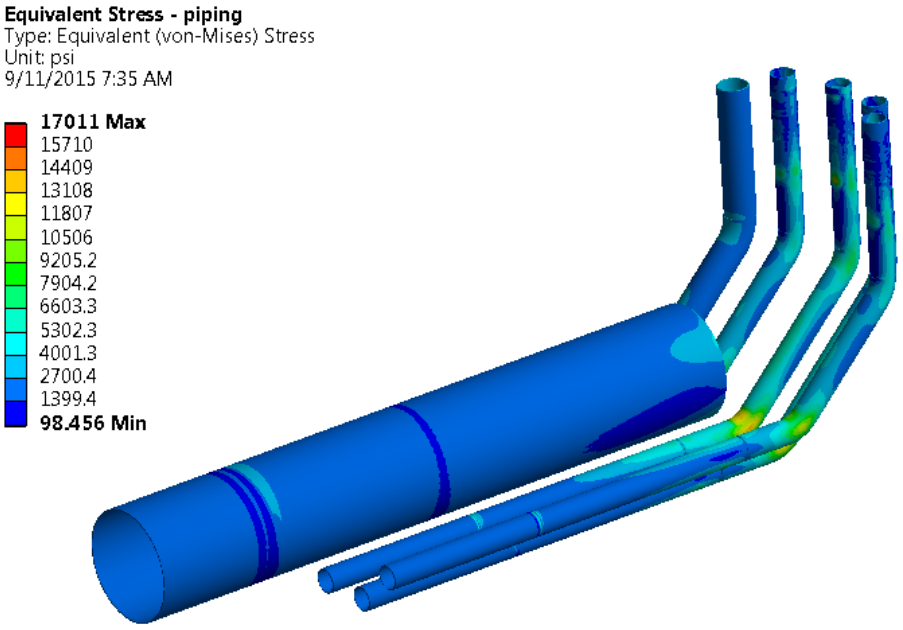

Figure 52. Stresses in piping of bottom elbow of vertical expansion joint

Transfer Line Supports

The horizontal transfer line run of 70 meters is supported by three truss assemblies. These are located at the center anchor module, and the two extreme ends. The vertical expansion joints allow the piping internal to the vacuum jacket to translate axially toward the center anchor (necessary for a stress-free cool down). Seismic axial loads on this piping are reacted solely by the center anchor support. Because there are bellows on the vacuum jacket close to the end anchor, the three anchors will share some of the axial load from the vacuum jacket itself. For this analysis, however, it was assumed that the center anchor was responsible for reacting all axial loads. The end anchors will be identical in design to the center anchor, but are expected to carry substantially less load.

A simplified FE model of the transfer line straight section was created to correspond to the proposed support spacing shown in Fig. 53. Loading is 1.4 g in Y, and 1.27 g in X and in Z.

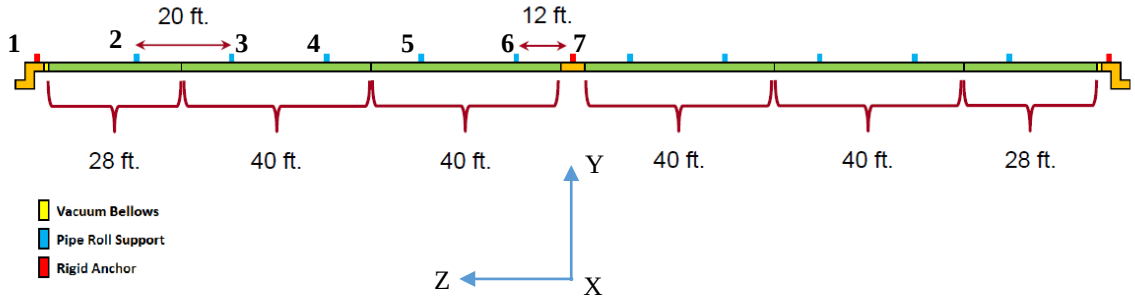

Figure 53. Schematic of transfer line straight section supports

In addition to the axial forces due to seismic loading, there is also the possibility of an axial force imbalance due to different pressures on each side of the vacuum break, as might develop during a venting fault scenario. The largest force would occur when one side of the break is evacuated, while the other (having suffered a cryogen line break, for instance) is pressurized to 22 psia. The vacuum jacket at the vacuum break is 26 in OD pipe with 0.25 in wall. This gives a cross sectional area of 511 in^2, for an additional force of 11240 lbs.

The analysis showed that, for the worst-case combinations of gravity, seismic loading, and pressure differential, the maximum X-direction (perpendicular to the pipe run) force on a support is 2856 lbs (rounded to 3000 lbs in Table XIVa). The maximum Z-direction (axial, i.e., parallel to the pipe run) force on a support is 41806 lbs (30566 lbs from seismic loading, and 11240 from differential pressure loading, the sum being rounded to 42000 lbs in Table XIVa), all of which appears at the central anchor, which is the only support designed to take this load. The maximum y-direction (vertical) force on a support is 3143 lbs (rounded to 3200 lbs in Table XIVa).

Table XIVa. Support Forces for Stress Analysis – Straight Section

Direction	Relevant to supports	Force - lbs
X	**1-7**	**3000**
Y	**1-7**	**3200**
Z	**7**	**42000**

The numbers in Table XIVa assume that all supports are designed to take x-direction loads. If only half of the supports are designed for this load, then the correct design load is 6000 lbs.

The anchor support is shown in Fig. 54. It is a weldment of rectangular tubes and plate, which are assumed to be A36 structural steel. Using an allowable stress of $0.6F_y$ gives an allowable stress of 0.6(36) = 21.6 ksi. This gives a maximum allowable membrane stress of 21.6 ksi, and a maximum allowable membrane plus bending stress of 32.4 ksi, using ASME stress classifications.

The welding rod is assumed to be E70XX. It is assumed that all welds except for the fillet welds indicated (which are done in the final steps of field assembly) will be full penetration welds.

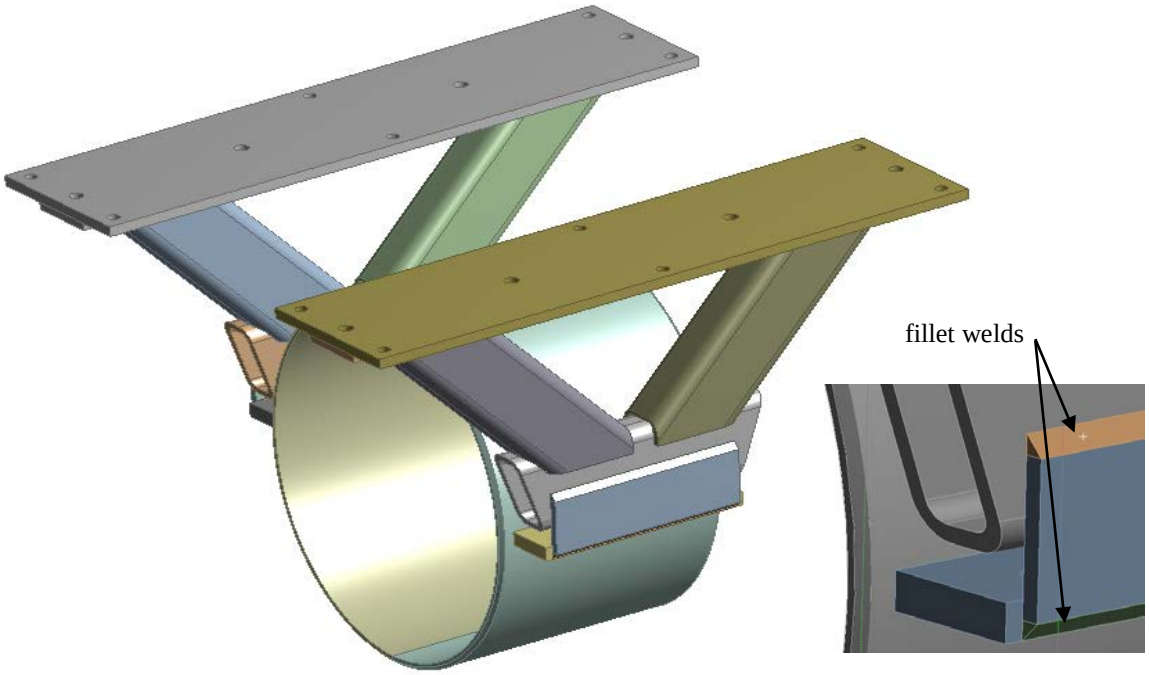

Figure 54. Solid model of anchor support

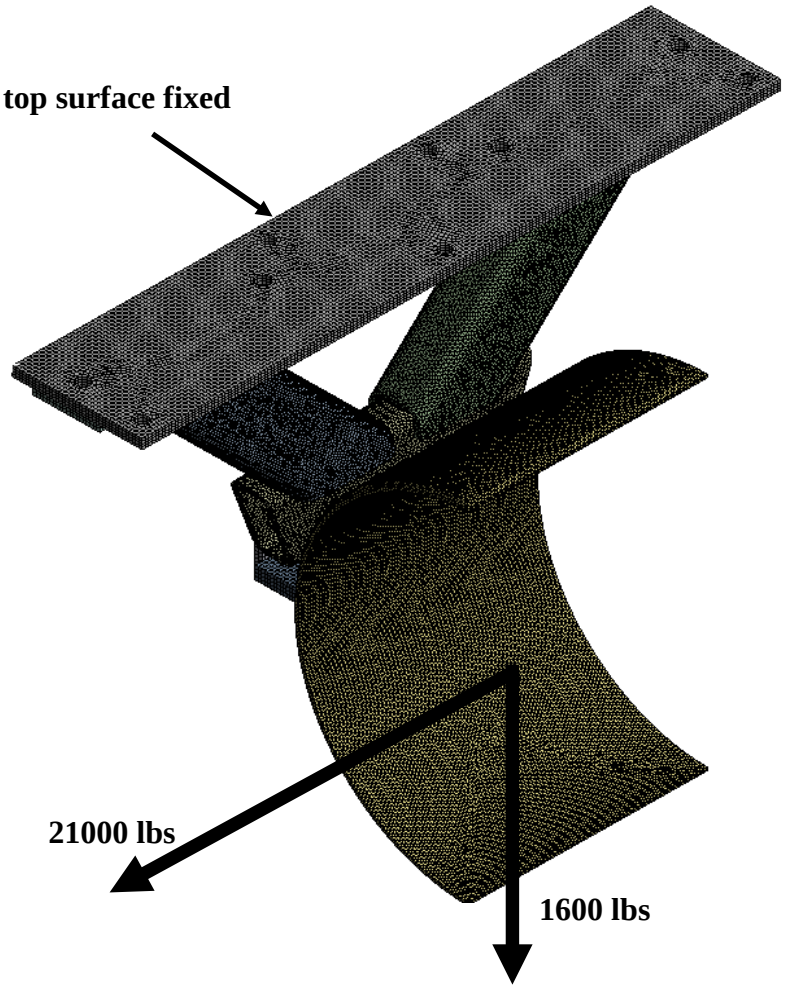

Figure 55. Finite element model of anchor support for stress analysis

The finite element model is shown in Fig. 55.

The X-direction forces (perpendicular to the axis of the vacuum vessel) are reacted by a dedicated horizontal strut with its own attachment to the wall, and are not a part of this analysis. Therefore, only one combination of loads is considered: The vertical and axial force shown, plus an acceleration on the truss structure itself of 1.4 g vertically, and 1.27 g horizontally, such that the truss mass adds to the loads shown.

The resulting stresses in the anchor support are shown in Fig. 56. The maximum stress is a concentration at the end of the 15 inch fillet weld holding the ½ inch steel plate to the side of the horizontal 4x6x0.5 inch rectangular tube. All of the structural steel tube stresses and the stresses in the shells and plates, apart from the weld, are well below the membrane stress allowable of 21.6 ksi.

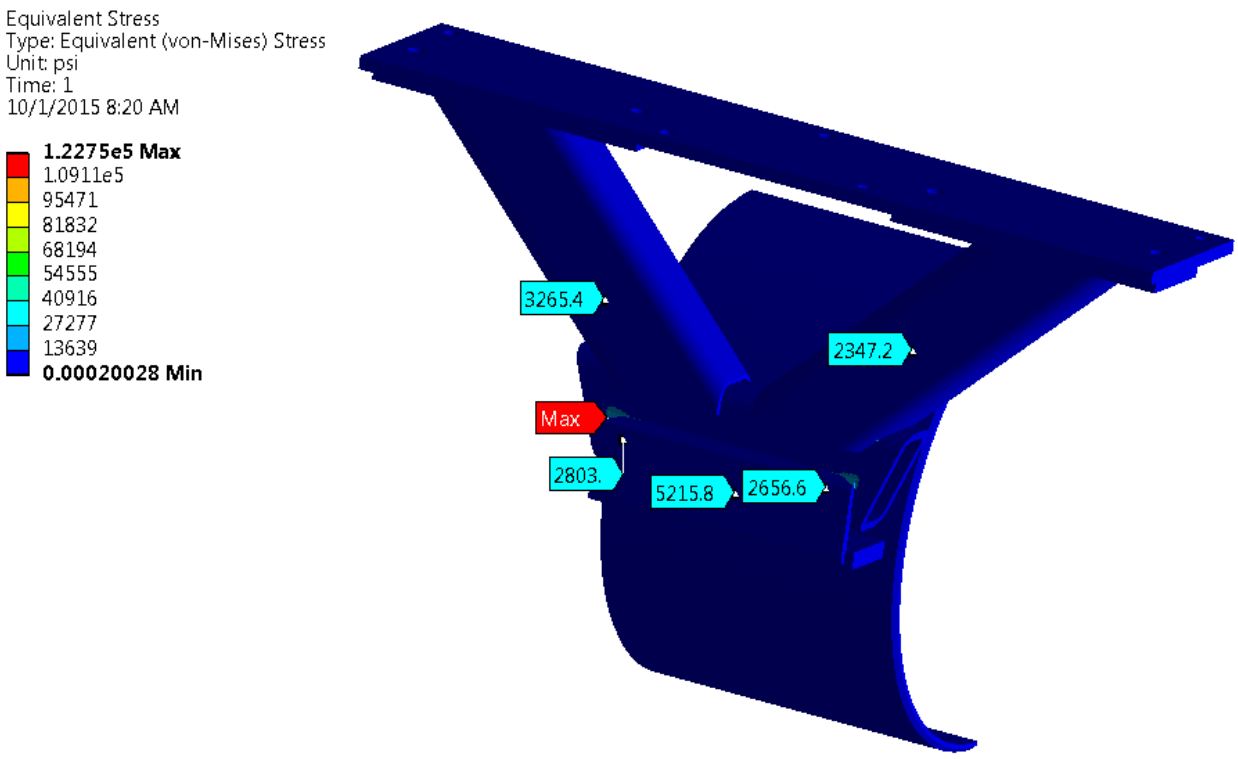

Figure 56. Stress plot of anchor support

The maximum stress in the weld is shown in detail in Fig. 57. The maximum value is a concentration, expected not only because the location is at the end of the weld, but because of the sharp discontinuity of attachment.

The fillet welds can be checked for size by resolving the two loads and applying this force to the nominal weld throat area to calculate a nominal shear stress. The allowable stress is the smaller of 0.3 times the weld metal strength and 0.4 times the yield stress of the A36 base metal. The base metal governs, with an allowable shear stress of 14.4 ksi. For the 15 inch long welds, with ½ inch legs, the total throat area is $15(0.707)(0.5) = 5.3$ in^2. The resolved force is (for the half model) is $(21000^2 + 1600^2)^{1/2} = 21060$ lbs. The nominal shear stress on the weld throat is then 16194/5.3 = 3055 psi, which is much less than the allowable stress of 14.4 ksi.

An additional check was performed using the ASME approach of stress linearization, but assuming the strength of the A36 base metal (which is less than the strength of E70XX rod). A stress classification line was passed through the weld throat, one element away from the stress concentration at the corner, as shown in Fig. 58. The results show a membrane stress of 18.7 ksi, and a membrane plus bending stress of 29.4 ksi, both below the allowable stresses.

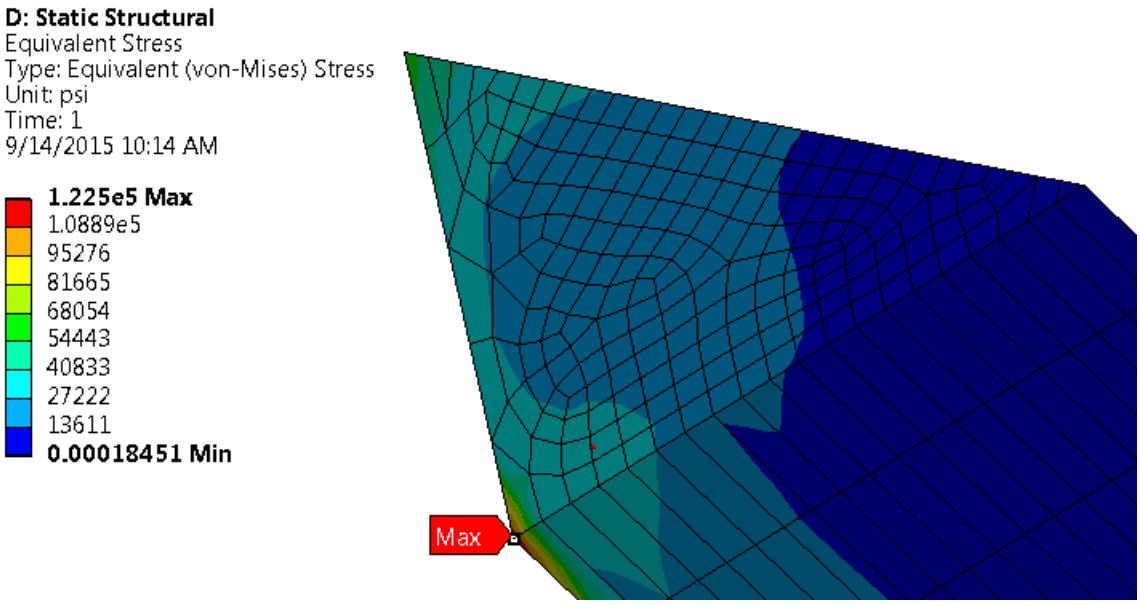

Figure 57. Detail of fillet weld stress

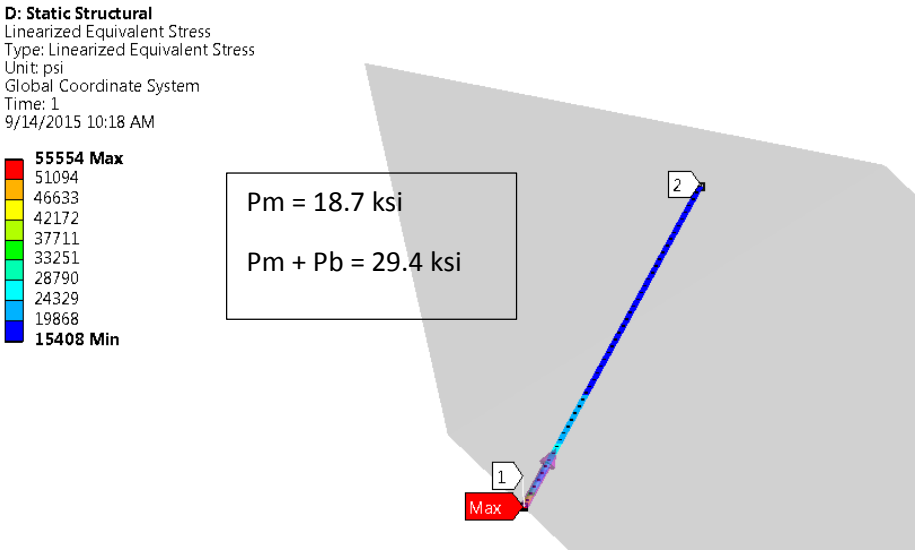

Figure 58. Stress classification line passed through end of fillet weld

Forces for use in designing the concrete anchors must be calculated with allowable strength load combinations and load factors (see appendix A).

Inspection of the three strength load combinations given in the Appendix shows that the worst case is 1.6 g vertical acceleration, 3.2 g horizontal acceleration, and 1.2x22 psi pressure differential. Recalling that the model for the stress analysis used vertical acceleration of 1.4 g, and a horizontal acceleration of 1.27 g, the previously calculated forces can be scaled to represent the support reactions corresponding to the higher loading. These scaled forces for anchor design are given in Table XIVb. These forces were applied to the finite element model of the support, along with the appropriate accelerations to ensure that the mass of the support itself is accounted for.

Table XIVb. Forces applied to FE model for anchor force analysis – Straight Section

Direction	Relevant to supports	Force - lbs
X	**1-7**	**7600**
Y	**1-7**	**3700**
Z	**7**	**90500**

The resulting force and moment reactions on the mounting plate, required for the concrete anchor design, are given in Fig. 59. The differences between these numbers and the forces that were input reflect the weight of the anchor support itself.

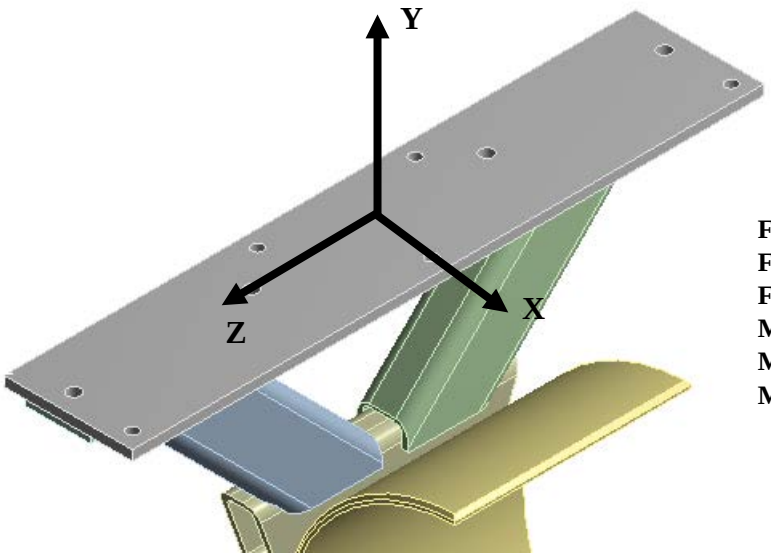

Figure 59. Forces and moments on anchor support mounting plate

Cryomodule Feedcap

The cryomodule feedcap model is shown in Fig. 60. Since bellows in the cryomodule prevent the cryogenic lines from developing tension to react their internal pressures, the stainless steel cylinder, adapter plate, and welded pantlegs of the vacuum break from the bottom elbow model of the vertical transfer line were included to provide a path for this loading.

The shield in the feedcap is copper, weighing approximately 180 lbs. It is attached directly to two horizontal 40 mm equal leg angles which are cantilevered from the shield plate. These angles also support a system of “trapeze” -like structures that provide surfaces for the piping to lay against. For the thermal part of this analysis, the heat paths through these structures is included, since this should lead to the most conservative estimate of total heat load. But in the structural analysis, no credit was taken for contact with these surfaces, i.e., the pipes were not supported except at their junctions with the shield plate. There are two additional angles cantilevered from the bottom of the shield, which aid in support of the trapeze systems, and assist the upper angles in support of the shield.

The copper shield is connected to lines E and F. This connection is active during the thermal analysis, but no interaction is accounted for in the structural analysis. This is based on the assumption that the connection through a copper braid, which has negligible stiffness.

The shield and its supports are designed to cool down without the development of significant stress.

There are several short lengths of flex hose on the lines in the feedcap. These were simulated with springs connecting the pipe ends and given the stiffness of an equivalent length of solid pipe. The springs offered only longitudinal stiffness, with no resistance to lateral motion, consistent with the flex hose behavior.

The feedcap endplate is not included in the analysis. The hanger and pendulum assemblies which connect to it are rigidly constrained at the surfaces to which they attach to the endplate, as is the outer circumference of the vacuum shell. The endplate is included explicitly in the feedcap support model (covered later in this report), where it is subjected to a worst case loading of the entire feedcap mass.

The following loads were considered:

1. Cool down
2. All pipes energized to their MAWP
3. 0.89 g acceleration in X (seismic)
4. 1.4 g acceleration in Y (deadweight + seismic)
5. 0.89 g acceleration in Y (seismic)
6. 2 mm displacement of end of line B in X (misalignment load)
7. 2 mm displacement of end of line B in Y (misalignment load)

Two critical load combinations (depending on component) were found. Both are variants of Combination 5. Loading condition 1 is cool down plus MAWP plus 1.4 g acceleration in Y plus 0.89 g acceleration in Z plus 2 mm offset of line B in Y. Loading condition 2 is cool down plus MAWP plus 0.89 g acceleration in X plus 1.4 g acceleration in Y plus 2 mm offset of line B in X.

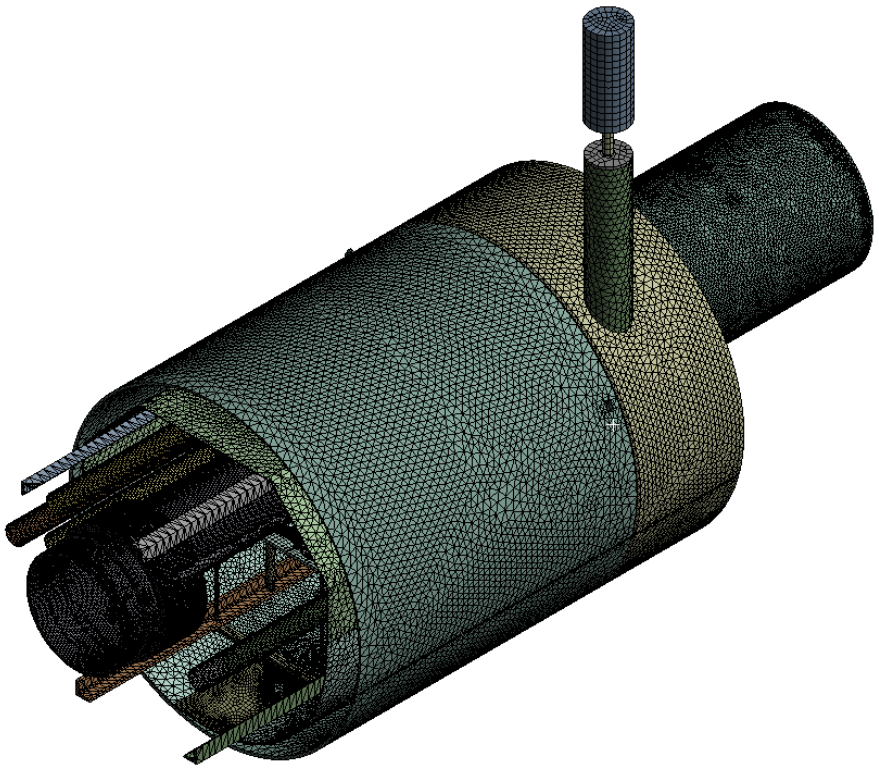

Figure 60. FE model of cryomodule feedcap

Thermal Results

The temperature profile in the stainless steel shield plate is shown in Fig. 61. The temperatures vary from 37.3 K to 53.7 K, consistent with the two sink temperatures applied by the lines E and F.

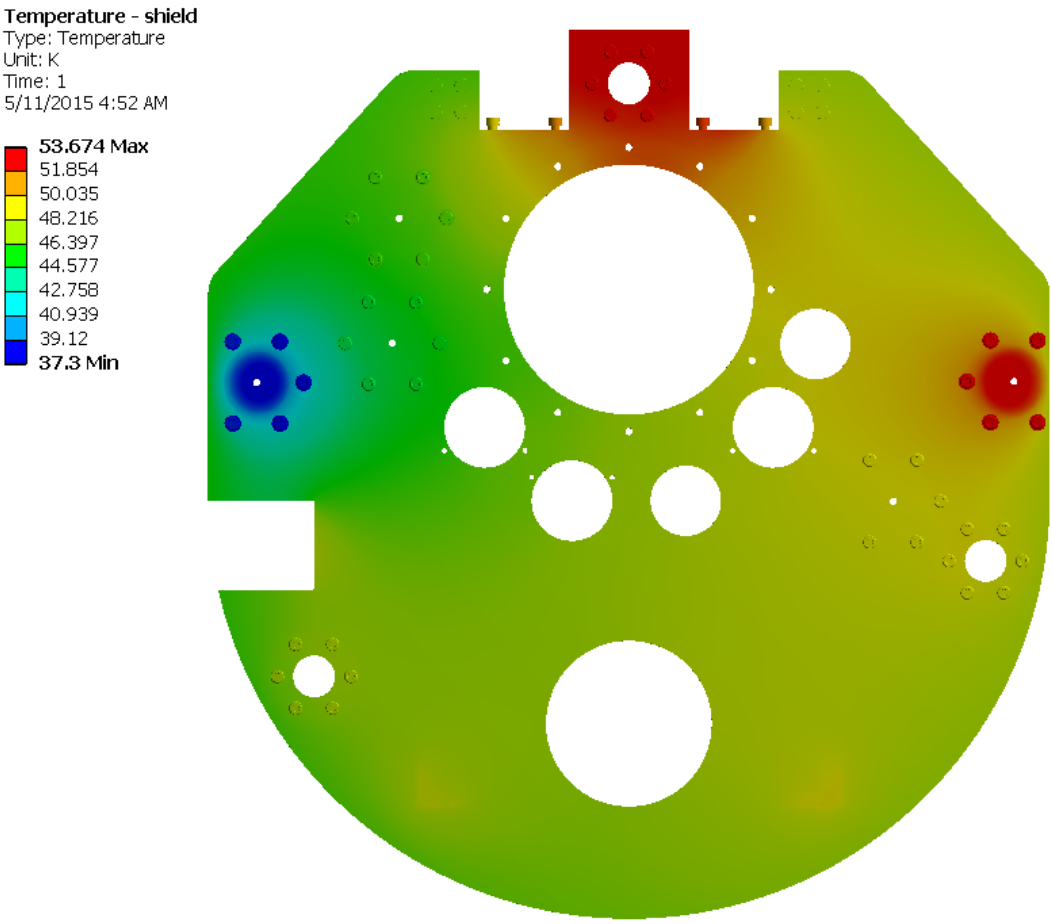

Figure 61. Temperature in SS304 shield plate

The heat leaks through each of the three pendulum assemblies and each of the three hangers are summarized in Table XV, using the nomenclature of Fig. 62.

Table XV. Heat Leak from Shield Plate supports

Support		Heat Leak - W
Pendulum Assembly	1	0.38
	2	0.39
	3	0.39
Hanger	1	0.43
	2	0.43
	3	0.43

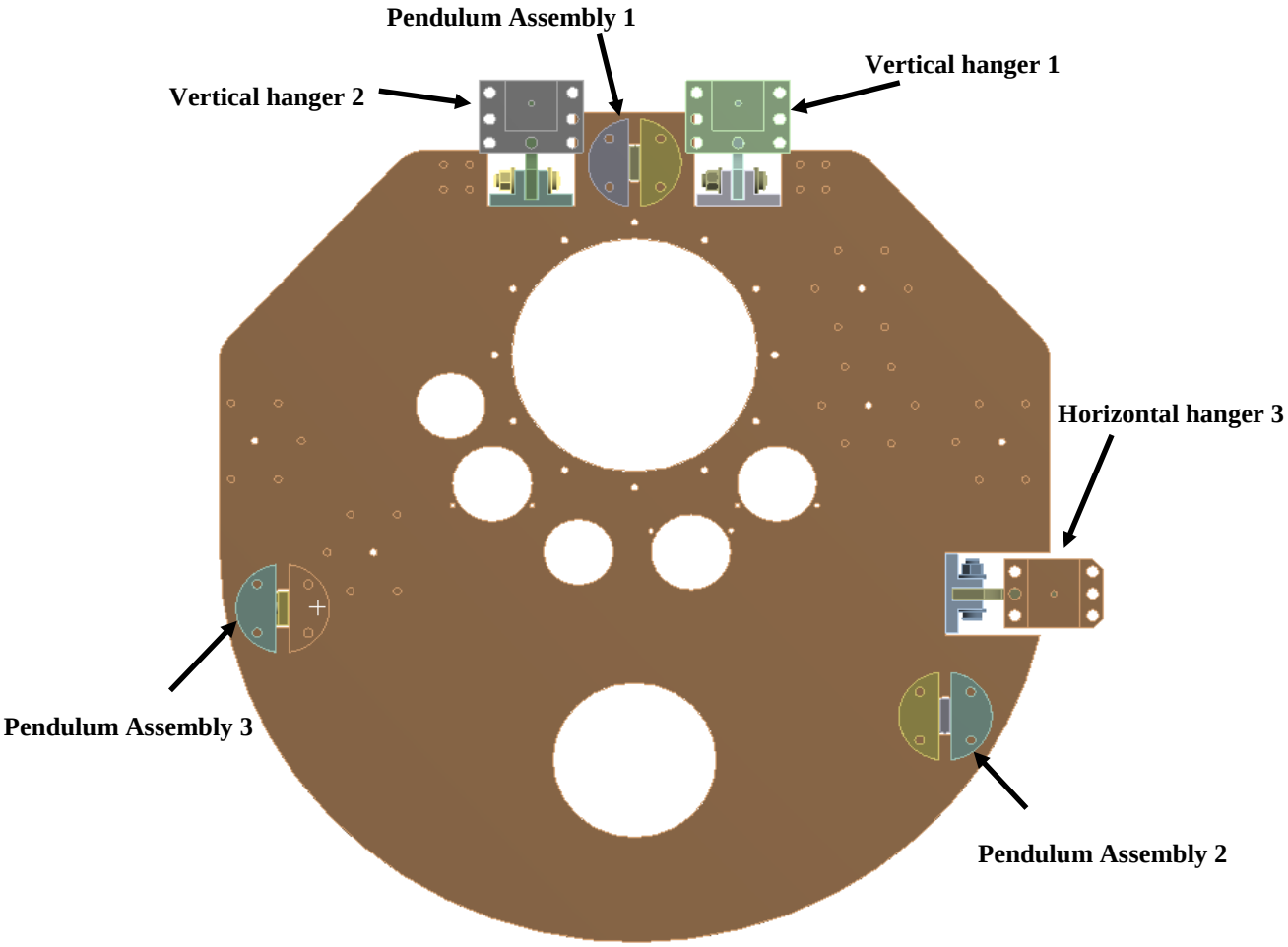

Figure 62. Shield plate support identification

The temperature profile in the copper shield is shown in Fig. 63. The range of temperature is similar to that of the shield plate, with the minimum temperature being about seven degrees warmer, and the maximum temperature being about 2 degrees less.

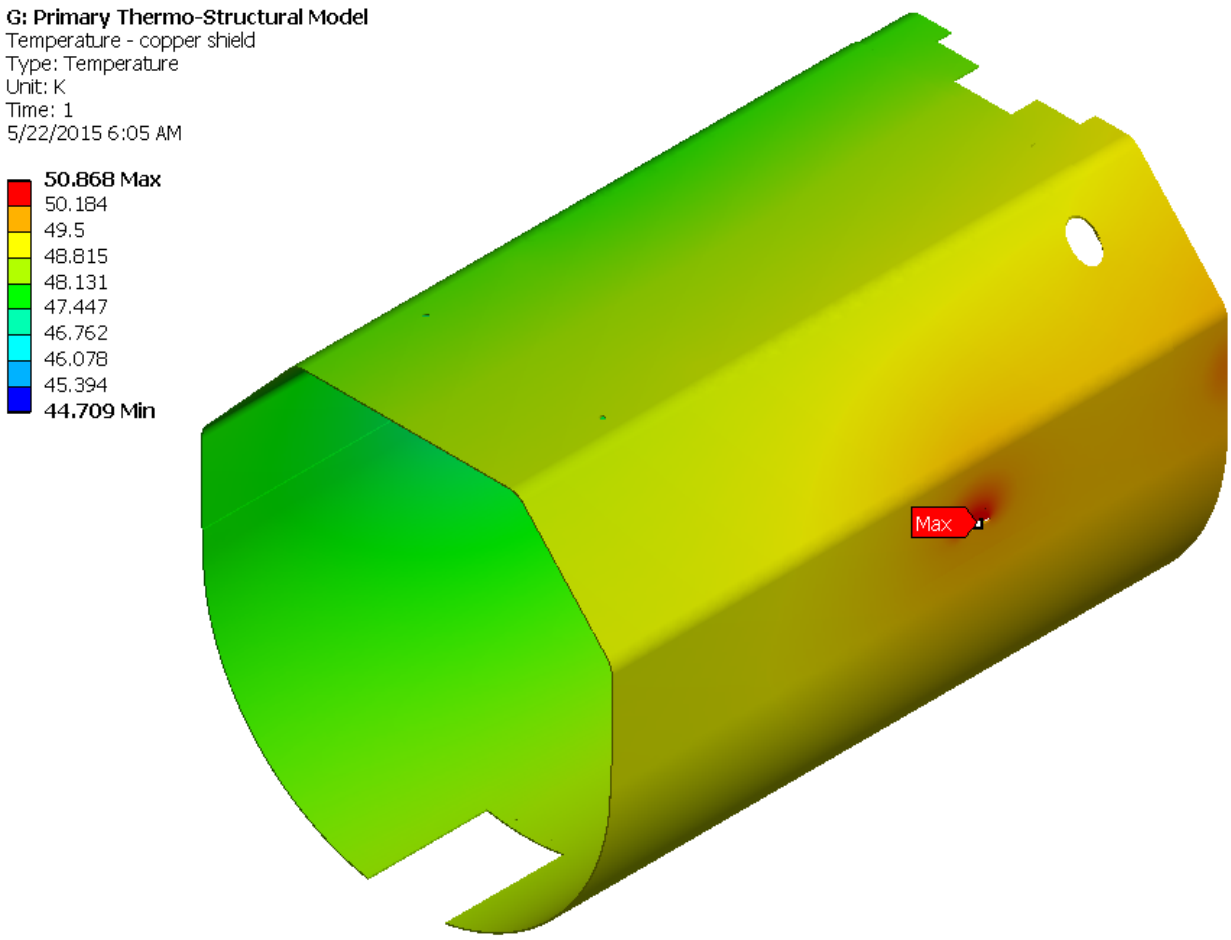

Figure 63. Temperature in copper shield

Stress Results

As stated previously, two critical load combinations (depending on component) were found. Both are variants of Combination 5. Loading condition 1 is cool down plus MAWP plus 1.4 g acceleration in Y plus 0.85 g acceleration in Z plus 2 mm offset of line B in Y. Loading condition 2 is cool down plus MAWP plus 0.85 g acceleration in X plus 1.4 g acceleration in Y plus 2 mm offset of line B in X.

The forces on the G-10 pendulum assemblies and hangers that support the shield plate are summarized in Table XVI. The convention is that a positive force produces tension on the component. (Note that the largest loads occur when the system is pressurized to its MAWP in all lines. Due to the presence of bellows at the interface with the cryomodule, all pressure force is reacted by the three pendulum assemblies)

Table XVI. Forces on pendulum assemblies and hangers - lbs

Loading	Pendulum Assemblies			Hangers		
	1	2	3	1	2	3
Cool Down	**-23**	**357**	**330**	**174**	**386**	**296**
MAWP	**-6123**	**-3663**	**-2814**	**474**	**262**	**-203**
Accel - X	**+/-91**	**+/-333**	**+/-427**	**+/-209**	**+/-211**	**+/-489**
Accel - Y	**443**	**-219**	**-187**	**371**	**361**	**0**
Accel - Z	**+/-334**	**+/-147**	**+/-128**	**+/-22**	**+/-26**	**+/-5**
2 mm line B, X	**+/-43**	**+/-174**	**+/-220**	**+/-73**	**+/-73**	**+/-131**
2 mm line B, Y	**+/-345**	**+/-173**	**+/-150**	**+/-106**	**+/-104**	**+/-4**
* - positive force produces tension on the component						

The maximum load on each support is calculated by summing the maximum possible values for each load case, for whatever combination of load cases produces the maximum and minimum support force, with the stipulation that the X seismic acceleration is assumed to never occur simultaneously with the Z seismic acceleration.

Table XVII summarizes the maximum tensile and maximum compressive forces on each G-10 component, and the resulting stress. The stress is based on a cross sectional area of 0.27 in^2 for a pendulum assembly, and 0.15 in^2 for a hanger assembly. (It should be noted that the minimum cross sectional area of the hangers is at a section through the hole in the end, not the middle of the hanger. This implies that the hanger could in fact be made thinner in the middle.) The allowable stress for G-10 in tension is 18.5. The allowable stress for G-10 in compression is 20.5 ksi.

Table XVII. Stresses in pendulum assemblies and hangers

Component		Maximum Tensile Force - lbs	Maximum Compressive Force - lbs	Maximum Tensile Stress - psi	Maximum Compressive Stress - psi
Pendulum Assembly	1	1165	-6426	4315	-23800
	2	1038	-4205	3844	-15574
	3	1127	-3467	4174	-12840
Hanger	1	1408	-388	9387	-2587
	2	1397	-389	9313	-2593
	3	920	-827	6133	-5513

The table shows that the compressive stress in pendulum assembly 1 is in excess of its allowable. This is readily remedied by reducing the diameter of the internal hole.

The pendulum assemblies are attached to the endcap/feedcap and the shield with 8 mm bolts. Assuming a coarse thread, the stress area of a bolt is 0.0567 in^2, and the maximum working load of a single bolt is 2465 lbs, based on the previously established working stress of 43.5 ksi. A minimum of four bolts are used to make a connection, giving a total capacity of 9860 lbs in tension. From Table XVII, the maximum load on a pendulum assembly is 6426 lbs. This is well below the capacity of the bolting.

The ends of the pendulum assemblies and the anchors use commercial spherical bearings. These bearings will be rated for loads well in excess of the maximum load of 6426 lbs.

The stress in the most highly loaded vertical hanger bracket (for vertical hanger 1) is shown in Fig. 65. Apart from mild concentrations at the discontinuities, the stresses are well below the allowable of 20 ksi.

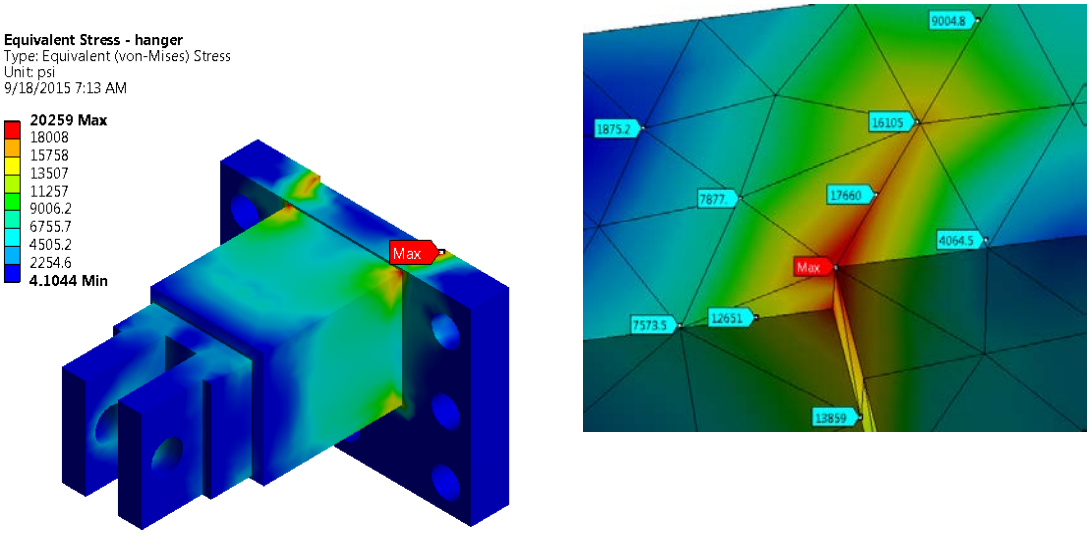

Figure 65. Stress in vertical hanger 1 bracket for loading

The hanger brackets are connected to the feedcap endplate with six 10 mm bolts (note that these bolts were not included in the model, since the feedcap endplate itself was not included). Using the maximum hanger tension of 1408 lbs, and a lever arm of 4.2 inches, the moment resisted by the six bolts is 1408(4.2) = 5914 in-lbs. Assuming that only the four bolts in the corners resist the moment, then, for a vertical distance between bolt centerlines of 2 inches, 5914 = 2F(2), where F is the force in one bolt. This gives F = 1478 lbs. For a 10 mm coarse thread, the stress areas is 0.179 in^2, giving a stress of 1478/0.179 = 8.3 ksi. This is well below the allowable bolting stress of 43.5 ksi.

The stresses in the bracket of the most highly stressed pendulum assembly (pendulum assembly 1) is shown in Fig. 65 for loading condition 2. Highly local bearing stress concentrations occur at the inner edge of the pin hole, but there is a substantial adjacent volume of low stressed material for stress redistribution. Stresses overall are well below the maximum allowable of 20 ksi.

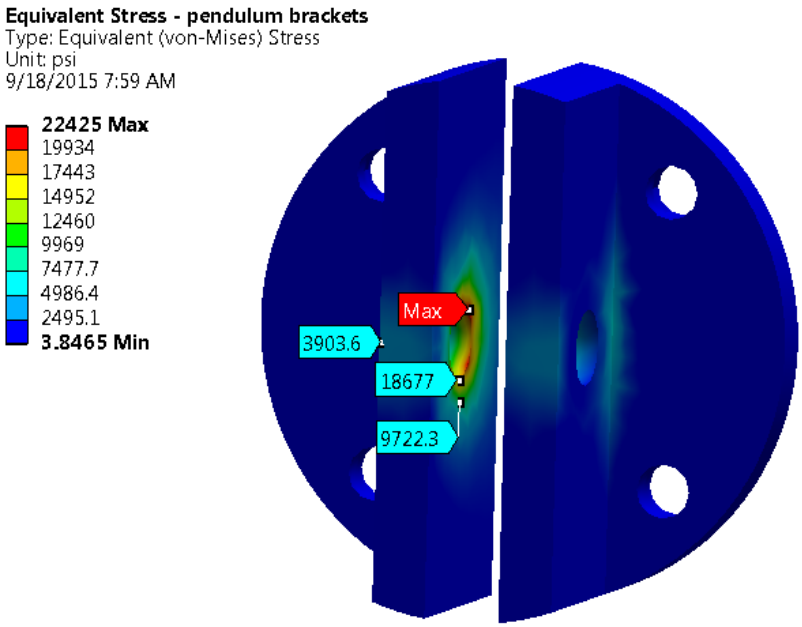

Figure 65. Stress in pendulum assembly 1 bracket for loading condition 2

The highest compressive load on a pendulum assembly is 6426 lbs. As this is a compressive load on a pin-ended member, buckling of the pendulum assembly must be checked. The buckling load was estimated from the Euler buckling load for a simply-supported column. The critical Euler buckling load is given by

$$P_{cr} = \pi^2 \frac{EI}{L^2}$$

Where P_{cr} = buckling load
E = Young's modulus = 2.7e6 psi
I = moment of inertia of cross section = 0.027 in^4
L = length = 5 in

Substituting gives P_{cr} = 28000 lbs, which is well above the loads the pendulum assembly will experience. It should be noted that this calculation is particularly conservative, not just for using the pin-ended Euler formula, but because the pendulum assembly uses steel caps on the ends of the G-10 hollow rod, and thus not the entire length is subject to the low modulus of G-10.

The highest compressive load on a hanger assembly occurs for the horizontally oriented hanger, which can be compressed by the X-direction seismic loading. This compression (see Table XVII) is 827 lbs. Repeating the calculation above with I = 0.003 in^4, and L = 3.1 in, gives P_{cr} of 8320 lbs, which is well above the maximum expected compressive load.

The maximum stress in the line B reducer occurs for loading condition 1, which is cool down plus MAWP plus 1.4 g acceleration in Y plus 0.85 g acceleration in Z plus 2 mm offset of line B in Y.

The stress in the reducer region is shown in Fig. 66. The stresses exceed the membrane stress allowable of 20 ksi only at a stress concentration at the junction of the gusset and line B. A stress classification line was passed through the thickness of line B at the gusset junction (Fig. 67). For this SCL, the primary membrane stress is 8.2 ksi, and the primary membrane plus bending stress is 21.3 ksi. Both of these stresses are below the allowables of 20 ksi and 30 ksi, respectively.

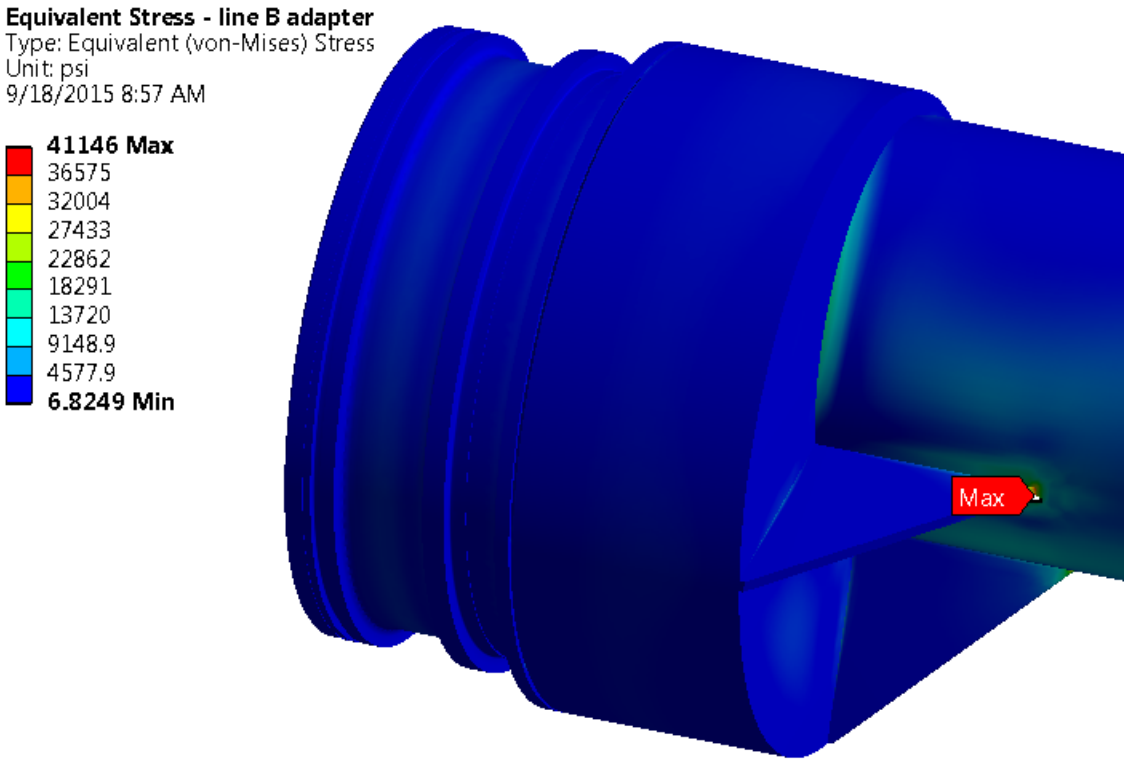

Figure 66. Stress in line B reducer

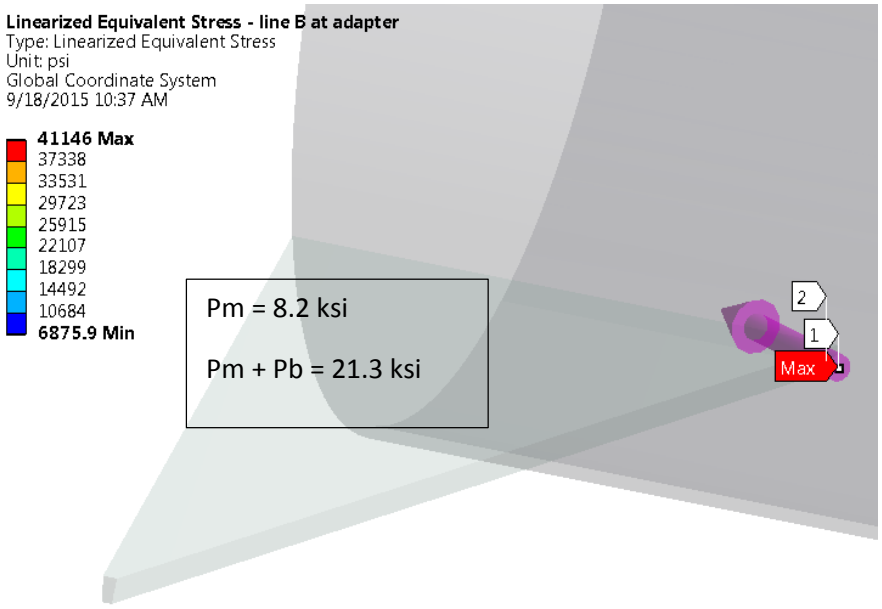

Figure 67. SCL through the most highly stressed region of line B

The shield plate is most highly stressed by the MAWP loading, and is predominately in bending, with very little membrane stress. Therefore, the surface stress can be allowed to reach the membrane plus bending allowable of Pb = 30 ksi.

The resulting stresses are shown in Figs. 68 for loading condition 1. Apart from a very local concentration at the attachment point of vertical hanger 1 (Fig. 69), all surface stresses are below the 30 ksi allowable.

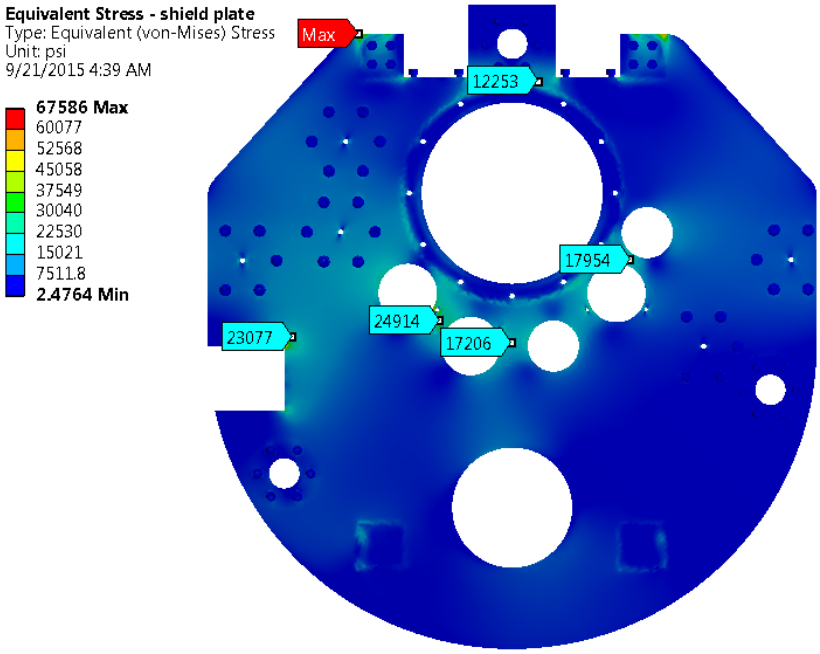

Figure 68. Stresses in shield plate for loading condition 1

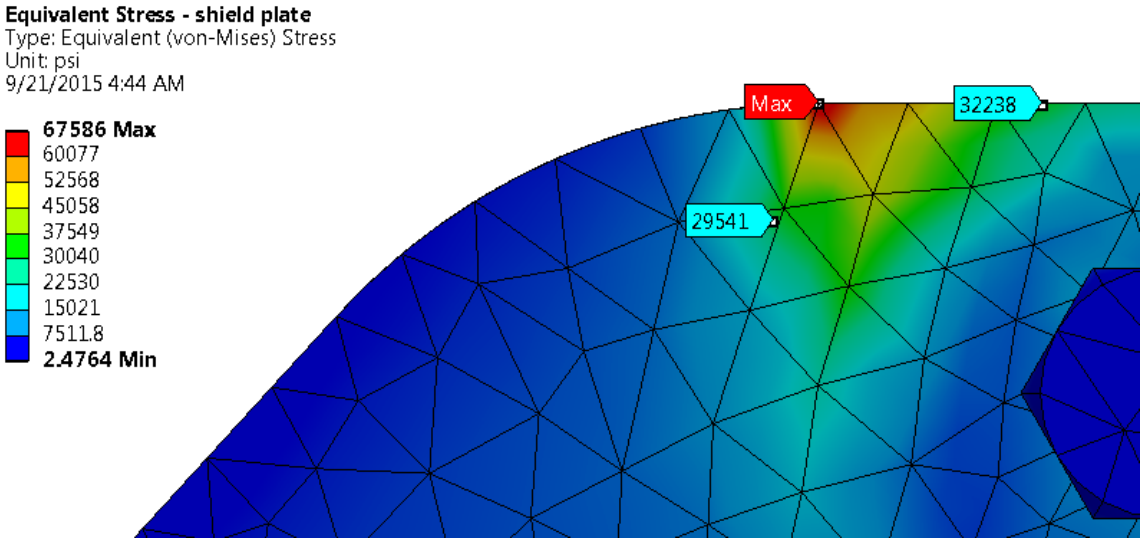

Figure 69. Close-up of stress concentration at connection to angle

The stresses in the piping are shown in Fig. 70 for loading condition 2. The maximum occurs in the small line coming from the valve. The primary contribution is the cool down, in which the small line contracts toward the valve, which is long but fixed at its warm end. An SCL was passed through this location, as shown in Fig. 71. The primary membrane stress, Pm, was 7.3 ksi. The primary membrane plus bending stress, Pm + Pb, was 23.5 ksi. Both of these stresses are below the allowables of 20 ksi and 30 ksi, respectively.

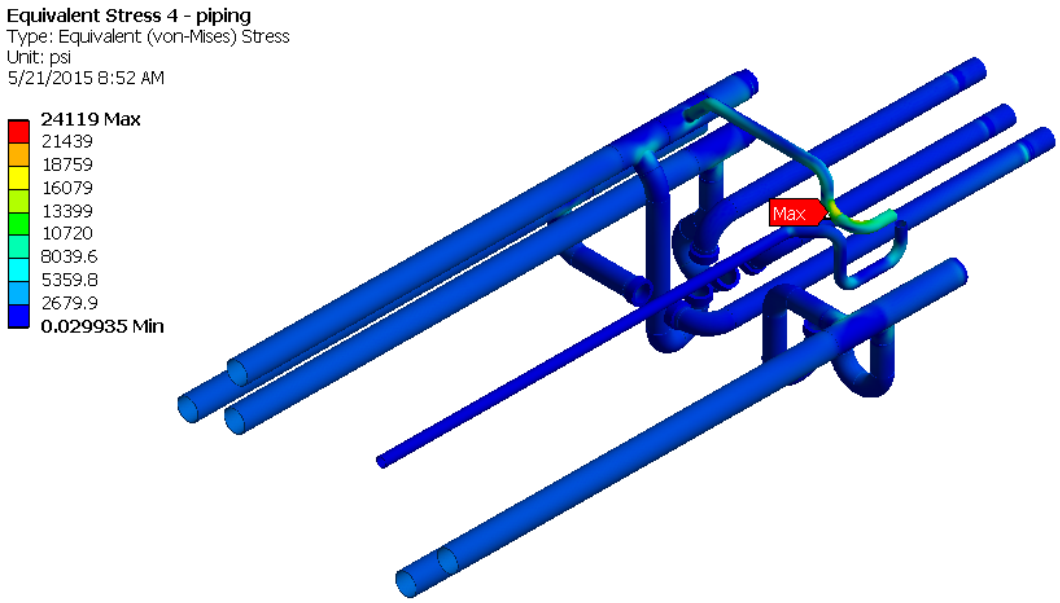

Figure 70. Stresses in piping for loading condition 2

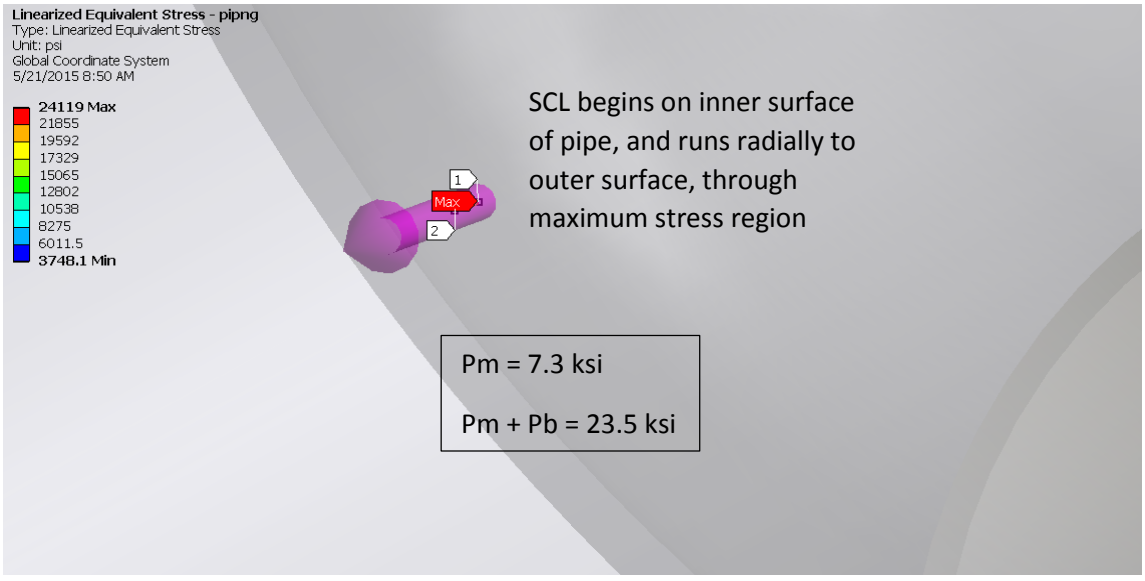

Figure 71. Stress classification line through most highly stresses pipe

Line E and line F attach with blind pipe stubs to the shield plate for the purposes of heat-sinking. The attachment for line E is the most highly stressed of the piping fittings that attach to the plate. The stresses in this fitting are shown in Fig. 72. The maximum stress of 18.2 ksi is below the allowable membrane stress of 20 ksi.

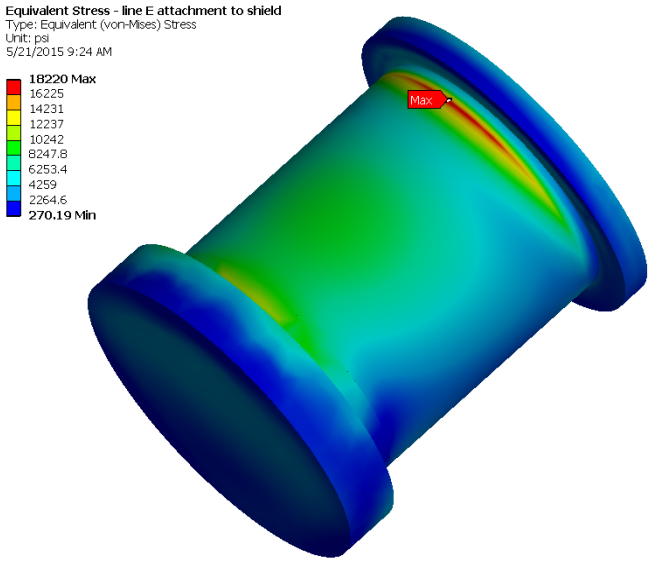

Figure 72. Stress in line E pipe stub to shield for loading condition 2

The connection of the lines to the shield plate were simulated such that the 8 mm bolts alone carried the joining loads. There was no credit taken for interface compression due to preload.

The most highly stressed bolt is in the mounting flange of line C, and occurs for loading condition 2. The axial stresses in this bolt are shown in Fig. 73. Since the bolt is simulated at its nominal diameter, an adjustment is necessary to express the FE stress in terms of the actual stress area. The ratio of nominal area to stress area for an 8x1.25 bolt is 1.37. The FE stresses in the bolt shank range between -30 ksi and 30 ksi, giving an adjusted stress of 41.2 ksi, which is below the allowable of 43.5 ksi. It should be noted that the bolts each carry shear and bending, which in the actual joint are shared by the flange compression.

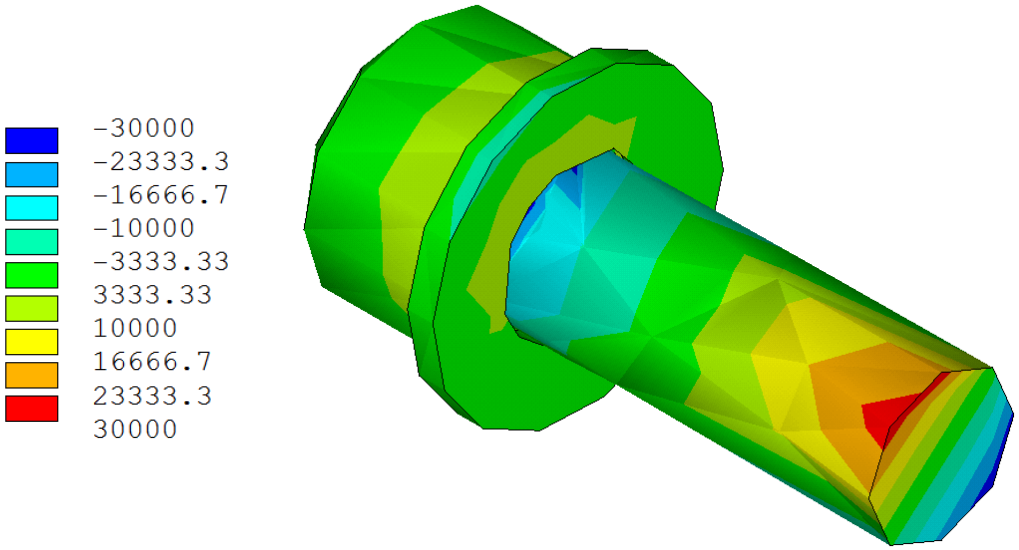

Figure 73. Axial stress in most highly stressed bolt

Lines A, C, and D attach to the shield plate through hollow G-10 insulating cylinders. These cylinders are both threaded and epoxied into SS304 sockets at each end. The axial stress in the G-10 is shown in Fig. 74. This stress is largest for loading condition 1. The maximum stress of 14.1 ksi, which occurs in the cylinder for line C, is below the tensile allowable of 18.5 ksi. The minimum compressive stress of -20.8 ksi is a concentration occurring at the change in diameter on the stub, but even as a concentration is only slightly in excess of the allowable of -20.5 ksi.

The stresses in the line B G-10 piece, also shown in Fig. 74, well below both the tensile and compressive stress allowables for G-10.

Simulating both G-10 threads and bonding to the sockets is difficult, so only bonding was considered. Shear stresses on the bonding surfaces of the G-10 are shown in Fig. 75 for loading condition 2. Apart from stress concentrations at the margins, these stresses are approximately 2500 psi for lines A and C. At this time the epoxy bond strength is not specified. From these

results, assuming a safety factor of 2, an appropriate lap shear strength value for the bond would be at least 5000 psi.

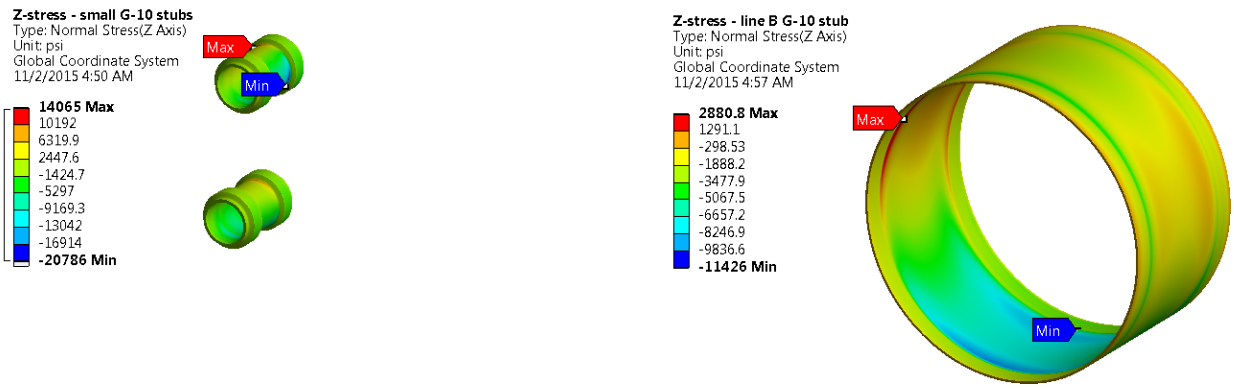

Figure 74. Axial stress in G-10 stubs at shield plate – Loading condition 1

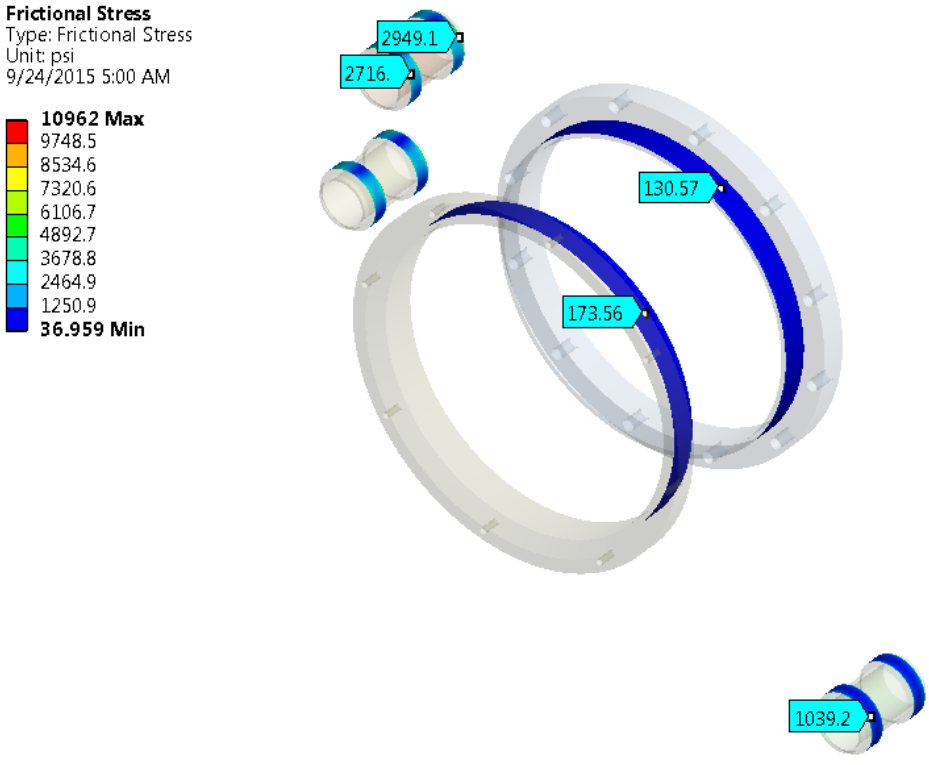

Figure 75. Shear stresses in epoxy bonds – Loading condition 2

The stress in the stainless steel sockets for the G-10 offsets for lines A and C for loading condition 1 are shown in Fig. 76. (The socket for line D is much lower in stress, and the scheme used to attach the line B cylinder is different in concept). The sockets for lines A and C are most highly stressed likely because those lines are more susceptible to lateral loads caused by cool down. The maximum socket stress occurs at a concentration at the junction of the flange and cylinder. An SCL was passed through this region (Fig. 77), and the stresses decomposed to a primary membrane stress of 8.5 ksi, and a primary membrane plus bending stress of 13 ksi. Both of these stresses are below the allowables.

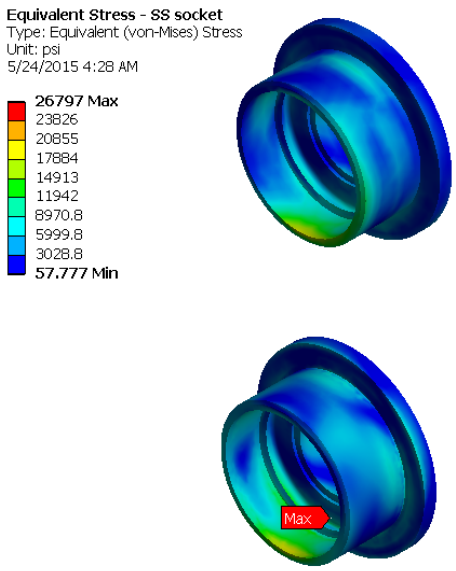

Figure 76. Stresses in SS304 sockets – loading condition 1

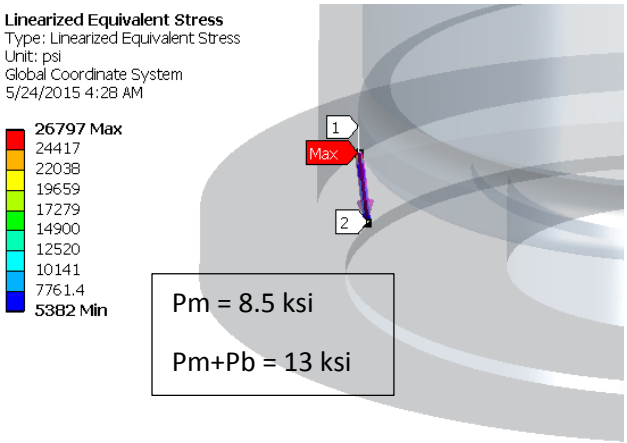

Figure 77. Stresses in SS304 sockets – loading condition 1

The copper shield is supported by two horizontal SS304 45x45x8 mm angles which are cantilevered from the top of the shield plate. Two additional angles are cantilevered from the bottom of the shield plate, and share some of the shield load by providing additional support to the upper angles. The shield assembly details are such that cool down should occur with little stress. Therefore, the stresses for the two loading combinations are assessed in the absence of the cool down contribution.

The stresses in the shield are shown in Fig. 78, for loading combination 2. This combination uses the X-direction seismic acceleration, which causes high stresses where shield bends over the angles. It is likely that, given the temper assumed, some yielding will occur across the section. Displacement of the shield in the X-direction, in true scale, is shown in Fig. 79. The maximum is 1.22 inches, in the direction opposite of the X-direction seismic loads. This deformation is predominately elastic, and when relieved of the seismic load, the shield will likely reassume its original position, with little permanent offset.

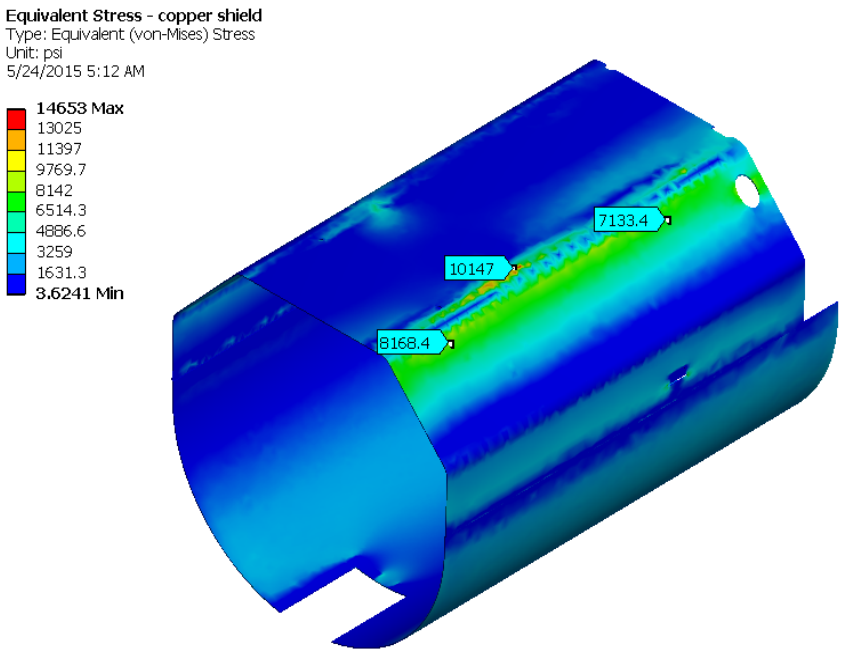

Figure 78. Stresses in copper shield – loading condition 2 (minus cool down)

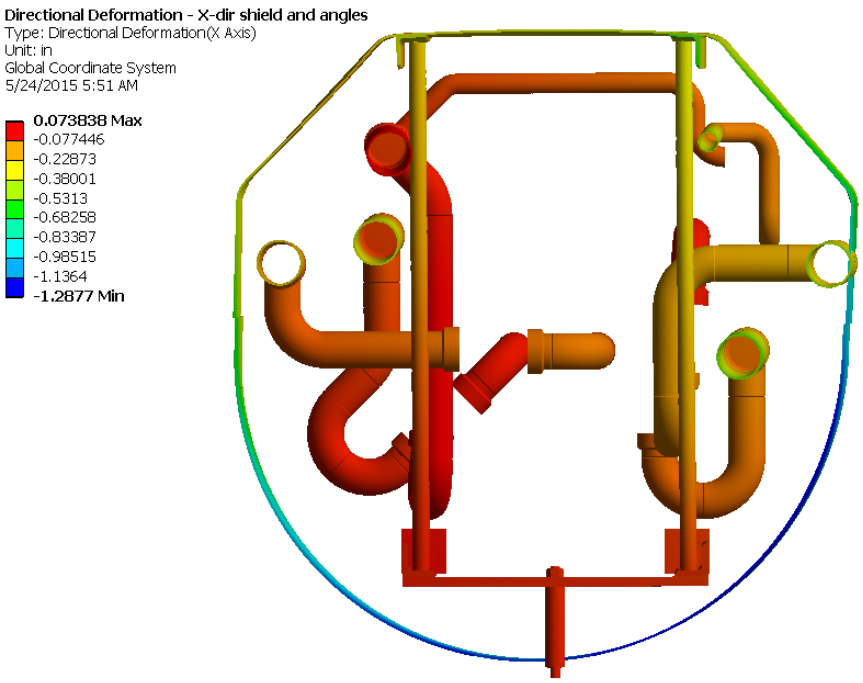

Figure 79. True scale displacements for loading condition 2

The stresses in the angles that support the shield are a maximum at the attachment point to the shield plate. Fig. 80 shows the angle dimensions, section properties, and the maximum calculated forces on the attachment point for loading combination 2. (Note that the shear value is large, but is primarily an internally reacted force resulting from the contraction of the shield, i.e., shear force on one angle is equilibrated by that in another, so the shear doesn't entirely represent external loads)

When the loads of Fig. 80 are used in beam bending, shear, and normal stress calculations, the result is a maximum tensile stress of 10.8 ksi, and a maximum shear stress of 1.4 ksi. These values are well below the membrane stress allowable stress of 20 ksi.

Assuming that the angle is welded to its mounting plate with full penetration, these stresses also apply to weld.

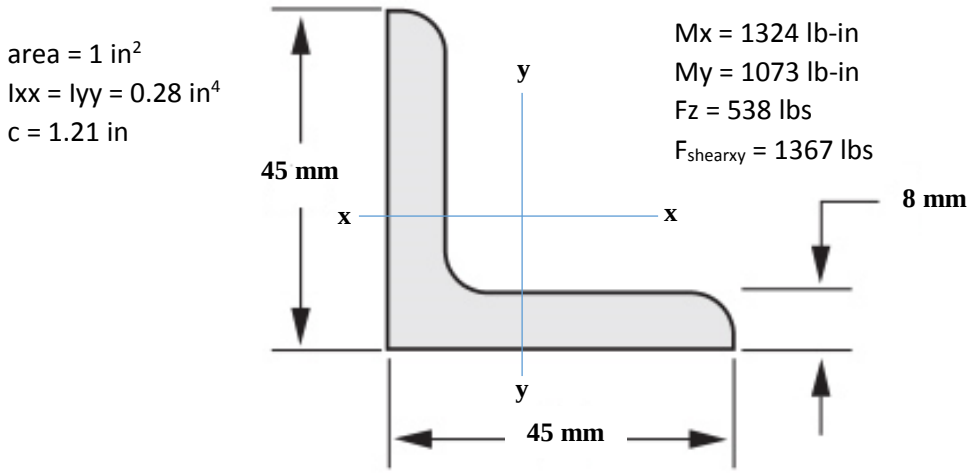

Figure 80. Angle geometry, section properties, and maximum loads

Cryomodule Feedcap Support

The cryomodule feedcap support supports the entire vacuum load on the circular endplate of the feedcap (~25000 lbs), as well as the feedcap gravity and seismic loads. The FE model is shown in Fig. 81. The mass of the previous feedcap model (1415 lbs) was lumped at the location of the center of mass in the cryomodule feedcap model. This location is concentric with and 21.4 inches in Z from the inner face of the endplate. This mass was mathematically attached to the perimeter of the endplate.

For the stress analysis of the members of the support, the model was subjected to five load cases. Note that, for conservatism, no factoring is performed on the seismic or pressure loads.

1. 1.27 g in +X and 1.4 g in +Y + vacuum in cryomodule
2. 1.4 g in +Y and 1.27 g in –Z + vacuum in cryomodule
3. 1.27 g in +X and 0.2 g in +Y + vacuum in cryomodule
4. 0.2 g in +Y and 1.27 g in –Z + vacuum cryomodule
5. 0.2 g in +Y and 1.27 g in +Z, positive 7 psi in vacuum space of cryomodule

Figure 81. FE model of feedcap support

Stresses in the feedcap support are shown in Fig. 82. The highest calculated stress of 9.9 ksi is less than the primary membrane stress allowable for SS304 of 20 ksi. Should the columns and angles (but not the end plate) be made of structural steel, one choice would be A36. This steel has a yield stress of 36 ksi. If an allowable is chosen as 0.6 of yield stress, then structural steel components would have an allowable membrane stress of 21.6 ksi, somewhat above that of SS304. In either case, the actual stresses are less than the allowable stress.

To check the bolting of the diagonal brace to the column, the maximum force was extracted at the joint and compared to the joint strength. The joint is assumed to use six 0.75x10 Gr. 5 bolts, with a proof load of 28400 lbs, an ultimate tensile load of 40100 lbs, and a stress area of 0.334 in^2. The analysis shows that the maximum joint loads occur for loading condition 2, where the maximum tensile force is 11900 lbs, and maximum shear force is 12600 lbs. Assuming an even distribution of these forces over the bolt group, the bolt tensile stress is then 6.0 ksi, and the bolt shear stress is 6.3 ksi. Assuming an allowable of 2/3 of proof strength gives (2/3)(28400)/0.334 = 56.7 ksi for tensile loading. For shear, half this value, 28.3 ksi, is taken as the allowable stress. For both stresses, the allowable is far above the calculated maximum bolt stress.

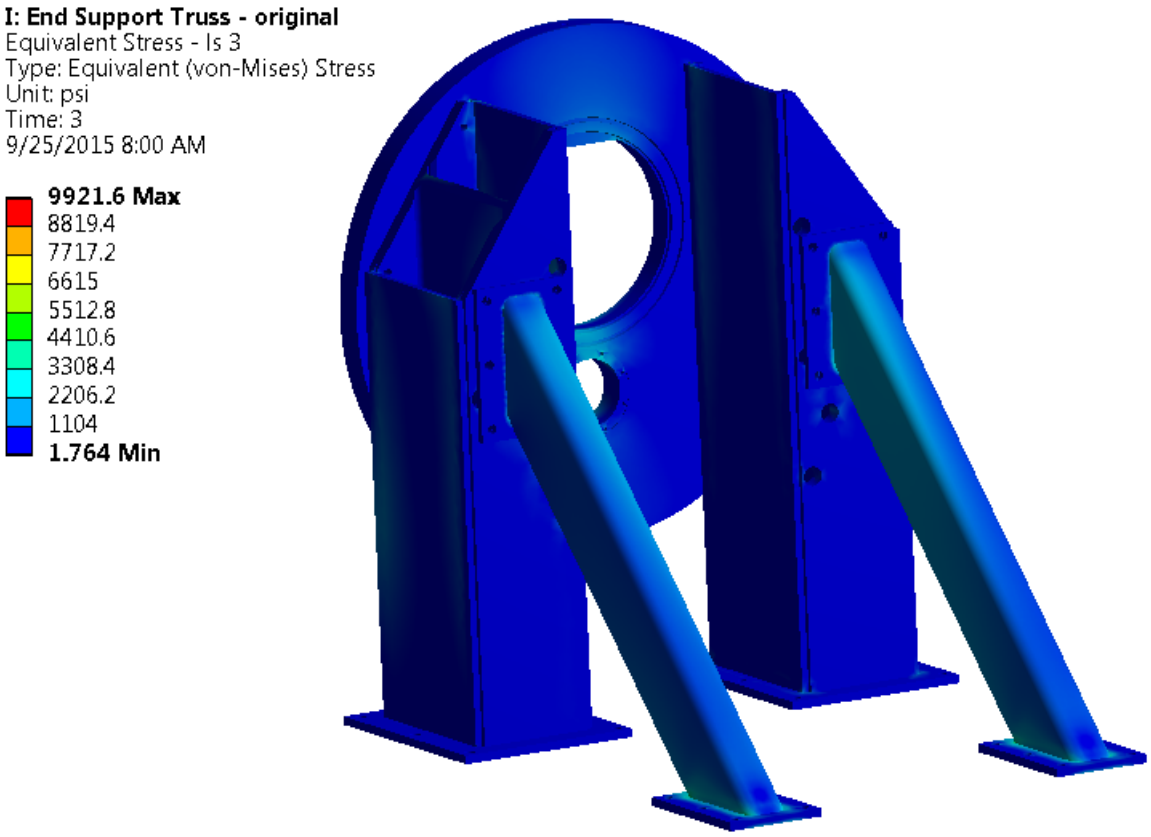

Figure 82. Stresses in feedcap support – 1.27 g X-acceleration plus 1.4 g Y-acceleration

Forces for use in designing the concrete anchors for the endcap support must be calculated with allowable strength load combinations and load factors (see Appendix A). An overstrength factor of 2.5 was specified. The model was subjected to six load cases:

1. 1.4 g in +Y + 1.4 times vacuum in cryomodule
2. 3.2 g in +X + 1.6 g in +Y + 1.2 times vacuum in cryomodule
3. 1.6 g in +Y + 3.2 g in +Z + 1.2 times vacuum in cryomodule
4. 1.6 g in +Y + 3.2 g in –Z + 1.2 times vacuum in cryomodule
5. 0.5 g in +Y + 3.2 g in –Z + 0.9 times vacuum in cryomodule
6. 0.5 g in +Y + 3.2 g in +Z + 0.9 times 7 psi in vacuum space of cryomodule

The resulting reaction forces at the floor plates are given in Table XVIII, for the orientations of Fig. 83.

Table XVIII. Floor reactions for concrete anchor sizing – lbs
(Note: Negative Fy indicates tension in anchor)

Floor Plate	Load Case	Fx	Fy	Fz
Column 1	1	4698	18260	-2473
	2	11088	4238	-5977
	3	3398	11661	183
	4	4628	21877	-3959
	5	3651	15727	-3893
	6	-2063	-8020	3350
Column 2	1	-4698	18250	-2484
	2	3042	29291	2190
	3	-3397	11662	182
	4	-4628	21857	-3978
	5	-3651	15711	-3909
	6	2064	-8007	3361
Truss 1	1	209	-15083	-14695
	2	374	-13972	-13655
	3	154	-8031	-7640
	4	206	-18248	-18017
	5	159	-14594	-14404
	6	-87	9153	9067
Truss 2	1	-209	-15073	-14684
	2	12	-12299	-11991
	3	-155	-8034	-7641
	4	-205	-18228	-17995
	5	-159	-14577	-14385
	6	87	9140	9053

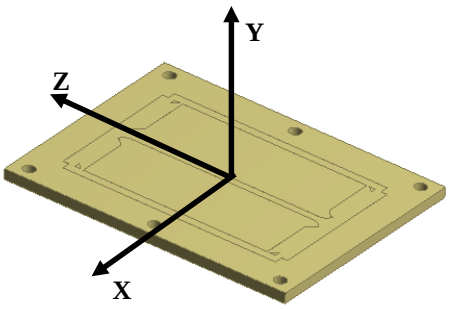

Column Support Floor Plate

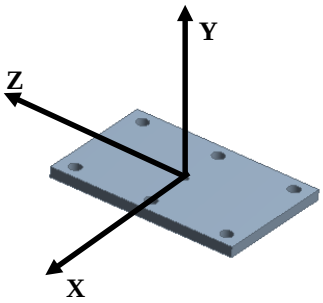

Truss Support Floor Plate

Figure 83. Coordinate systems for anchor force orientation

References

1. ASME B31.3-2010, “Process Piping” American Society of Mechanical Engineers, 2010
2. ASME B31E-2010, “Standard for the Seismic Design and Retrofit of Above-Ground Piping Systems,” American Society of Mechanical Engineers, 2010
3. ASME Boiler and Pressure Vessel Code, Section VIII, Div. 1,”Rules for Construction of Pressure Vessels,” American Society of Mechanical Engineers, 2013
4. ASME Boiler and Pressure Vessel Code, Section VIII, Div. 2, “Alternative Rules: Rules for the Construction of Pressure Vessels,” American Society of Mechanical Engineers, 2013
5. ASME Boiler and Pressure Vessel Code, Section II, Part D, “Properties,” American Society of Mechanical Engineers, 2013
6. ASCE 7-10, “Minimum Design Loads for Buildings and Other Structures,” American Society of Civil Engineers, 2010
7. G-10 properties http://ncsx.pppl.gov/NCSX_Engineering/CloseOut_Documentation/Brown/Jobs8203_1803/Design_Integration_Files/NCSX%20-%202008/Cryostat/G10CR-G11CR-Properties1.pdf

Appendix A

Approach to the Analysis of the LCLS-II CDS ($I_p = 1.5$)

Summary

The LCLS-II CDS will be designed and analyzed by the procedures of B31.3-2010, "Process Piping." The effects of seismic loadings will be assessed by B31Ea-2010, "Standard for the Seismic Design and Retrofit of Above-Ground Piping Systems." ASCE-7 is used to calculate the seismic effect coefficients, and for guidance in the creation of load combinations.

Load Combinations – ASCE 7

B31.3 uses an allowable stress design methodology. There are no formal lists of load combinations to be considered. Section 301.5, "Dynamic Effects", states that, for wind and seismic loading, "the analysis considerations and loads may be as described in ASCE 7."

The loads on the CDS are:

1. Dead weight, D
2. Internal pressure in piping, F_{ip}
3. External pressure on vacuum vessel or other pipes, F_{ep}
4. Self-straining due to cool down from ambient to cryogenic temperatures, T
5. Seismic effects, E

Load combinations are defined in ASCE-7, para. 2.4, "Combining Nominal Loads Using Allowable Stress Design." Two loads on the system, F, and T, do not appear explicitly in the load combination list of 2.4.1. However, subsequent paragraphs clarify their inclusion.

Para. 2.4.1 states that "Where fluid loads F are present, they shall be included in the combinations 1 through 6 and 8 with the same factor as that used for dead load D."

Para. 2.4.4, states that, "Where applicable, the structural effects of load T shall be considered in combination with other loads. Where the maximum effect of load T is unlikely to occur simultaneously with the maximum effects of other variable loads, it shall be permitted to reduce the magnitude of T considered in combination with these other loads. The fraction of T considered in combination with other loads shall not be less than 0.75."

From the list of load combinations for allowable stress design given in 2.4.1, and applying the fluid pressure loads and self-straining loads as recommended in that paragraph, the following load combinations can be created:

1. $D + F_{ip} + F_{ep} + T$
5. $D + F_{ip} + F_{ep} + 0.7E + T$
8. $0.6D + 0.7E + 0.6F_{ip} + 0.6F_{ep}$

Note that although load combination 6b does include E, in the absence of live load L and snow load S, this load combination is not as demanding as load combination 5, and so is not included in this list.

In the actual analysis, the horizontal seismic acceleration loads will be factored by 0.7. The vertical seismic acceleration loads will be factored by 1.0

Calculation of Seismic Effects – ASCE 7

Two basic assumptions are made for determining the seismic effects:

1. Risk Category II – this is taken from Table 1.5-1 of ASCE-7, assuming that this work falls under "Buildings and other structures that represent low risk to human life in the event of failure."

2. Seismic Design Category E – this is taken from Section 11.6, assuming Risk Category II, and a mapped spectral response acceleration parameter at 1-s period, S_1, equal to 1.198 (>0.75, and taken from the 2014 revision of the SLAC seismic design specifications)

ASCE-7 permits either Allowable Strength or Allowable Stress design. In both cases, total seismic load, E, consists of a horizontal effect E_h, and a vertical effect E_v.

12.4.2(1) states: For use in load combination 5 in Section 2.3.2 or load combinations 5 and 6 in Section 2.4.1, E shall be determined in accordance with Eq. 12.4-1 as follows:

$$E = E_h + E_v \qquad (12.4\text{-}1)$$

12.4.2(2) states: For use in load combination 7 in Section 2.3.2 or load combination 8 in Section 2.4.1, E shall be determined in accordance with Eq. 12.4-2 as follows:

$$E = E_h - E_v \qquad (12.4\text{-}2)$$

In practice, E_h and E_v are coefficients that multiply the acceleration due to gravity.

The design and analysis of the LCLS-II transfer line is based on ASME B31.3, "Process Piping" and B31Ea-2010, "Standard for the Seismic Design and Retrofit of Above-Ground Piping Systems." The E calculated here will be used as the "seismic static coefficient" of B31Ea-2010.

Horizontal Seismic Load Effect, E_h

E_h is defined in 12.4.2.1 as

$$E_h = \rho Q_e \qquad (12.4\text{-}3)$$

Where Q_e = effects of horizontal seismic forces from V or F_p, and ρ is a redundancy factor. From 12.3.4.1, because we are designing non-structural components, ρ can be taken as 1.

For the transfer line, F_p is used. This is defined in Section 13.3.1 as

$$F_p = \frac{0.4 a_p S_{DS} W_p}{\frac{R_p}{I_p}} \left[1 + 2\frac{z}{h}\right] \qquad (13.3\text{-}1)$$

F_p is not required to be taken as greater than

$$F_p = 1.6 S_{DS} I_p W_p \qquad (13.3\text{-}2)$$

and F_p shall not be taken as less than

$$F_p = 0.3 S_{DS} I_p W_p \qquad (13.3\text{-}3)$$

Where F_p = seismic design force
S_{DS} = spectral acceleration, short period
a_p = component amplification factor
I_p = component importance factor that varies from 1.00 to 1.5 (see Section 13.1.3)
W_p = component operating weight
R_p = component response modification factor that varies from 1.00 to 12
z = height in structure of point of attachment of component with respect to base
h = average roof height of structure with respect to base.

The factors are chosen as follows:

S_{DS} – This is taken from the SLAC document "Seismic Design Specification for Buildings, Structures, Equipment, and Systems: 2014", Table 2. The highest value on this table is $S_{DS} = 2$.

a_p and R_p – These are taken from ASME B31Ea-2010, paragraph 3.1, which states ""the parameter a_p shall be 2.5 and the parameter R_p shall not exceed 3.5 when applying the stress limits of para. 3.4."

I_p – This is taken from Section 13.1.3. The transfer line is a Risk Category IV structure, requiring an importance factor $I_p = 1.5$

z and h – due to our tunnel installation, z = 0, and h is undefined.

Substituting the above values into Eqn. 13.3-1 gives $F_p = 0.86W_p$. The maximum value of F_p (Eqn. 13.3-2) is $F_p = 4.8W_p$. The minimum value (Eqn 13.3-3) is $F_p = 0.9W_p$.

Since the F_p calculated from 13.3-1 is less than the minimum calculated by 13.3-3, for the transfer line $F_p = 0.9W_p$.

Vertical Seismic Load Effect, E_v

Section 12.4.2.2 defines the vertical seismic load effect as

$$E_v = 0.2S_{DS}D \qquad (12.4\text{-}4)$$

Substituting the previously determined value of S_{DS} gives $E_v = 0.4D$.

Application of B31Ea-2010 – Seismic Loading

Paragraph 3.1 of B31Ea-2010 discusses the calculation and application of the seismic effects E. For seismic loading, it states: “The seismic loading shall be specified for each of three orthogonal directions. The seismic design should be based on either a three-directional excitation, east-west plus north-south plus vertical, combined by square-root sum of the squares (SRSS) , or a two–directional design approach based on the envelope of the SRSS of the east-west plus vertical and north-south plus vertical seismic loading.”

A two-directional approach is taken in the CDS analysis. The two orthogonal horizontal accelerations of 0.9 g are resolved to a single acceleration of 1.27 g and applied along the length of the pipe run in one load case, and perpendicular to the pipe run in another load case. In both load cases the vertical loading is included. The sign of the 1.27 g acceleration will be that which gives the highest stresses.

Application of B31Ea-2010 – Design by Analysis

Table 1 of B31Ea-2010 is used to determine if design-by-rule or design-by-analysis applies to a piping system. Given a peak spectral acceleration a = 0.9g, and the designation of the transfer line as “critical piping”, then by Table 1 the LCLS-II transfer line must be designed by analysis.

Para. 3.4 covers the design by analysis. It require consideration of two stress components:

1. The elastically calculated longitudinal stress in a pipe due to pressure, sustained bending, and seismically-induced bending must be calculated by a specific formula and limited to specific stress values, which are larger than the allowable stresses given in B31.3, Table A-1
2. The sum of shear and tensile forces due to seismic anchor motion, divided by the cross sectional area of the pipe, must be less than or equal to the yield stress of pipe material

The stress analysis approach for this work treats seismic loads no differently than other loads on the system. Therefore, while these two special cases will be treated, it is expected that both stresses will lie well below the allowables specified in B31Ea-2010.

Using Strength Load Factors for the Anchoring Loads – with Overstrength

The load factors and load combinations for allowable stress are used in the analysis of all CDS components except the concrete anchors. This is because the Hilti Profis program, which designs anchoring configurations based on user input, requires allowable strength load factors and load combinations to be used to calculate the anchor forces.

From ASCE-7, 2.3, there are 7 load combinations that must be considered in a strength design. Of these seven, three are relevant to the calculation of the anchoring loads. The elimination of the others is based on the fact that for the anchor loads, only dead weight, vacuum (fluid pressure), and seismic loading need to be considered.

The three load combinations are:

1. 1.4D

5. 1.2D + 1.0E

7. 0.9D + 1.0E

The vacuum loading is a fluid load, F, and is not explicitly included in the load combinations. Guidance for its use is given in 2.3.2: “When fluid loads F are present, they shall be included with the same load factor as dead load D in combinations 1 through 5 and 7.” This results in the following final load combinations:

1. 1.4D + 1.4F

5. 1.2D + 1.0E + 1.2F

7. 0.9D + 1.0E + 0.9F

We are required to consider an overstrength factor of 2.5. Guidance for the use of this factor is taken from 12.4.3:

1. For use in load combination 5 in Section 2.3.2 or load combinations 5 and 6 in Section 2.4.1, E shall be taken equal to E_m as determined in accordance with Eq. 12.4-5 as follows:

$$E_m = E_{mh} + E_v$$

2. For use in load combination 7 in Section 2.3.2 or load combination 8 in Section 2.4.1, E shall be taken equal to E_m as determinate in accordance with Eq. 12.4-6 as follows:

$$E_m = E_{mh} - E_v$$

Where E_m = seismic load effect including overstrength factor

E_{mh} = effect of horizontal seismic forces including overstrength factor as defined in Section 12.4.3.1

E_v = vertical seismic load effect as defined in Section 12.4.2.2

The effect of horizontal seismic load has been calculated previously as 0.9g. The approach taken in the analysis of the CDS has been to use the SRSS (1.27g) applied in either the longitudinal direction, or the lateral direction, but not in both directions simultaneously. With an overstrength factor of 2.5, this horizontal acceleration becomes 3.2g.

The effect of vertical seismic load has been calculated previously as 0.4g.

The pressure loading on the endcap support is either 15 psi vacuum, or 7 psi differential possible during fault conditions (e.g., rupture of a cryogenic line in the vacuum space).

Using these values, the three load combinations can be written in more detail.

Load Combination 1:

This combination becomes a vertical acceleration of 1.4g plus the pressure load of either 15 psi, or 7 psi differential, both factored by 1.4.

Load Combination 5:

This load combination becomes a vertical acceleration of 1.6g, and horizontal accelerations of 3.2g. The pressure load is either 15 psi vacuum, or a 7 psi overpressure, both factored by 1.2.

Load Combination 7:

This load combination (which is typically considered to address tipping) becomes a vertical acceleration of 0.5g, horizontal accelerations of 3.2g, and pressures loads of either 15 psi, or 7 psi overpressure, both factored by 0.9

Note that a given load combination can result in more than one load case, since the sign and direction of the horizontal acceleration can change, and there is more than one pressure loading to consider.

Summary

The loads which must be considered in the analysis of the LCLS-II CDS are shown in Table A-I.

Table A-I. Loadings on the LCLS-II CDS

Loading	Symbol per ASCE 7-10k, 2.4	Value
Dead weight	**D**	**mass x 1.0 g**
Horizontal Seismic Acceleration	**E_v**	**mass x 0.9 g(1)**
Vertical Seismic Acceleration	**E_h**	**mass x 0.4 g**
Maximum Allowable Working Pressure	**F_{ip}**	**varies with pipe**
Vacuum	**F_{ep}**	**15 psi external**
Pressure imbalance at vacuum breaks	**F_{ip}**	**7 psi differential**
Cool Down	**T**	**varies with pipe**

1) This is applied as the SSRS of 0.9 g's (1.27 g), in the direction perpendicular to the piping, *or* parallel to the piping, but not in both directions at once.

The loadings above are used in the three load combinations listed in Table A-II

Table A-II. Load Combinations for the Analysis of the LCLS-II CDS

Load Combination Number per ASCE 7-10, 2.4.1	Load Combination
1	**$D + F_{ip} + E_{ep} + T$**
5	**$D + F_{ip} + F_{ep} + 0.7E + T$**
8	**$0.6D + 0.7E + 0.6F_{ip} + 0.6F_{ep}$**

The load combinations provide only broad guidance. The analysis must consider the presence of all loads in a given combination, but also the possibility that higher stresses might result in the absence of a given load.

For the Fermilab Reference Design, the 0.7 load factor applied to E was applied to only the horizontal component; the vertical component was used with a factor of 1. The 0.6 factor on F_{ip} and F_{ep} was also replaced with a factor of 1. This is not meant to be viewed as a requirement for the analysis of any proposed system.

Specific load cases must consider the directions of the seismic loads. For example, in Load Combination 8, if a downward vertical seismic acceleration of 0.4 is assumed, then the combination of deadweight D and the vertical seismic acceleration becomes 0.2D.